NTNU
Norwegian University of
Science and Technology

Cathodic Protection of Steel-Aluminium Galvanic Couples for a New Generation of Lightweight Subsea Structures

Sondre Røstbø

Preface

This master's thesis was written during spring of 2016 at the Department of Materials Science and Engineering at Norwegian University of Science and Technology (NTNU), in Trondheim, Norway. The thesis is a continuation of the work carried out in the course TMT4500 Materials technology specialization project during fall of 2015.

I would like to thank my supervisor, Professor Kemal Nisancioglu, and co-supervisor Dr. Otto Lunder for their guidance and help throughout this project.

Gratitude goes to Staff Engineer Anita Storsve for assisting me during preparation of salt bridges, and with other technical challenges.

The mechanical workshop at Faculty of Natural Science and Technology (Finmekanisk verksted) deserves recognition for their help in developing experimental setups and preparation of samples.

Lastly, thanks goes to Mariia Stepanova, PhD candidate at NTNU, for always being helpful and assisting me in the lab whenever needed.

Sondre Røstbø

Abstract

A new generation of lightweight subsea structures is planned for application in oil and gas production. Due to increasing weight of subsea installations, the use of aluminium as a structural material is of continuous interest. A problem is that galvanic corrosion will occur since not all steel components can be replaced by aluminium, and the two metals need to be isolated from each other. Another solution is to protect both metals from corrosion by a common cathodic protection system.

The purpose of this thesis was to show by laboratory research if it is possible to protect steel-aluminium galvanic couples against corrosion by cathodic protection. Samples of X65 carbon steel, 6005 aluminium and an AlZnIn sacrificial anode were studied by galvanic corrosion testing, open circuit testing and potential sweep. Steel and aluminium samples were connected in a simulated crevice of 100 μm to study the effect of galvanic crevice corrosion. Weight loss measurements were performed to determine corrosion rates, and the sample surfaces were characterized by SEM and EDS. Electrochemical testing was performed in both artificial seawater and a 3.5% NaCl solution.

It was found that cathodic protection of steel-aluminium galvanic couples is possible in the absence of crevice corrosion. In a three-metal coupling, the sacrificial anode supplied cathodic current to both steel and aluminium. The reduction rate on steel was between 1 and 2 orders of magnitude larger than that on aluminium. The lower current density on aluminium was due to the fact that reduction only occurs on Fe-rich intermetallic particles in the Al matrix. During cathodic polarization of aluminium, an alkaline etching process caused detachment of these cathodic particles for surface pH sufficiently high. Calcareous deposits precipitated on steel under cathodic protection, but had little or no effect on the current density at a potential controlled by AlZnIn.

Cathodic protection applied to a galvanic crevice between steel and aluminium gave a high local corrosion rate of aluminium near the crevice mouth. The steel was completely protected. The local corrosion rate of aluminium was sufficiently high to give anodic net current despite being connected to a sacrificial anode. The phenomena was an initial stage related to a potential and current distribution across the crevice. A very high local reduction rate on steel caused a high pH and thus corrosion of aluminium. The reduction rate on steel decreased as a function of time along with the corrosion rate of aluminium.

Sammendrag

En ny generasjon lettvekt undersjøiske strukturer er planlagt for bruk i produksjon av olje og gass. På grunn av økende vekt av undersjøiske installasjoner, er det interesse for å bruke aluminium som strukturelt materiale. Et problem er at galvanisk korrosjon vil oppstå, siden ikke alle komponenter av stål kan erstattes av aluminium, og de to metallene må isoleres fra hverandre. En annen løsning er å beskytte begge metaller fra korrosjon felles system for katodisk beskyttelse.

Formålet med denne oppgaven var å vise ved laboratorieundersøkelser om det er mulig å beskytte stål-aluminium koblinger mot korrosjon ved katodisk beskyttelse. Prøver av X65 karbon stål, 6005 aluminium og en AlZnIn offeranode ble studert ved galvanisk korrosjonstesting, åpen krets testing and potensial sveip. Prøver av stål og aluminium ble koblet i en kunstig spalt på 100 μm for å studere effekten av galvanisk spaltkorrosjon. Vekttapsmålinger ble utført for å bestemme korrosjonsrater og prøveoverflatene ble karakterisert ved SEM og EDS. Elektrokjemisk testing ble utført i både kunstig sjøvann og en 3.5% NaCl løsning.

Det ble funnet at katodisk beskyttelse av stål-aluminium koblinger er mulig uten spaltkorrosjon. I en tre-metall kobling fikk både stål og aluminium katodisk strøm fra offeranoden. Reduksjonsraten på stål var mellom 1 og 2 tier potenser større enn på aluminium. Den lave strømtettheten på aluminium var på grunn av det faktum at reduksjon kun skjer på Fe-rike intermetalliske partikler i Al matrisen. Under katodisk polarisering av aluminium ble disse katodiske partiklene løsnet av en alkalisk etseprosess, for en høy nok pH ved overflaten. Kalkbelegg ble utfelt på stål under katodisk beskyttelse, men hadde liten eller ingen effekt på strømtettheten ved et potensial kontrollert av AlZnIn.

Katodisk beskyttelse av en galvanisk spalt mellom stål og aluminium gav en høy lokal korrosjonsrate av aluminium nær spalteåpningen. Stålet var fullstendig beskyttet. Den lokale korrosjonsraten av aluminium var høy nok til å gi anodisk netto strøm til tross for å være koblet til en offeranode. Fenomenet var en innledende fase relatert til en potensial- og strømfordeling langs spalten. En veldig høy lokal reduksjonsrate på stål førte til en høy pH og dermed korrosjon av aluminium. Reduksjonsraten på stål avtok som funksjon av tid sammen med korrosjonsraten av aluminium.

Contents

x

Chapter 1

Introduction

1.1 Background

Application of aluminium in subsea installations today is limited. Aluminium in marine applications is mostly used as tool and construction material for remote operated vehicles (ROVs), not permanent structures. As aluminium is widely used in sacrificial anodes, it is to some structural designers associated with poor corrosion resistance in seawater [1]. It also has different corrosion properties from steel, and the engineering experience with Al alloys is limited compared to steel [2].

By replacing steel components with aluminium in structures, a significant reduction in weight can be achieved. Aluminium has beneficial strength to weight ratio, in general good corrosion resistance, and is unsusceptible to hydrogen induced stress cracking (HISC) [3], [2]. Subsea structures are submerged by a lifting vessel during installation, and lifted up again for maintenance. The maximum weight of such structures is therefore limited, and a higher weight results in higher costs, related to installation, maintenance and operating conditions. It is therefore of continuous interest to use aluminium as a lightweight structural material [2]. Replacement of steel with aluminium is not limited to subsea structures; the benefits of the high strength to weight ratio and corrosion resistance can be useful in a wide range of marine applications.

Not all steel can be replaced when designing marine structures, and it is necessary to isolate steel from aluminium to avoid galvanic corrosion. Another solution may be to protect both steel and aluminium in galvanic contact by cathodic protection. A steel-Al coupling would normally cause the less noble aluminium to corrode; however, a cathodic protection system might be able to protect both metals. Another issue associated with joining metals is crevice corrosion. This form of corrosion can cause very high local corrosion rates, and could be detrimental for the lifetime of a structure.

1.2 Aim of the thesis

The purpose of this thesis is to show by laboratory testing whether or not steel-aluminium galvanic couples can be protected against corrosion by application of cathodic protection. The electrochemical behavior of the joined metals is to be determined, as well as the mechanisms for corrosion protection. Galvanic corrosion tests will be performed between samples of X65 carbon steel, 6005 Al and an AlZnIn sacrificial anode. Samples of X65 carbon steel and 6005 Al will also be coupled in a simulated crevice to study the effect of galvanic crevice corrosion. In addition, open circuit potential testing of the individual alloys will be performed, and potentiodynamic sweep tests will be carried out to study polarization behavior.

Experiments will be conducted in both artificial seawater and a 3.5% NaCl solution. Weight loss measurements will be performed after galvanic corrosion testing to determine corrosion rates. Surface characterization will be done both macroscopically and microscopically through SEM and EDS.

Chapter 2

Theory

2.1 Galvanic corrosion

Galvanic corrosion is a form of corrosion that occurs when two dissimilar metals are joined together in electric contact in the presence of an electrolyte. When coupled, the less noble metal will experience an increased corrosion rate and provide protective current to the more noble metal as illustrated in figure 2.1. The potential of the two metals will become equal, presuming that there is no ohmic resistance between them in the electrolyte nor in the connecting circuit [4].
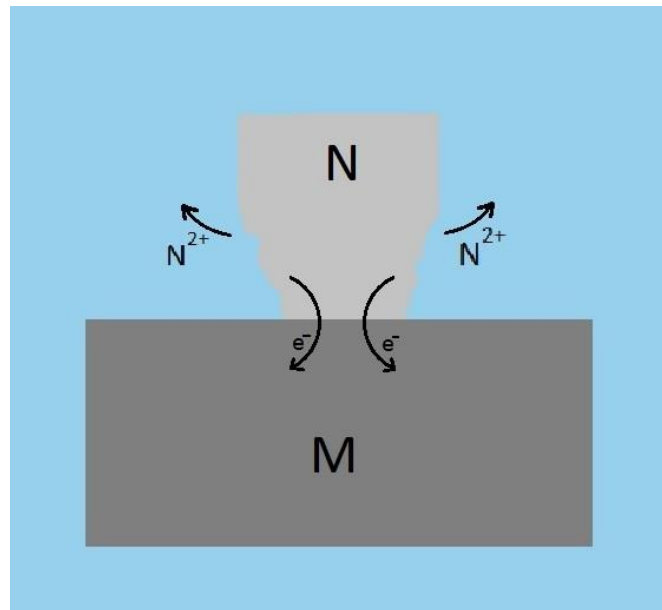

Figure 2.1. Illustration of galvanic corrosion between a noble metal M, and a less noble metal N.

For a noble metal M, and a less noble metal N, the following applies in an M-N coupling without ohmic potential drop [4]:

$$E_M = E_N = E_C \qquad (2.1)$$

Theory

A net galvanic current will flow from N to M to maintain the relation above. For the entire system, the total oxidation rate is equal to the total reduction rate. Possible oxidation reactions are:

$$M \rightarrow M^+ + e^- \tag{2.2}$$

$$N \rightarrow N^+ + e^- \tag{2.3}$$

Possible reduction reactions are:

$$2H^+ + 2e^- \rightarrow H_2 \tag{2.4}$$

$$2H_2O + 2e^- \rightarrow H_2 + 2OH^- \tag{2.5}$$

$$O_2 + 2H_2O + 4e^- \rightarrow 4OH^- \tag{2.6}$$

$$O_2 + 4H^+ + 4e^- \rightarrow 2H_2O \tag{2.7}$$

To measure the galvanic current between to metals, it is necessary to use a zero-resistance ammeter, in order to avoid disturbing the flow of electrons. The measured current is equal to the difference between oxidation rate and the reduction rate on the anode, or vice versa on the cathode:

$$I_{net} = \sum I_{ox,N} - \sum |I_{red}|_N = \sum |I_{red}|_M - \sum I_{ox,M} \tag{2.8}$$

Assuming the only possible oxidation reaction is metal dissolution, equation 2.8 becomes

$$I_{net} = I_{corr(M-\underline{N})} - \sum |I_{red}|_N = \sum |I_{red}|_M - I_{corr(\underline{M}-N)} \tag{2.9}$$

Presence of ohmic resistance, either in the electrolyte or in the metal path, results in a potential difference between the anode and the cathode:

$$E_M - E_N = I_{net} R_{el} + I_{net} R_{ext} \tag{2.10}$$

2.1.1 Steel-aluminium coupling

Pryor and Keir performed galvanic corrosion testing of pure aluminium ($> 99.99\%$) and mild steel in a normal NaCl solution. Results from three parallels can be seen in figure 2.2. The surface area for both samples is 100 cm^2, giving a current density range of approximately 8 to 24 μA/cm^2. Current flow behavior was not reproducible for one parallel, which has a significant scatter from the two others [5].
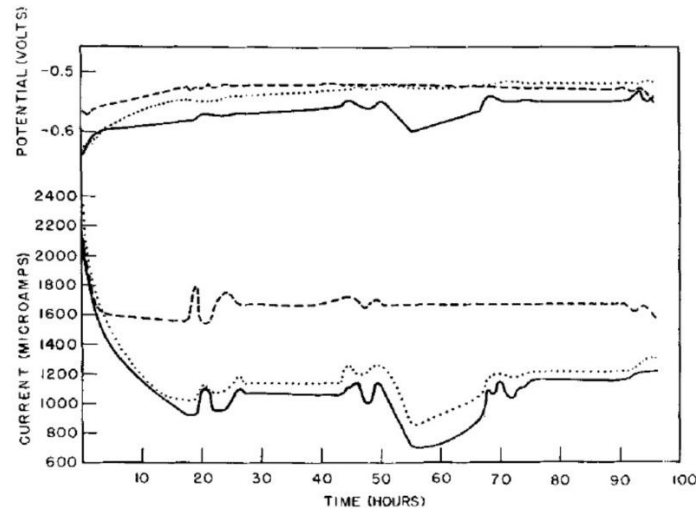
Figure 2.2. Three parallels of galvanic corrosion testing between pure aluminium and mild steel in normal NaCl solution. Curves relate current flow and potential to time. Sample area is 100 cm^2 for both samples. Potential is measured against SCE [5].

Mansfeld and Parry studied galvanic corrosion between Al alloys and stainless steel in a 3.5% NaCl solution. Current behavior was recorded and weight loss measurements of the Al alloys were performed after electrochemical testing. Before joining alloys, corrosion rates of uncoupled samples were found; corrosion rate of bare 6061 Al was reported as 0.15 ± 5 mg/cm^2 for a 24 hour test. Result from galvanic corrosion testing between 6061 Al coated with Alodine 600 (chromate conversion coating from Henkel), and 304 stainless steel (SS304) can be seen in figure 2.3 [6].
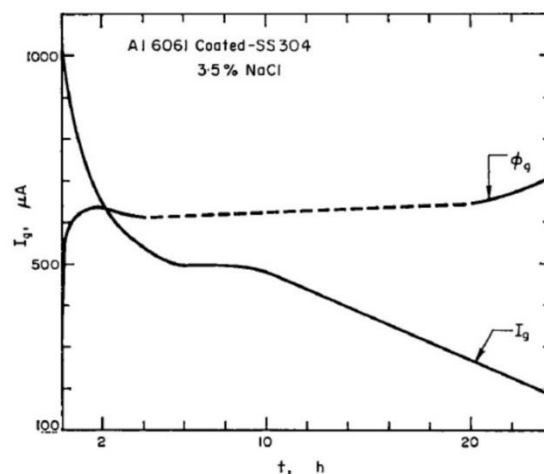

Figure 2.3. Galvanic current I$_g$ and potential φ_g of coated Al 6061/SS304 in 3.5% NaCl solution. Exposed area of samples is 20 cm^2 [6].

The initial current density is approximately 50 μA/cm^2, and decreases throughout the experiment. Weight loss for coated 6061 Al coupled to SS304 was found to be 0.24 mg/cm^2, and 0.33 mg/cm^2 for bare 6061 Al / SS304 [6].

5

2.2 Cathodic protection

Cathodic protection is a method of corrosion protection where the metal to be protected is polarized in cathodic direction by supplying a current on the metal. Two different systems are used: Sacrificial anodes and impressed current (inert anode). When using sacrificial anodes, the anode is in electric contact with the metal to be protected. Anodic dissolution will occur on the sacrificial anode, and current is provided to the more noble metal where a reduction reaction takes place.

When the potential of the metal to be protected is lowered from the open circuit potential, or corrosion potential, E_{corr} to a protection potential, E_p, the oxidation rate on the metal is reduced, and the corrosion decreases. If the metal is polarized below the reversible potential of metal dissolution, it will be completely protected. In a Pourbaix diagram, this will be in the immune region, see figure 2.4.

2.2.1 Reduction reactions

The two reduction reactions that may occur under cathodic protection is the oxygen reduction reaction (ORR) and the hydrogen evolution reaction (HER), (equation 2.5 and 2.6 in alkaline environment). The oxygen reduction reaction is expected to be mass transport controlled, i.e. controlled by transport of oxygen to the metal surface. The rate of the reaction can be calculated by combining Faraday's law and Fick's first law:

$$J_{O_2} = \frac{i}{nF} = -D\frac{dc}{dx} \qquad (2.11)$$

Where J is the flux towards the surface, i is current density, n is number of electrons involved, F is Faradays constant, D is the diffusion coefficient and $\frac{dc}{dx}$ is the concentration gradient.

$$i = -\frac{nFD(C_b - C_s)}{\delta_N} \qquad (2.12)$$

Where δ_N is the thickness of Nernst's diffusion layer and C_s and C_b is concentration at the surface and bulk solution respectively. At limiting current density the surface concentration becomes zero:

$$i_{lim} = -\frac{nDFC_b}{\delta_N} \qquad (2.13)$$

The mechanism for hydrogen evolution in alkaline environment is described by equation 2.14-16 [7]:

$$H_2O + M + e^- \rightleftarrows MH_{ads} + OH^- \tag{2.14}$$

$$H_2O + MH_{ads} + e^- \rightleftarrows M + H_2 + OH^- \tag{2.15}$$

$$2MH_{ads} \rightleftarrows 2M + H_2 \tag{2.16}$$
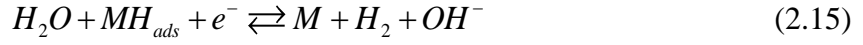
Where 2.15 and 2.16 are two possible mechanisms, described by Heyrovsky and Tafel respectively [7]. M signifies a vacant site, and H_{ads} an adsorbed hydrogen atom.

In contrast to the ORR, the HER is activation controlled i.e. transfer of electrons. The theoretical Tafel slope of the reaction can be calculated from the Tafel approximation of the Butler-Volmer equation:

$$i = i_0 \left[\exp\left(\frac{(1-\alpha)nF}{RT} \eta \right) - \exp\left(\frac{-\alpha nF}{RT} \eta \right) \right] \tag{2.17}$$

Where i is current density, i_0 is exchange current density, α is a charge transfer coefficient, and η is overpotential. The Tafel slope becomes:

$$\frac{\partial E}{\partial \log i} = -\frac{RT \ln(10)}{\alpha nF} \tag{2.18}$$

With a charge transfer coefficient of 0.5 and a temperature of 25 ℃, the Tafel slope becomes -118 mV/dec. Stern [8] reported the Tafel slope of reduction of water on an iron surface to be -174 mV/dec, which was explained by an increase in pH at the metal surface and the following concentration polarization.

2.2.2 Cathodic protection of steel

Figure 2.4 shows the Pourbaix diagram for iron (steel) in water, with potential given versus the Standard Calomel Electrode (SCE). This report will give potentials versus the Ag/AgCl reference electrode in saturated KCl. The difference between the Ag/AgCl electrode (saturated KCl) and SCE is 0.043 V [9], such that $E_{Ag/AgCl} = E_{SCE} + 0.043$.
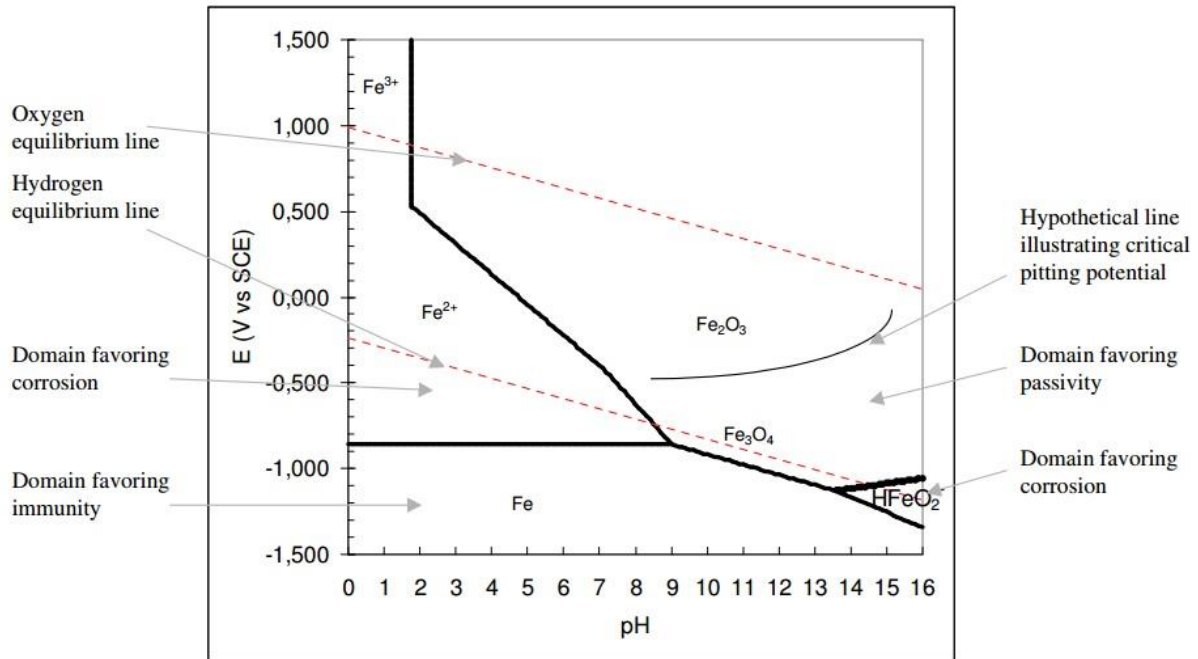
Figure 2.4. Pourbaix diagram of iron in water [10].

Carbon steel and low alloy steel submerged in seawater should be polarized to a potential between -800 mV and -1050 mV versus the Ag/AgCl reference electrode to be protected. However, cathodic protection of such steels should be considered as a method of corrosion control, rather than complete immunity [3], [11].

Refait et.al reported decrease in corrosion rate of carbon steel due to cathodic protection with zinc-based anodes to be one order of magnitude. The testing was carried out in natural seawater, in the tidal zone of a seaport with a test period of 7 years. Under cathodic protection, the average corrosion rate decreased from 90 µm/year to 9 µm/year [12].

2.2.3 Calcareous deposits

When cathodic protection is applied to steel submerged in seawater, calcareous scale deposits consisting of mainly $Mg(OH)_2$ and $CaCO_3$ will form on the metal surface. The calcareous deposits are known to reduce protection current requirement on steel by inhibiting the oxygen reduction reaction. The following reactions describe formation of the deposits [4], [13]:

$$CO_2 + H_2O \rightarrow H_2CO_3 \tag{2.19}$$

$$H_2CO_3 \rightarrow H^+ + HCO_3^- \tag{2.20}$$

$$HCO_3^- \rightarrow H^+ + CO_3^{2-} \tag{2.21}$$

$$Ca^{2+} + CO_3^{2-} \rightarrow CaCO_3 \tag{2.22}$$

$$Mg^{2+} + 2OH^- \rightarrow Mg(OH)_2 \tag{2.23}$$

Precipitation of $CaCO_3$ is initiated by a reaction between water and carbon dioxide from the atmosphere (equation 2.19). The following acid-base equilibria (equation 2.20, 2.21) are shifted to the right due to local increase in pH from equation 2.5 and 2.6, and calcium carbonate is precipitated. High pH also shifts equation 2.23 to the right, precipitating magnesium hydroxide [13].

The pH at which $CaCO_3$ and $Mg(OH)_2$ precipitates can be calculated using the solubility product constant for the compounds and their concentration in seawater. Yang et al. [14] calculated the precipitation pH of $CaCO_3$ to be 7.58, and 10 for $Mg(OH)_2$. Okstad [15] performed similar calculations and found that $CaCO_3$ forms at a pH of 6.0 and $Mg(OH)_2$ at 9.1. As the surface of cathodically protected steel slowly becomes increasingly alkaline, it is expected that $CaCO_3$ precipitates before $Mg(OH)_2$.

The protective properties of the calcareous deposits is greatly affected by the Ca/Mg ratio. Okstad studied the properties of calcareous deposits on carbon steel as a function of applied potential and flow velocity. It was reported that the kinetics for precipitation of $Mg(OH)_2$ was faster than for $CaCO_3$; $Mg(OH)_2$ was formed at all applied potentials (-800 to -1200 mV versus SCE), and all flow velocities (1, 5 and 10 cm/s). No calcium phase was found for the most noble potentials due to low pH on the steel surface and inhibition by Mg. Also, no $CaCO_3$ was found for the most active potentials with low flow velocity where the pH was high, which gives a high driving force for $Mg(OH)_2$ precipitation. $CaCO_3$ was formed at -1000 and -1100 mV_{SCE} for all flow velocities. Increased convection resulted in precipitation of $CaCO_3$ at more active potentials. For the lowest flow rate, 1 cm/s, the Ca/Mg ratio was highest at -1000 mV_{SCE} and decreased for both increasing and decreasing potential. Figure 2.5 illustrates the findings [15].
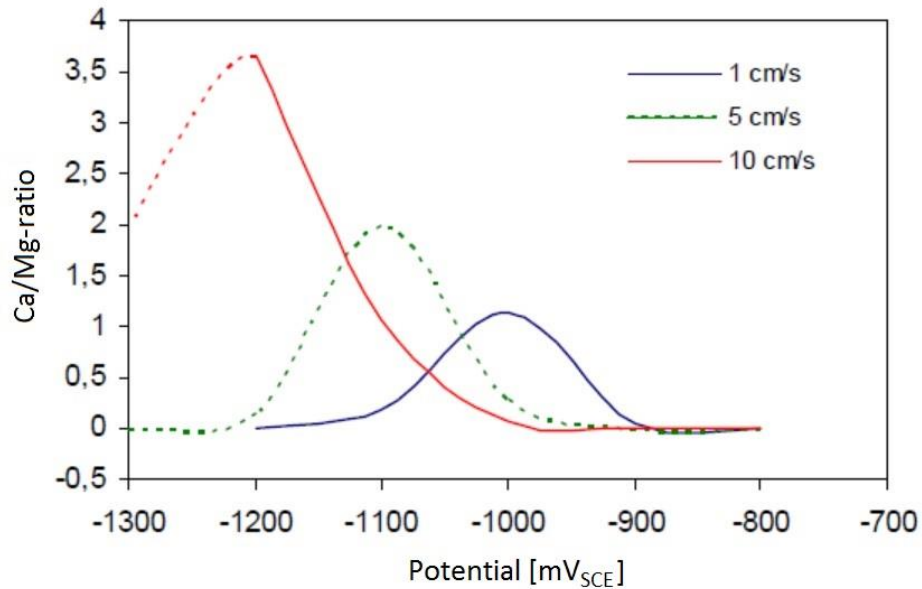
Figure 2.5. Ca/Mg ratio in calcareous deposits as a function of applied potential and flow velocity. Results are based on EDS-analysis and visual observations by Okstad. Dashed lines represent assumed data. Adapted from Okstad [15].

Okstad et al. studied significance of hydrogen evolution during cathodic protection of carbon steel in seawater and found that calcareous deposits reduces the rate of oxygen reduction while having little effect on the hydrogen evolution reaction [16]. It was also reported that the hydrogen evolution reaction was dominating for potentials more negative than -900 mV$_{SCE}$. At more noble potentials, there was contribution from the oxygen reduction reaction [16]. The Tafel slope of hydrogen evolution on steel in NaCl and in seawater with calcareous deposits was reported to be approximately -200 mV/dec for both cases. Catalyzing of the hydrogen evolution reaction was reported in a study by Salle et al., where the kinetics of the HER was found to be significantly higher on $Mg(OH)_2$ covered Mg surface compared to uncoated Mg [17].

Elbeik et al. evaluated the effectiveness of $CaCO_3$ as a protective film for mild steel by measuring corrosion current of both uncoated and $CaCO_3$ coated samples. Experiments were performed in both oxygenated and de-oxygenated seawater to determine corrosion current and potential associated with the oxygen and hydrogen reduction reaction. They reported a reduction in corrosion current for oxygen reduction due to $CaCO_3$ to be a factor of five, while for hydrogen, the corrosion current was halved. Results are shown in table 2.1 [13].

Table 2.1. Corrosion current density and potential for CaCO$_3$ coated and plain mild steel in seawater. Adapted from Elbeik et al. [13].

Sample type	I$_{corr}$ (O$_2$) [μA/cm^2]	E$_{corr}$ (O$_2$) [V$_{SCE}$]	I$_{corr}$ (H$_2$) [μA/cm^2]	E$_{corr}$ (H$_2$) [V$_{SCE}$]
Mild steel	223.9	-0.49	25.1	-0.78
CaCO$_3$ coated mild steel	44.7	-0.62	14.1	-0.85

2.2.4 Cathodic protection of aluminium

By the standard EMF series, aluminium is a highly active metal, but a very stable oxide forms on the surface quickly, passivating the metal. The oxide film provides good corrosion properties, and makes aluminium applicable in marine environments. From the Pourbaix diagram for aluminium (figure 2.6), one can see that aluminium oxide is an amphoteric compound, and is not stable in alkaline or acidic environments. This becomes an issue when cathodic protection is applied to aluminium; if the reduction reactions are rapid, the pH will increase at the surface, possibly destabilizing the oxide [18]. From experimental measurements, a revised Pourbaix diagram was obtained in a study by Perrault [19], and the results showed that the aluminium oxide may become unstable due to formation of hydrides. It was indicated that the immune zone of aluminium does not exist in practice.
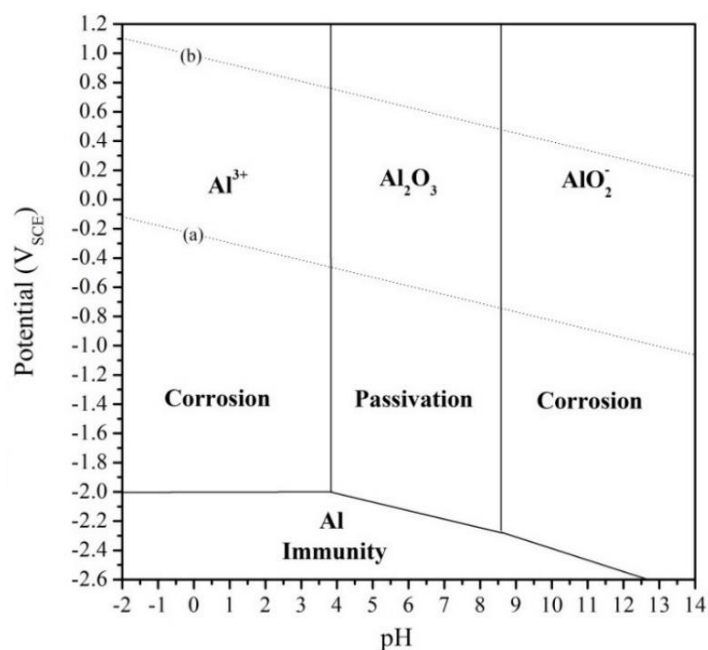

Figure 2.6. Pourbaix diagram of pure aluminium in aqueous solution at 25 °C. Lines (a) and (b) correspond to reduction of oxygen and hydrogen [20].

Aluminium is a less noble material than steel, but the current density required for cathodic protection of aluminium in seawater is roughly one order of magnitude less than for protection of steel [21]. The low current requirement is related to the small cathodic area on aluminium; reduction reactions occur on intermetallic sites, i.e. a very small fraction of the surface area [18]. This is in contrast to steel where the entire surface is available for reduction reactions. This difference is evidenced by comparing the polarization curves for steel and aluminium, shown in figure 2.7. The polarization curve for steel shows a limiting current behavior related to the reduction of oxygen, whereas no such behavior can be seen for the aluminium specimens. The curves for aluminium show a behavior resembling that of Tafel kinetics, and the current densities are far less than what can be seen one steel. Thus, the reduction process on aluminium is not controlled by transport [21].
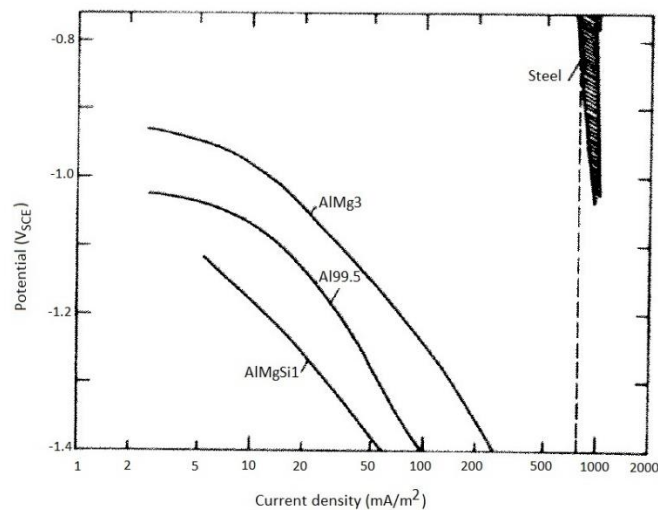

Figure 2.7. Cathodic polarization curves for aluminium and steel specimens in seawater at a flow rate of 8 cm/s [21].

Gundersen and Nisancioglu performed potensiostatic tests of commercial Al alloys in flowing natural seawater to investigate the mechanism for cathodic protection of aluminium. The following mechanism was proposed [21]: When immersed in seawater, reduction reactions occur at exposed iron-rich intermetallic particles in the Al matrix. These processes create an alkaline diffusion layer (equation 2.5, 2.6) near the particles. The high pH causes dissolution of the protective oxide film on the metal, and the Al matrix around the cathodic inclusion will corrode. The reduction reactions on the particle will be enhanced by increased particle area and iron enrichment, which in turn increases alkalinity of the adjacent diffusion layer. Corrosion of the Al matrix around inclusions will continue, and will eventually lead to detachment of particles (figure 2.8). The particle sites will be covered with corrosion products and possibly

calcareous deposits, which prevents exposure of new intermetallic particles. The alkalinity will drop and reaction rates decrease.
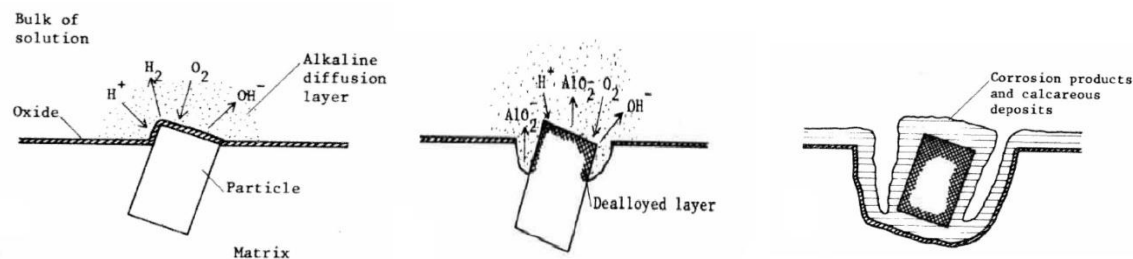

Figure 2.8. Principal sketch of the mechanism of cathodic protection of aluminium. Development of alkaline diffusion layer, followed by increased particle exposure and iron enrichment and finally detachment of the particle [21].

Figure 2.9 shows typical current-time behavior for aluminium under cathodic polarization. The increase in current density can be explained by increasing exposed area and iron enrichment of intermetallic particles in the Al matrix. The decrease in current follows from detachment of particles.
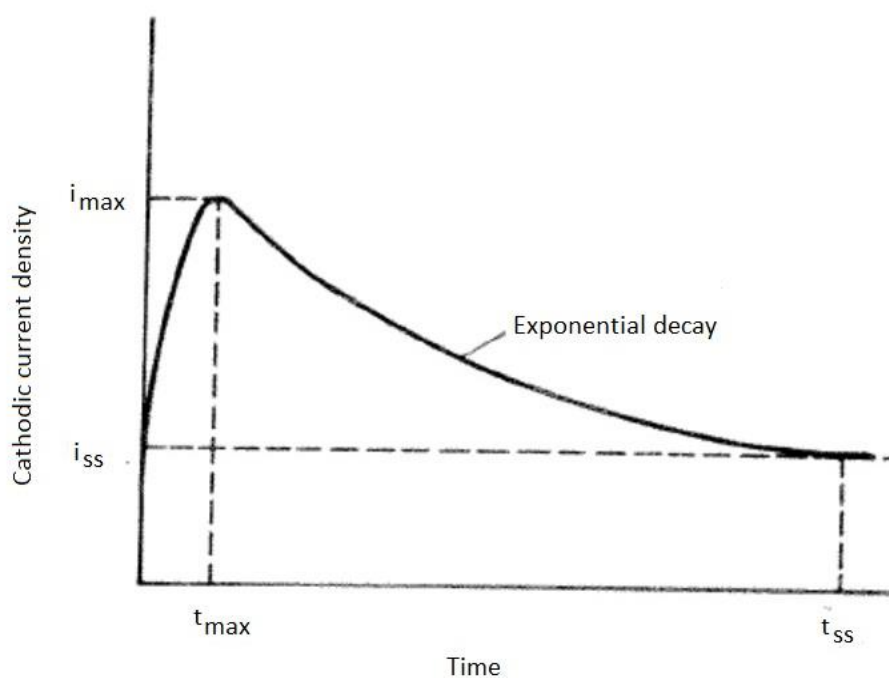

Figure 2.9. Current-time behavior of aluminium under cathodic polarization [21].

The alkaline etching process of aluminium was studied as a function of applied potential by Nisancioglu et al. Micrographs of the pits after polarization at different potentials can be seen in figure 2.10. As the potential increases in cathodic direction, the pits become larger, and new intermetallic particles are exposed in the Al matrix. The increased alkalinity gives rise to a surface morphology consisting of densely packed hemispherical pits [22].
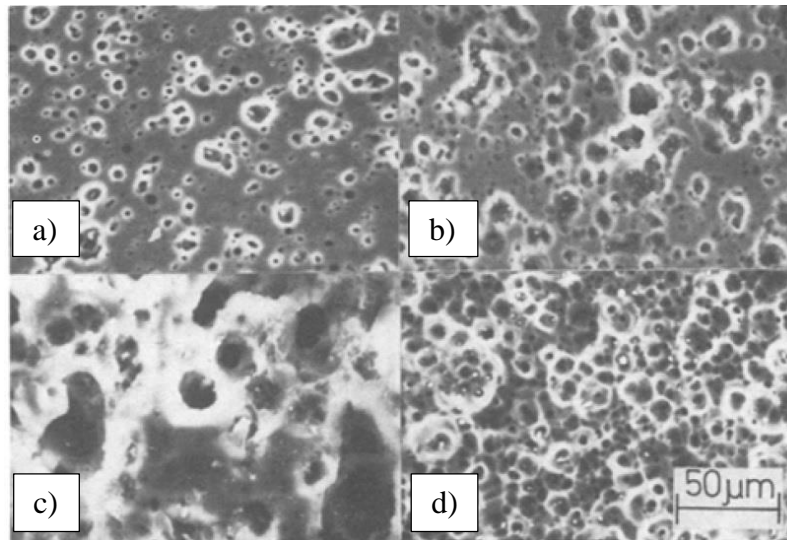
Figure 2.10. Pit morphology on Al specimens polarized for 24 hours in 0.52 M NaCl solutions. a) -1.3V, b) -1.35 V, c) -1.37V, e) -1,38V. All potentials are with respect to SCE. Adapted from Nisancioglu et al. [22].

2.3 Crevice corrosion

Crevice corrosion is a form of localized corrosion that occurs in crevices or narrow cavities between metals. It is often seen when two metals are joined together by methods such as rivet/sheet or screw/washer. The chemistry of the solution inside the cavity becomes different from that of the bulk solution. A potential difference between the inside and outside of the crevice occurs due to overpotential and ohmic potential drop, and the metal suffers from corrosion as a result of the increasingly aggressive crevice environment. The following mechanism is proposed [4]:

$$M^+ + H_2O \rightarrow MOH + H^+ \tag{2.24}$$

Metal dissolution (equation 2.2, 2.3) will occur inside the crevice, and H^+ ions will form from hydrolysis of the metal ions. The protons will be consumed in reduction of oxygen (equation 2.7) and the pH will remain unchanged. However, due to limited diffusion inside the narrow cavity, the concentration of dissolved oxygen decreases, thus creating a concentration overpotential between the inside and outside of the crevice. H^+ ions will accumulate inside the cavity, which causes migration of anions order to maintain electroneutrality. In environments containing chloride ions, this process will form hydrochloric acid in the cavity.

The potential difference associated with the crevice is further enhanced by ohmic potential drop due to formation of solid metal hydroxide and hydrogen gas bubbles, such that

$$E_{out} - E_{in} = I_{net}R + \eta_c \tag{2.25}$$

14

The potential distribution along the crevice will vary, depending on position due to the non-uniform conditions causing the change in potential. Thus, the current distribution along the crevice will become non-uniform. The resulting crevice corrosion attack will be associated with the electrochemical kinetics of the metal. An active-passive metal can suffer from extensive corrosion deep inside the crevice, as the potential drop in this area polarizes the metal into the active region. A passive metal however, is more resistant to crevice corrosion, and the corrosion is expected to mainly be seen at the mouth of the crevice in form of pitting corrosion [4].

Joma et al. studied crevice corrosion of aluminium and copper in a sheet/rivet coupling and in a thin layer cell with sodium sulfate as electrolyte. They reported that the changes in pH associated with a crevice causes dissolution of cuprous oxide and copper replating near the crevice. Results from a test between pure Al and pure Cu in the thin layer cell can be seen in figure 2.11. The surface areas of the metal samples were 7 cm^2, and the crevice distance was 150 μm [23].
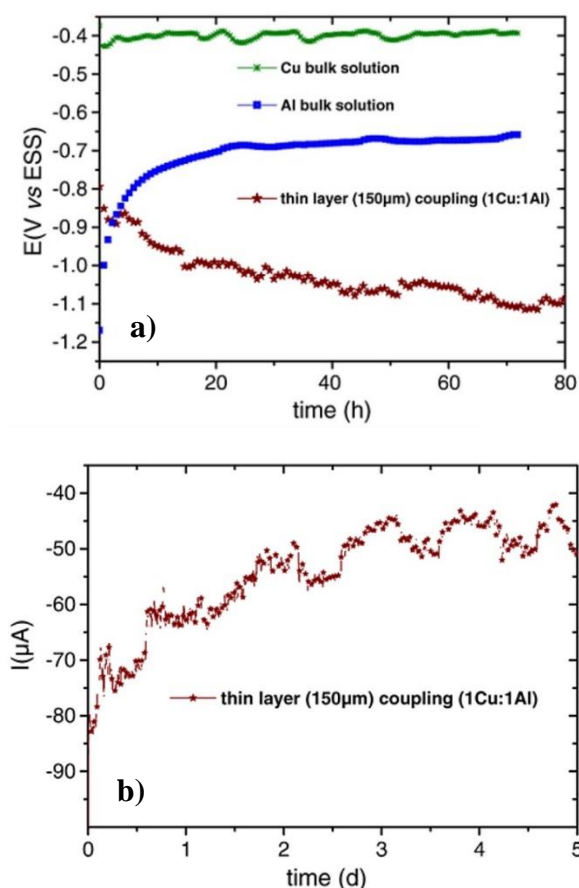

Figure 2.11. a) Comparison between the OCP for pure Al and Cu in a bulk solution, and the galvanic potential for Al-Cu coupled samples in a thin-layer electrolyte (0.1M Na$_2$SO$_4$). b) Evolution of the galvanic current as a function of time (surface area = 7 cm^2 for both samples) [23].

15

Joma et al. also used the thin-layer cell to record cathodic current on AISI 316L Stainless Steel coupled against an inert plan with a crevice of 150 μm. The current was recorded at a potential of -1.1 V(SSE) which is in the oxygen reduction domain. From figure 2.12, it can be seen that the current reaches a steady state value after 60 hours, as oxygen is depleted in the cavity [23].
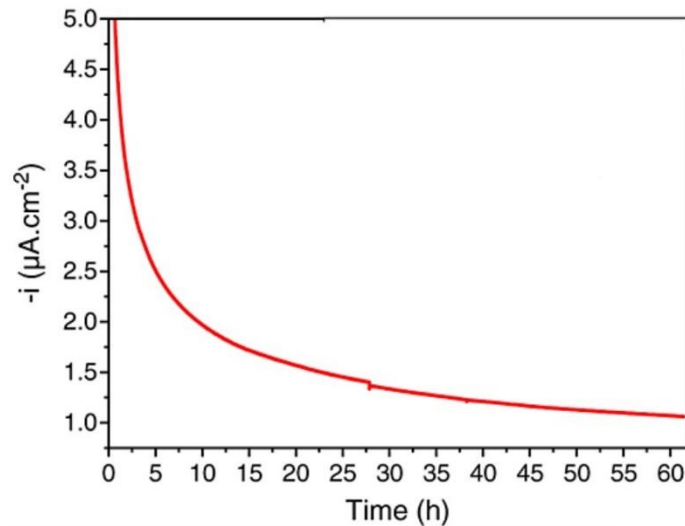

Figure 2.12. Cathodic current curve for oxygen reduction on AISI 316L SS in 0.01 M Na_2SO_4, coupled against an inert plan with a crevice of 150 μm. The potential is -1.1V(SSE) [23].

Application of cathodic protection against crevice corrosion was studied by Li et al. [24]. They recorded potential and current distributions in a cathodically protected crevice between a simulated disbonded coating and mild steed in dilute NaCl solution. Change in pH and conductivity of the solution was also reported, results can be seen in table 2.2 and figure 2.13.

Table 2.2. Experimental conditions and results of CP against crevice corrosion on steel [24].

No.	E_h (V/SCE)	C_{NaCl} (M)	δ (mm)	$\sigma_{initial}$ (μS/cm)	t_p (h)	σ_{final} (μS/cm)	pH_{final}	Corrosion on steel
1	−0.95	0.006	1.0	720	25	1850	8.7	Slight
2	−1.05	0.006	1.0	720	25	2000	9.2	Very slight
3	−1.15	0.006	1.0	720	25	1750	9.5	Very slight
4	−1.25	0.006	1.0	720	13	1350	9.7	Very slight
5	−1.05	0.06	1.0	6500	25	7400	9.8	No
6	−1.05	0.0006	1.0	115	25	560	8.6	Slight
7	−1.05	0.006	0.5	720	25	1650	9.8	Slight
8	−1.05	0.006	1.5	720	25	1850	10.6	Very slight

Table 2.2 shows the potential of the crevice mouth (E_h), electrolyte concentration, crevice thickness (δ), solution conductivity (σ), test duration and final pH of the crevice. The initial pH was 6.6. Thus, a significant increase in both solution conductivity and pH due to formation of hydroxyl ions and migration of sodium ions into the crevice was reported [24].

Figure 2.13 shows the potential and current distributions along the crevice in 0.0006 M NaCl solution. The crevice thickness and control potential was 0.1 mm and -1.15 V(SCE) respectively. A significant potential gradient was seen in the crevice, which decreased as a function of time. The current also was initially concentrated near the mouth of the crevice, decreasing inwards. The potential and current distributions became stable after 25 hours. The increasingly uniform distribution of potential and current was explained by depletion of oxygen inside the crevice and an increase in solution conductivity [24].

In figure 2.13 b), it can be seen that an anodic current was measured on the steel approximately 65 mm into the crevice, 1 hour after test initiation. Li et al. explain this by local cell corrosion formed due to the heterogeneity of the material and chemical environment. The anodic current disappeared, which implies that cathodic protection might prevent local corrosion within the crevice [24].
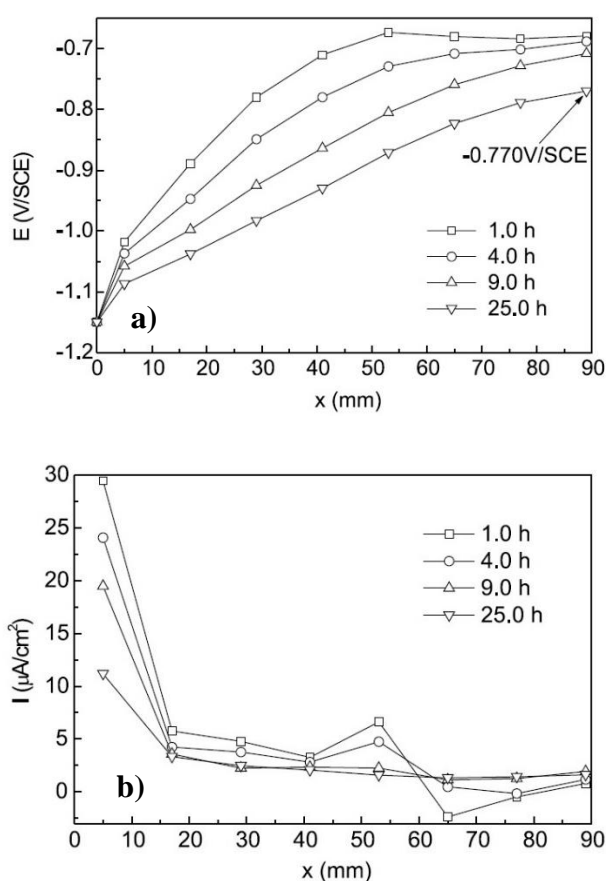

Figure 2.13. Results of CP against crevice corrosion on steel in 0.0006 M NaCl. a) Potential distribution. b) Current distribution. Potential at the crevice mouth is -1.15 V(SCE) and crevice thickness is 1.0 mm [24].

2.4 Sodium chloride solution and artificial seawater

To make experimental testing simulate real conditions, it is desirable to use real seawater as electrolyte. However, this requires a continuous supply of fresh natural seawater as the biological properties found in the ocean changes quickly if seawater is kept in storage. Furthermore, seawater is a complex system with many factors and is difficult to simulate in a laboratory. Commonly used substitutes are a 3.5% sodium chloride solution and synthetic seawater. The former is known to be more aggressive than natural seawater due to lack of calcium and magnesium ions, which form calcareous deposits on metal surfaces [25]. The synthetic seawater is preferred, which has the same protective properties as natural seawater in terms of Mg and Ca deposits, but lacks the biological factors.

Another important difference between NaCl solution and seawater is that seawater has a natural buffer capacity due to several equilibria. Thus, the pH of seawater is more stable than that of a NaCl solution. Local changes of pH is an important factor for corrosion, especially for aluminium. This supports the assumption of NaCl solution being a more aggressive solution that seawater [26].

Möller et al. conducted corrosion testing of low carbon steel in 3.5% NaCl solution and both synthetic and natural seawater. They found that the corrosion rate was approximately four times higher in NaCl solution than in natural seawater. Corrosion rates in synthetic and natural seawater were similar [25].

The corrosion products differed between the electrolytes; Fe_3O_4 (Magnetite) and γ-FeOOH (Lepidocrocite) was found on samples immersed in NaCl solution, while mainly γ-FeOOH was found on samples immersed in seawater [25].

2.5 Summary of theory

- Galvanic coupling between two dissimilar metals will cause the less noble metal to corrode. Cathodic protection applied on both metals simultaneously in a three-metal system is yet to be attempted.
- The mechanism of corrosion protection of steel and aluminium by CP differs greatly, and is related to the metallurgical and electrochemical properties of the metals.

- Reduction current during cathodic protection of steel depends to a large degree on the properties of the calcareous deposits that form on the steel surface. The composition of the deposits depend on many factors including applied potential and convection.

- Cathodic polarization of aluminium causes alkaline etching of the intermetallic inclusions present in the Al matrix due to increased pH at the surface related to reduction of oxygen and hydrogen evolution. The etching process causes an exponential decay in the reduction current as the cathodic sites are removed.

- Crevice corrosion will cause high local corrosion rates between joined metals due to formation of an aggressive acidic environment inside the narrow cavity between them. Concentration and ohmic overpotential result in a potential and current distribution along the crevice.

- Cathodic protection applied to a crevice will cause an alkaline environment inside the cavity.

Chapter 3

Experimental

This section contains the experimental setups, procedures, material and electrolyte specifications, and equipment details. Preparing and cleaning of test samples was inspired by the project work of Bergin [27], as well as ASTM standards [28, 29]. Experimental procedures and techniques were developed in the work performed in the author's specialization project [30].

3.1 Material specification

The experimental testing in this project has involved three different materials: X65 carbon steel, 6005 aluminium alloy and an AlZnIn sacrificial anode alloy. The sample material was available at NTNU from previous projects and studies. The steel samples were cut from a part of an oil pipe, the 6005 Al was provided by the supervisor as a larger extruded plate (T4 condition), and the AlZnIn were cylindrical-shaped sacrificial anodes. The chemical composition of the metals can be found in the tables below.

Table 3.1. Chemical composition of X65 Carbon steel [27].

Element [wt%]								
C	Si	Mn	P	S	V	Nb	Ti	Fe
0.16	0.45	1.65	0.02	0.01	0.09	0.05	0.06	Balance

Table 3.2. Chemical composition of 6005 Aluminium [31].

Element [wt%]						
Mg	Si	Fe	Mn	Cr	Cu	Al
0.51	0.59	0.41	0.14	0.02	0.18	Balance

Table 3.3. Chemical composition of AlZnIn sacrificial anode [32].

Element [wt%]							
Zn	In	Cd	Si	Fe	Cu	Pb	Al
2.650	0.026	0.00021	0.049	0.076	0.00044	0.00007	Balance

3.2 Sample preparation

The test specimens were pretreated in various ways, depending on the material and which experiment the specimen was subjected to. All mechanical preparation was done at the mechanical workshop at Faculty of Natural Science and Technology at NTNU.

3.2.1 Open circuit and galvanic corrosion

For experiments involving self-corrosion and galvanic corrosion, the X65 CS and 6005 Al samples were cut into small plate specimens with the dimensions 80×20×2 mm. The AlZnIn specimens were cut with dimensions of 40×20×2 mm. The steel samples were milled on both sides, and the edges were grinded in order to remove corrosion products present from the base material. Samples of 6005 Al and AlZnIn were mechanically grinded and polished.

Prior to testing the samples were cleaned, weighed and coated. To clean the samples thoroughly, they were first cleaned in distilled water, followed by acetone. Finally, the samples were rinsed with ethanol (96%) to prevent the acetone from evaporating and leaving impurities on the metal surface. The specimens were then dried with an electrical heat gun and weighed on an analytical weight with an error of ± 0.1 mg.

In order to control the exposed area of the specimens, a coating was applied on the metal surface as shown in figure 3.1. This was also done to prevent metal exposure in the solution-air interface. Samples of 6005 Al and AlZnIn were coated with bee wax by covering the desired exposed area with a masking tape before immersing the samples in molten wax. The coating covering the masking tape was then cut off, leaving an exposed metal area of 2×1.9 cm (width of sample × width of masking tape).
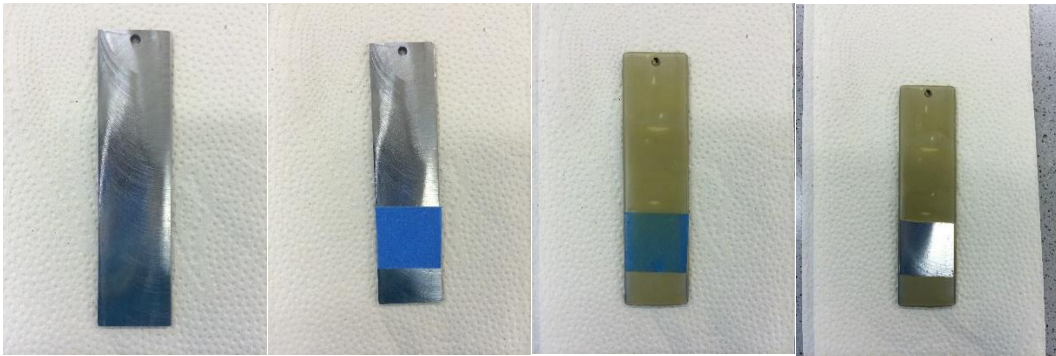
Figure 3.1. Principle of coating application. The exposed area of the metal sample is covered with masking tape before coating is applied. Desired area of the coating is cut off prior to testing.

Steel samples were coated with Miccro Super XP 2000 Stop-Off Lacquer, shown in figure 3.2. The reason for using different coatings is that bee wax has poor adhesion when applied to steel, and the Miccro lacquer does not adhere well on aluminium, resulting in crevice corrosion. Similar to bee wax, the Miccro lacquer was also applied by immersing the samples into the liquid coating, but the masking tape was removed immediately after immersion, before the lacquer was allowed to cure.

Figure 3.2. Steel sample coated with Miccro Super XP 2000 Stop-Off Lacquer.

In order to reduce ohmic resistance between metals during testing, a connection method was introduced to exclude the use of extra clamps and long wires, which contribute to resistance in the electric circuit. Screw holes were made at the top of the samples, making a connection point. One end of a two-end banana plug wire was cut off and the insulation was removed, exposing about 3 cm of the conducting copper wire. The wire was forced against the metal sample by using a screw and a washer (3 mm) as shown in figure 3.3.

Figure 3.3. Connection of wire to metal sample. The insulation on one end of a banana plug wire is stripped off and forced in contact with the sample with a screw and a washer.

3.2.2 Galvanic crevice corrosion

For experiments involving crevice corrosion, a different sample geometry was needed due to the experimental setup. The X65 CS and 6005 Al samples were cut into plate specimens with dimensions of $20\times20\times2$ mm, and grinded to 800 grit size. The samples of AlZnIn had the same geometry and surface treatment as for galvanic corrosion and open circuit testing. The specimens were also cleaned and weighed as described earlier.

The device for conducting galvanic crevice corrosion testing can be seen in figure 3.4. The two specimens are fitted into sample holders made of polyoxymethylene (POM), which are kept together by four screws. The metal samples are kept apart by two Teflon strips ($3\times20\times0.1$ mm) placed between them, creating a crevice of 100 μm. By placing the Teflon strips onto the metal surface, the exposed area becomes 1.4×2 cm.

In order to measure current and potential, a wire was attached to the samples. A screw hole was drilled 1.8 mm into the specimens, allowing the wire to be connected to the metal with a cable shoe and a screw. To control the exposed area and current density, a coating was applied on the samples except the surface making the crevice. As the whole device was immersed into the electrolyte during testing, it was necessary to coat all contacts as well. The Miccro lacquer was used for steel, and nail polish from H&M was used for aluminium. The nail polish was chosen for its easy appliance and removal. The wire-metal contacts were coated with Miccro lacquer.
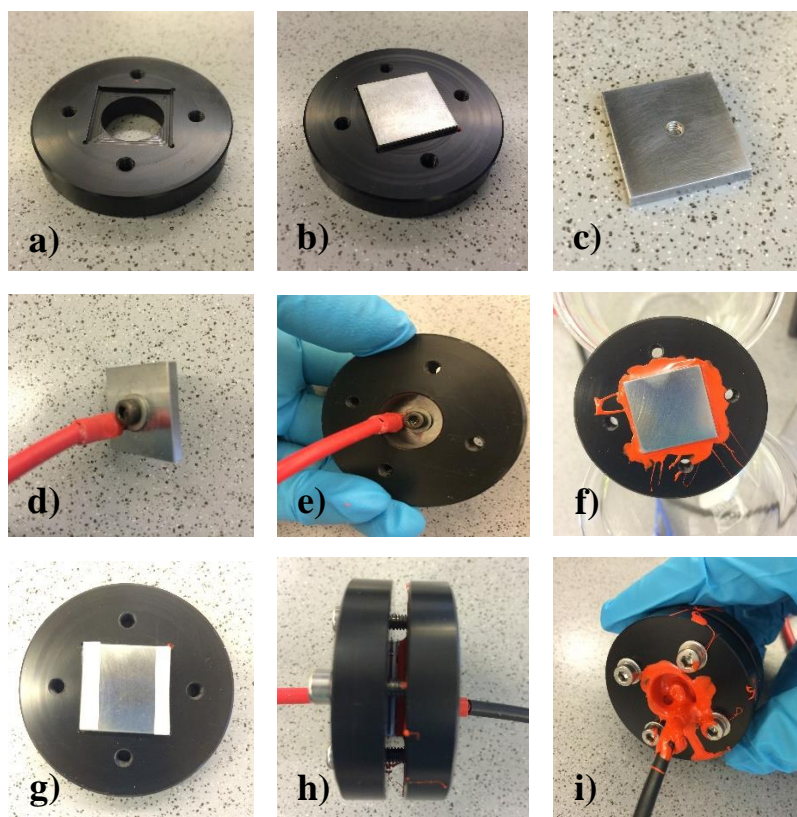
Figure 3.4. Crevice device coupling. a) Plastic sample holder. b) Sample placement. c) Backside of sample with connection point. d) Sample connected to wire. e) Backside of sample holder with connection. f) Steel sample with coating covering all areas except the exposed crevice-area. g) Teflon strips placed onto the Al sample. h) Complete coupling. i) All electrical connections coated before testing.

3.3 Equipment and setup

The electrochemical cells used in the tests were made of a glass beaker filled with electrolyte. The specimens were immersed in the solution, and the cell was kept in a water bath holding a constant temperature of 25 ℃. Initially, a saturated Silver/Silver Chloride electrode was used as a reference electrode which has a potential of 0.198V vs the standard hydrogen electrode (SHE) [9]. About half way through the project, the Ag/AgCl electrode was replaced by a Saturated Calomel Electrode (SCE) for increased stability. A salt bridge containing agar and saturated KCl solution was used make ionic contact between the reference electrode and the cell. Gamry potentiostats were used for electrochemical measurements. The experimental setup can be seen in figure 3.5.
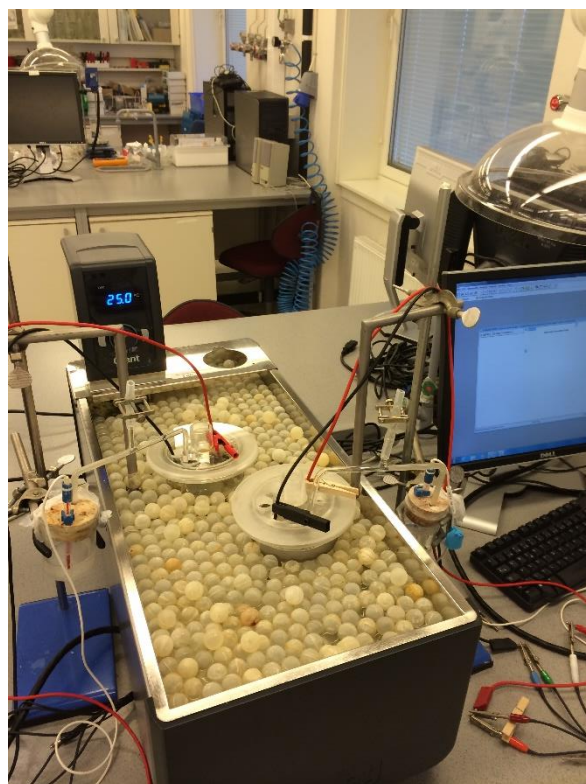
Figure 3.5. Experimental setup. The cells are placed in a water bath keeping a constant temperature of 25 ºC. A salt bridge maintains ionic contact between the test cell and the reference electrode. Metal samples are connected to a potentiostat (computer).

A schematic drawing of the circuit used for open circuit testing can be seen in figure 3.6. The potential of the sample was measured with a voltmeter.
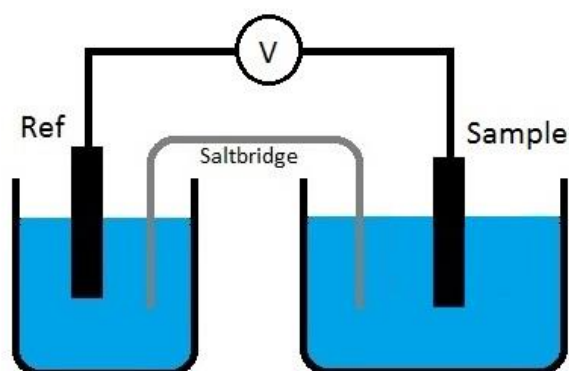

Figure 3.6. Schematic illustration of the setup used in open circuit testing. The potential of the metal sample is measured against a reference electrode with a voltmeter.

The circuits used for galvanic corrosion testing can be seen in figure 3.7. For two-metal testing, the noblest alloy was connected as working electrode, and the other alloy as counter electrode. By running galvanic corrosion testing in Gamry, the potentiostat keeps the potential between the two samples at zero, acting as a zero resistance ammeter. The coupling potential and the net

galvanic current is measured. For three-metal testing, two potentiostats were required for measuring current on two electrodes. The setups also applies to galvanic crevice corrosion testing, the only difference being that X65 CS and 6005 Al are coupled in the crevice device while the anode is placed adjacent to the coupling in the solution.
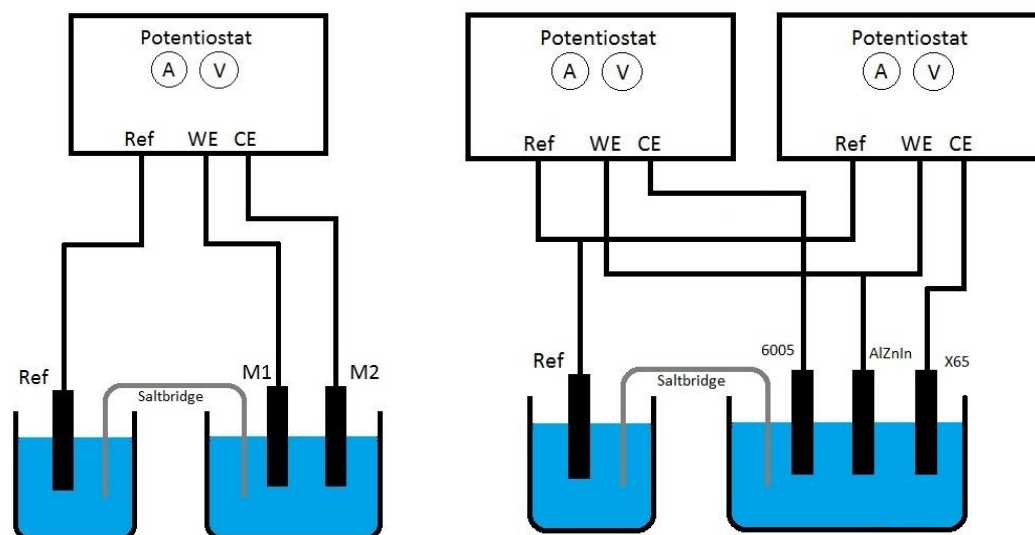

Figure 3.7. Schematic illustration of the experimental setup used in galvanic corrosion and galvanic crevice corrosion testing. The two-metal circuit is shown to the left, and three-metal coupling to the right. For galvanic crevice corrosion, the X65 carbon steel and 6005 Al are kept in close contact by a crevice device.

3.4 Electrolytes

Artificial seawater and a 3.5 wt% sodium chloride solution were used as electrolytes. The NaCl solution was made by dissolving 3.5 parts by weight of sodium chloride in 96.5 parts of distilled water. The artificial seawater was prepared according to ASTM's standard [28] with minor deviation; bromides were excluded for HSE reasons. The standard also suggests that several stock solutions should be made separately and mixed together just before using the solution. Based on the project work of Bergin [27], this was regarded unnecessary and all ingredients were mixed and stored together. The pH of the solution was adjusted to 8.2 just before experiments were carried out. The composition of the artificial seawater can be found in table 3.4.

Table 3.4. Composition of artificial seawater [28].

Compound	Concentration [g/L]
$MgCl_2 \cdot 6H_2O$	11.112
$CaCl_2$	1.158
$SrCl_2 \cdot 6H_2O$	0.042
KCl	0.695
$NaHCO_3$	0.201
H_3BO_3	0.027
NaF	0.003
$NaCl$	24.534
Na_2SO_4	4.094

3.5 Procedures

All electrochemical testing was done by immersing the metal samples in a cell filled with approximately 900 mL of electrolyte. The salt bridge was installed close to the working electrode, and the respective circuitry was connected. When the test was completed, the specimens were taken out, rinsed with distilled water and ethanol before they were dried.

3.5.1 Open circuit

The open circuit testing of the different alloys was performed with a voltmeter, using the setup shown in figure 3.6. The duration of the OCP tests was 24 hours. The potential was measured and logged frequently during the first two hours of the test, and during the final hours.

3.5.2 Galvanic corrosion

Galvanic corrosion testing was performed using the setup shown in figure 3.7, with a primary duration of 24 hours. One special-purpose test was run for 96 hours. Gamry potentiostats were used to run galvanic corrosion tests, and galvanic current and coupling potential was measured and logged every 5 minutes.

3.5.3 Galvanic crevice corrosion

Galvanic crevice corrosion tests were run with the same circuitry as for galvanic corrosion tests, using the crevice device shown in figure 3.4. Test duration was 72 hours. The crevice device was placed vertically in the test cell with the opening of the crevice pointing upwards, allowing gas to escape. A pipette was used to force electrolyte into the crevice just prior to testing. Once

the test was completed, the crevice device was carefully taken out of the cell and opened. A pH strip was placed onto the surfaces of the samples in attempt to measure the pH inside the crevice. As electrical contacts were immersed into the electrolyte during testing, the protective coating on the contacts was removed after testing, and all connections were controlled for corrosion and/or exposure to the solution.

3.5.4 Potential sweep

A single steel sample covered with calcareous deposits was polarized in a potentiodynamic sweep test to determine the Tafel slope of hydrogen evolution. A platinum electrode was used as counter electrode, and the sweep rate was 0.1 mV/s.

3.6 Weight loss measurements

After electrochemical testing, the samples were thoroughly cleaned and weighed in order to determine corrosion rate. Before chemical cleaning of the samples, the coating was removed. For samples coated with bee wax, the coating was first scraped off carefully using a plastic ruler. For complete removal, the samples were boiled in distilled water for approximately 30 seconds. The Miccro lacquer was manually peeled off the metal surface, and nail polish was easily removed by rinsing with acetone.

Chemical cleaning for removal of corrosion products was performed in accordance with ASTM G1 [29]. The cleaning procedure for steel and aluminium can be seen in table 3.5.

Table 3.5. Solutions and duration of chemical cleaning of various alloys [29].

Alloy	Cleaning solution	Time	Temperature
X65 CS	500 mL HCl (SG 1.16) 3.5 g Hexamethylenetetramin Reagent water to make 1000 mL	6×30 sec	25 ºC
6005 Al AlZnIn	50 mL phosphoric acid (SG 1.69) 20 g chromium(IV) oxide Reagent water to make 1000 mL	10 min	90 ºC to boiling

The chromic phosphoric acid does not attack aluminium, only the corrosion products [33]. The steel however, suffers some metal loss while immersed in the hydrochloric acid solution. To determine weight loss caused by corrosion of carbon steel, the samples were chemically cleaned in several cycles of 30 seconds immersion. Between each cycle, the samples were cleaned with

solvent, and weight loss was determined and corrected for metal loss by use of an untested reference sample. Number of cleaning cycles was plotted against accumulated weight loss to determine weight loss caused by corrosion. Such a plot can be found in appendix A.

3.7 Surface characterization

The surface of the samples was characterized both before and after chemical cleaning. On a macroscopic level, the samples were inspected visually and photographs were taken. For microscopic characterization, micrographs were taken in LV-SEM (Low Vacuum Scanning Electron Microscopy). EDS (Energy Dispersive Spectroscopy) was used to acquire the chemical composition of the metal surface, primarily corrosion products, deposits and intermetallic inclusions in aluminium.

The SEM used for EDS and micrographs was a LV-SEM Hitachi S-3400N. Photographs were taken with an iPhone 5s.

3.7.1 Characterization of calcareous deposits

Steel samples covered with calcareous deposits were generally analyzed with EDS and chemically cleaned afterwards. In order to study the chemical composition of the calcareous deposits close to the metal surface, the deposits on a sample was scraped off mechanically, exposing the metal surface. This allowed EDS analysis of the part of the deposits which formed close to the test initiation.

3.8 Overview

The following tests were performed:

- Open circuit corrosion of all three alloys in NaCl solution and in artificial seawater.
- Galvanic corrosion test of
  - X65 carbon steel and 6005 aluminium in NaCl solution and in artificial seawater.
  - X65 carbon steel and AlZnIn in NaCl solution and in artificial seawater.
  - 6005 aluminium and AlZnIn in NaCl solution and in artificial seawater.
  - All three alloys in NaCl solution and in artificial seawater.
  - All three alloys in artificial seawater (special-purpose, 96 hours).
- Galvanic crevice corrosion test of
  - X65 carbon steel and 6005 aluminium in NaCl solution and in artificial seawater.
  - All three alloys in NaCl solution and in artificial seawater (X65 carbon steel and 6005 aluminium in crevice under cathodic protection).

- Potentiodynamic sweep test of an X65 carbon steel sample with calcareous deposits in artificial seawater.

In addition, a considerable amount of parallels of the galvanic corrosion tests (no crevice) was performed in the author's specialization project [30], and can be found in appendix C. Polarization curves for all three alloys were also recorded, and will be presented in the next chapter.

Chapter 4

Results

This chapter will present the results from the experiments described in the previous chapter. All potentials will be given versus the saturated Ag/AgCl electrode, which has a potential of +0.198 versus the standard hydrogen electrode [9]. The results will be presented in the following order: Open circuit, galvanic corrosion, galvanic crevice corrosion, potentiodynamic sweep, weight loss, macroscopic surface characterization and finally microscopic surface characterization. Furthermore, 3.5% NaCl solution and artificial seawater will be referred to as NaCl and seawater respectively.

4.1 Open circuit

The results from open circuit testing can be seen in figure 4.1-4.3. The potential was measured frequently during the first hours of the experiment, and during the final hours.
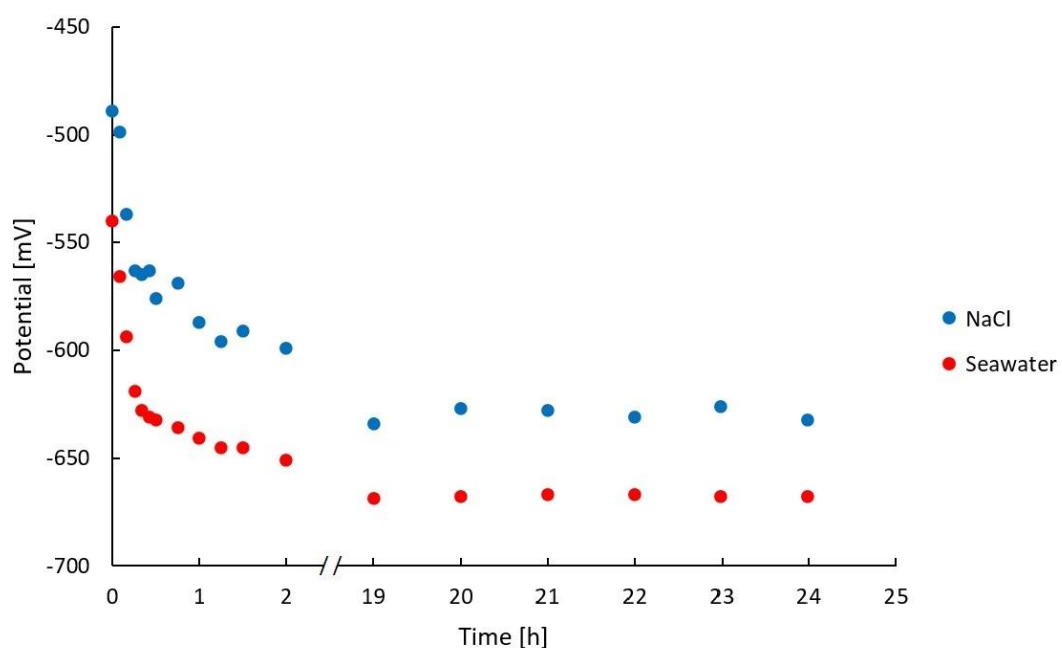
Figure 4.1. Open circuit corrosion test of X65 carbon steel in NaCl and seawater.
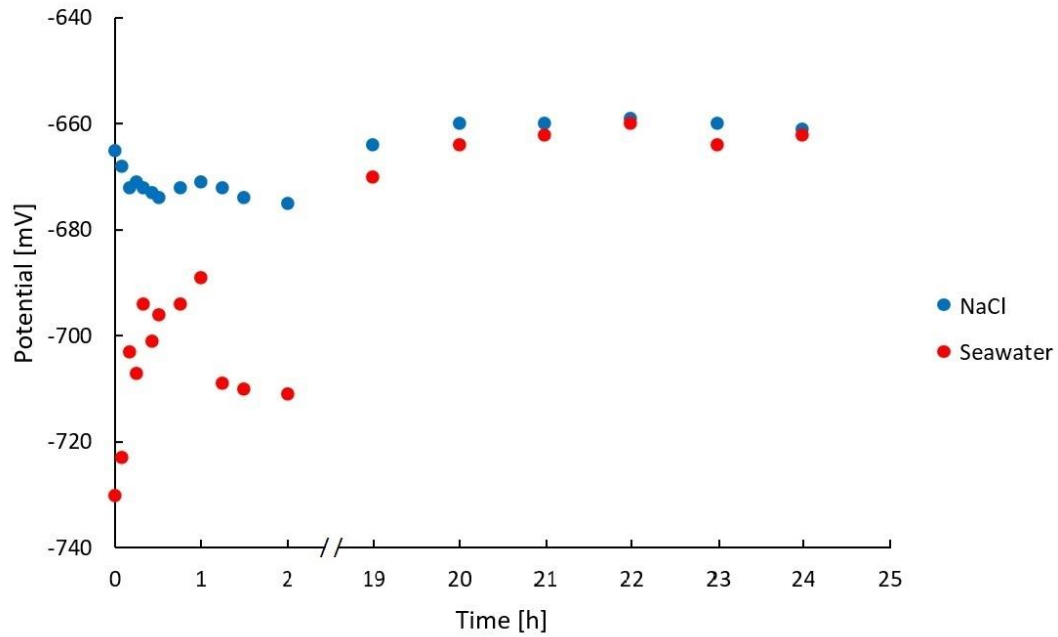
Figure 4.2. Open circuit corrosion test of 6005 aluminium in NaCl and seawater.
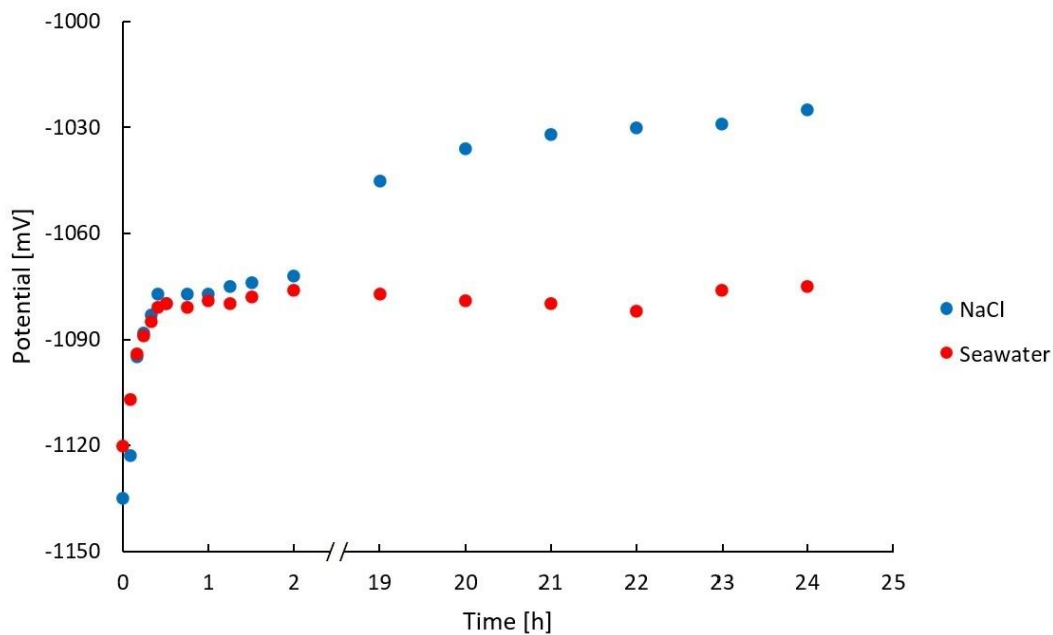
Figure 4.3. Open circuit corrosion test of AlZnIn in NaCl and seawater.

From the measured potential, it appears that the alloys are more active in seawater. The steel became more active as a function of time, while the opposite can be seen for the aluminium and the anode. The potential of steel and aluminium became almost the same, with a difference of 10-20 mV.

34

4.2 Galvanic corrosion

4.2.1 Two-metal coupling

The results from galvanic corrosion testing of X65 carbon steel and 6005 aluminium in NaCl and seawater can be seen in figure 4.4 and 4.5. The steel sample was defined as working electrode.
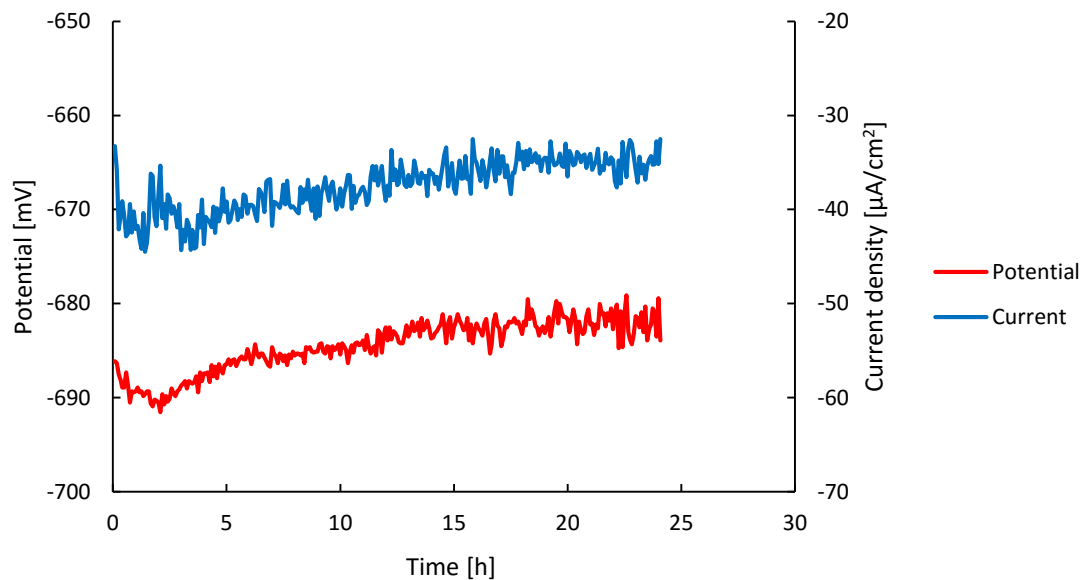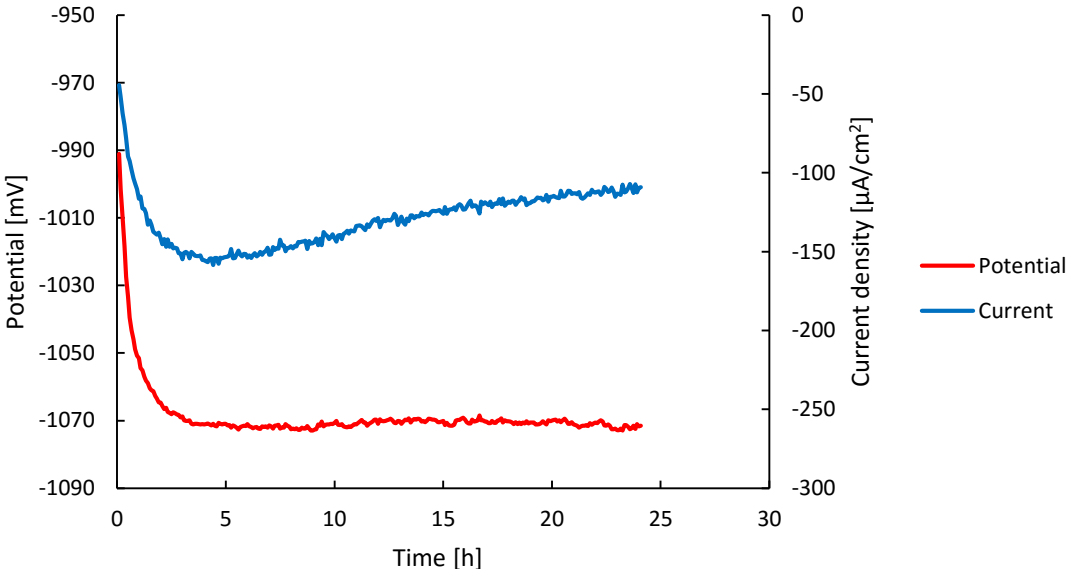

Figure 4.4. Galvanic corrosion test between X65 carbon steel and 6005 aluminium in NaCl. Recorded coupling potential and galvanic current as a function of time.
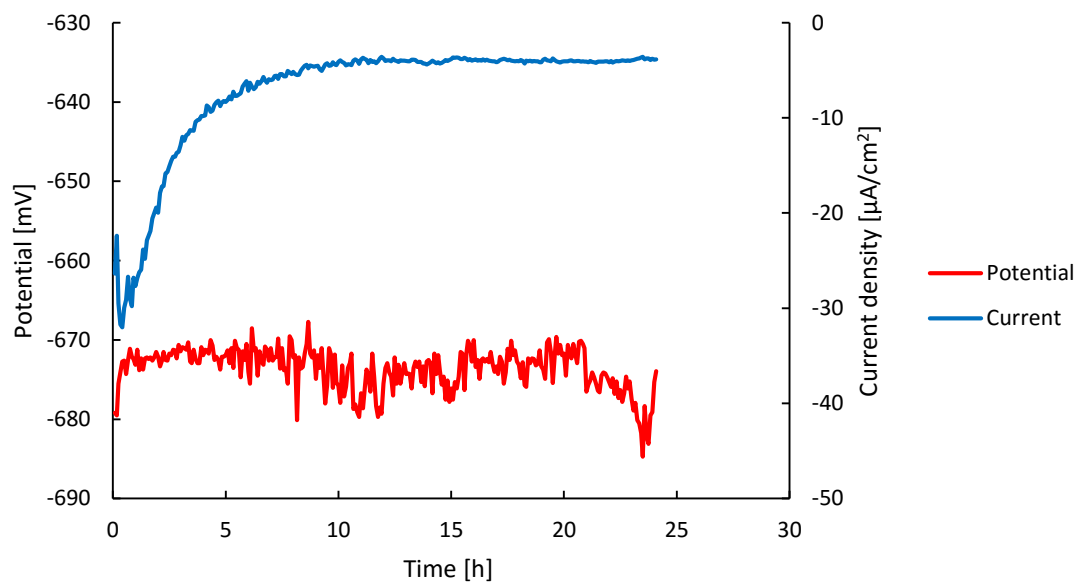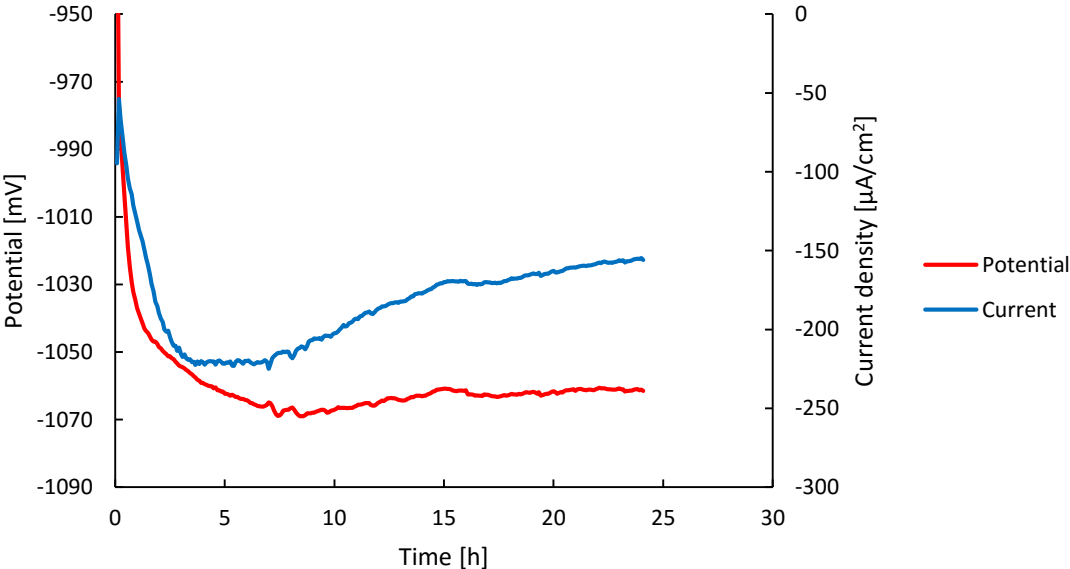

Figure 4.5. Galvanic corrosion test between X65 carbon steel and 6005 aluminium in seawater. Recorded coupling potential and galvanic current as a function of time.

Results

The current showed a relatively stable behavior in NaCl, varying approximately 10 µA/cm^2 during testing. In seawater, an exponential decay in current density occurred, stabilizing close to zero net current. Similar potential behavior was seen for the two test solutions.

The results from galvanic corrosion testing between X65 carbon steel and AlZnIn in NaCl and seawater can be seen in figure 4.6 and 4.7. The steel sample was defined as working electrode.
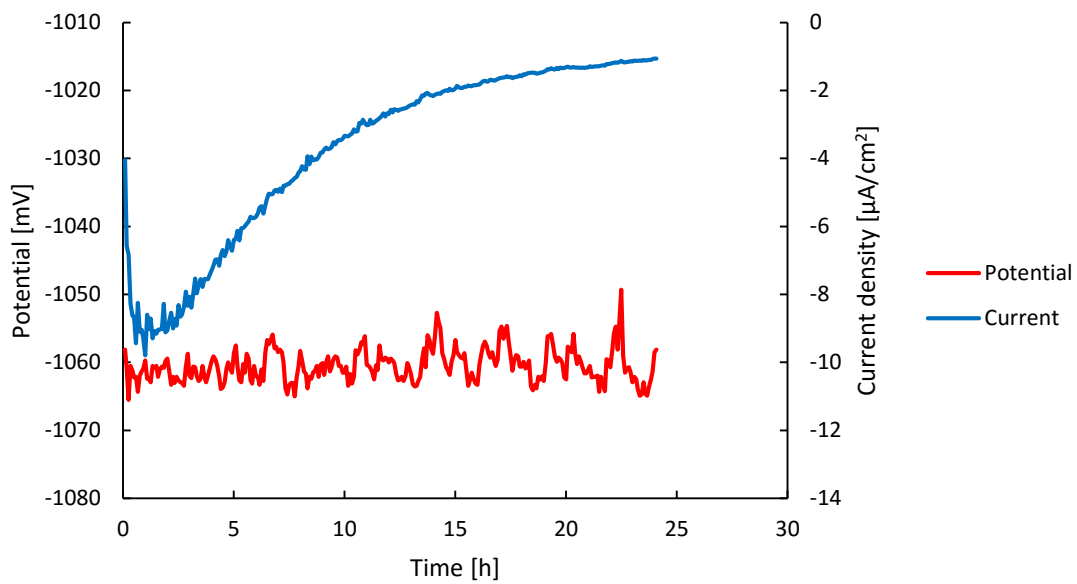

Figure 4.6. Galvanic corrosion test between X65 carbon steel and AlZnIn in NaCl. Recorded coupling potential and galvanic current as a function of time.
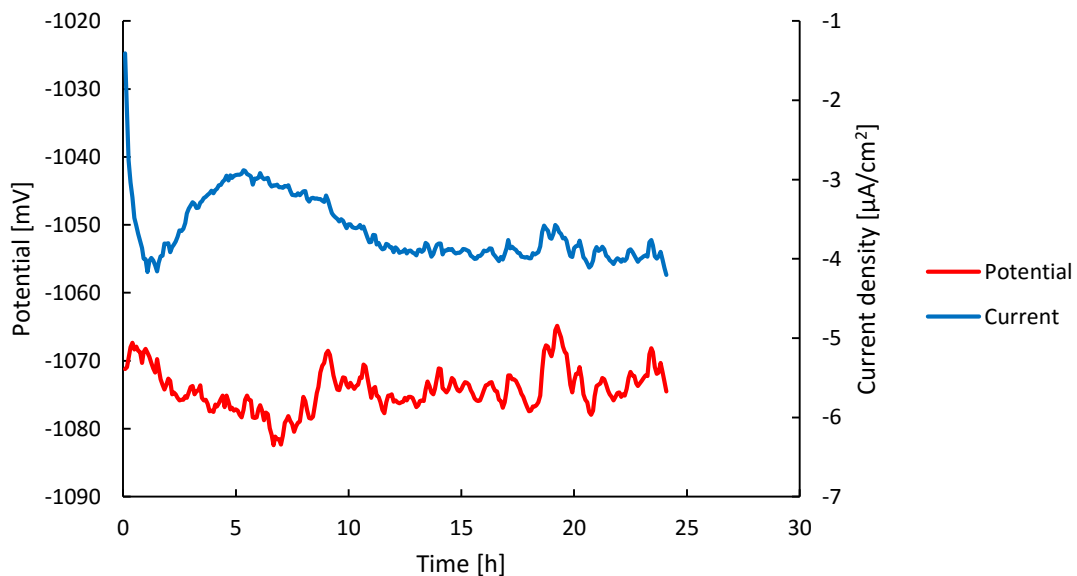

Figure 4.7. Galvanic corrosion test between X65 carbon steel and AlZnIn in seawater. Recorded coupling potential and galvanic current as a function of time.

36

The current showed similar behavior in the two test solutions, starting with a steep increase in the beginning followed by a slow decay as time progressed. By comparing the current curves in figure 4.6 and 4.7, it can be seen that the current density is significantly larger in seawater than in NaCl. The coupling potential is close to that of the anode, and almost identical between the solutions.

The results from galvanic corrosion testing between 6005 aluminium and AlZnIn can be seen in figure 4.8 and 4.9. The 6005 Al was defined as working electrode.

Figure 4.8. Galvanic corrosion test between 6005 aluminium and AlZnIn in NaCl. Recorded coupling potential and galvanic current as a function of time.

Figure 4.9. Galvanic corrosion test between 6005 aluminium and AlZnIn in seawater. Recorded coupling potential and galvanic current as a function of time.

Results

From figure 4.8 and 4.9 it can be seen that 6005 Al showed different behavior between the two test solutions. The current curve in NaCl has a steep minimum about 1 hour into the test, followed by an exponential decay towards zero. In seawater, the current curve reaches a minimum and more or less stabilizes. However, although the current progressed differently between the solutions, the measured current densities are relatively small, with no values larger than -10 μA/cm^2. The potential was somewhat more active in seawater with a difference of approximately 10 mV, thus not significant.

4.2.2 Three-metal coupling

The results from galvanic corrosion testing between X65 carbon steel, 6005 aluminium and AlZnIn in NaCl and seawater can be seen in figure 4.10 through 4.12. Recall the circuitry presented in figure 3.7; the electrochemical data for steel and aluminium were recorded simultaneously with two potentiostats. All values of current were measured as cathodic. However, the absolute value of the current density is plotted on a logarithmic scale due to large difference in the current values measured on steel and aluminium.
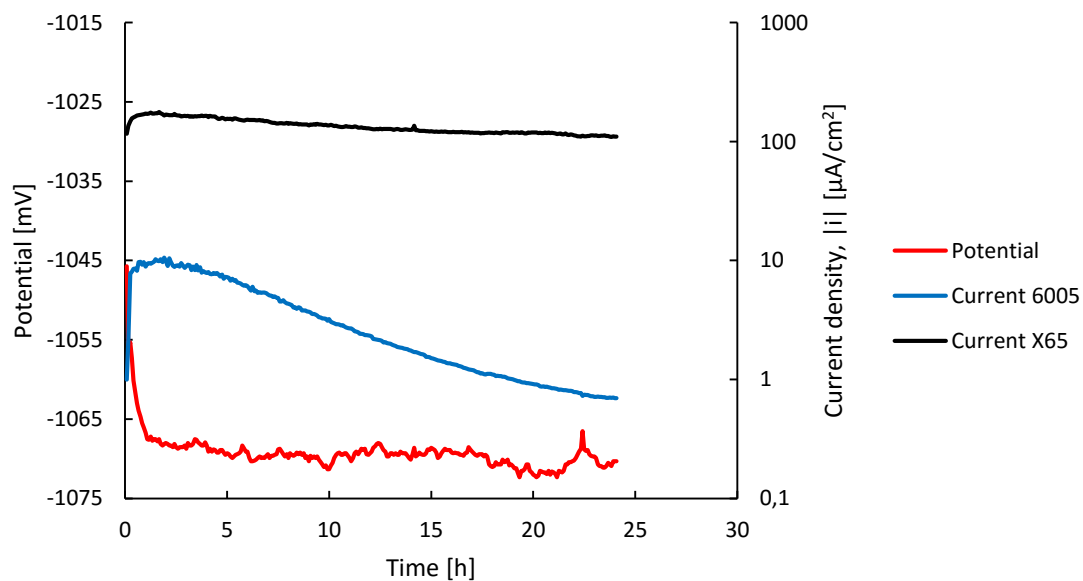

Figure 4.10. Galvanic corrosion test between X65 carbon steel, 6005 aluminium and AlZnIn in NaCl. Recorded coupling potential and galvanic current as a function of time.
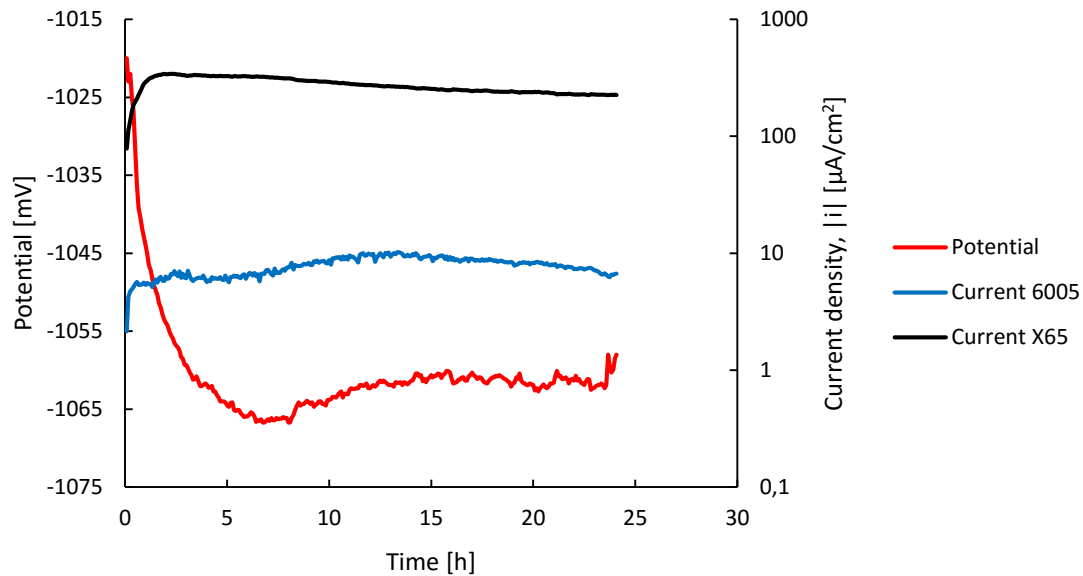
38

Figure 4.11. Galvanic corrosion test between X65 carbon steel, 6005 aluminium and AlZnIn in seawater. Recorded coupling potential and galvanic current as a function of time.
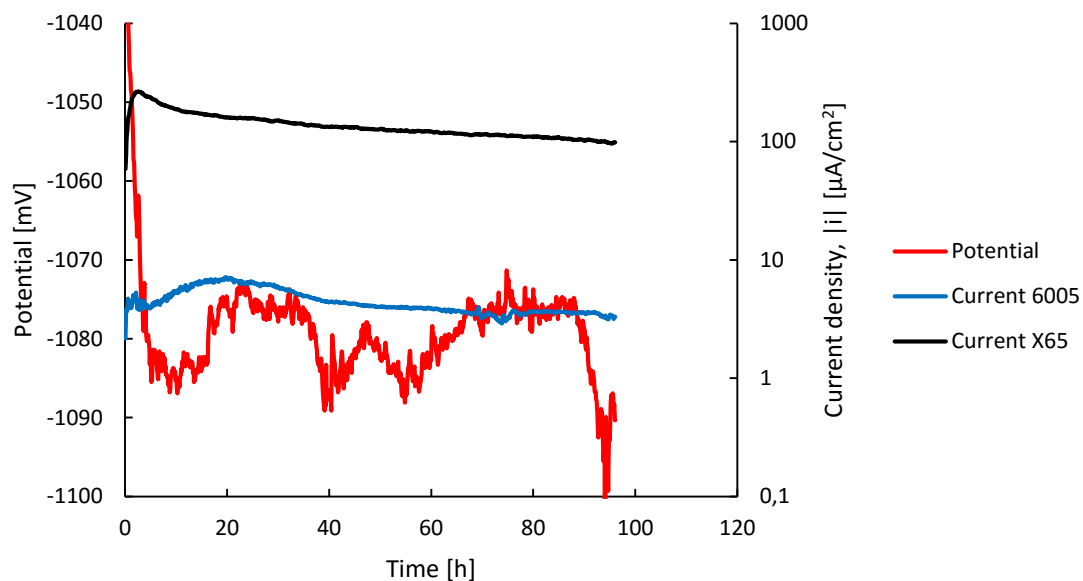

Figure 4.12. Long-term (96h) galvanic corrosion test between X65 carbon steel, 6005 aluminium and AlZnIn in seawater. Recorded coupling potential and galvanic current as a function of time.

From figure 4.10 through 4.12 one can see that the current density on steel is between one and two orders of magnitude larger than that on aluminium. The electrochemical behavior of each metal resembles the corresponding results found for two-metal testing against AlZnIn. The current density on steel decays slowly after reaching an initial peak in both test solutions. For aluminium, a decay towards zero can be seen in NaCl, but not in seawater. Futhermore, by comparing the results from testing in NaCl and seawater, it can be seen that the reduction rate

on steel is significantly greater in latter. The 96-hour test was primarily performed to see whether or not the current density on aluminium would decay as a function of time similar to what was seen in NaCl. From figure 4.12 a very slight decay in current density on aluminium can be seen after approximately 24 hours, where the measured current is halved over the following 72 hours. Moreover, the potential was more unstable and somewhat more active than in the 24-hour tests.

4.3 Galvanic crevice corrosion

The following data will be from the galvanic crevice corrosion tests. Recall that the duration was 72 hours in contrast to the galvanic corrosion tests. Electrolyte was forced into the cavity prior to testing, and the pH was measured on the metal surfaces once the tests were completed.

4.3.1 Two-metal coupling

The recorded current and potential in galvanic crevice corrosion testing of X65 carbon steel and 6005 aluminium can be seen in figure 4.13 and 4.14. The steel sample was defined as working electrode.
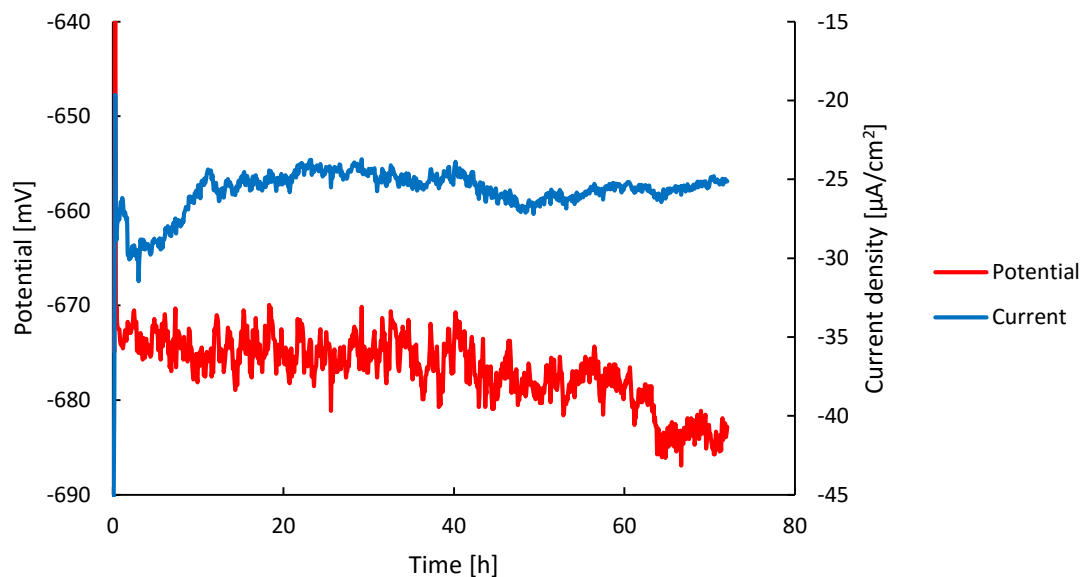

Figure 4.13. Galvanic crevice corrosion test between X65 carbon steel and 6005 aluminium in NaCl. Recorded coupling potential and galvanic current as a function of time. The samples were coupled in a simulated crevice of 100 μm.
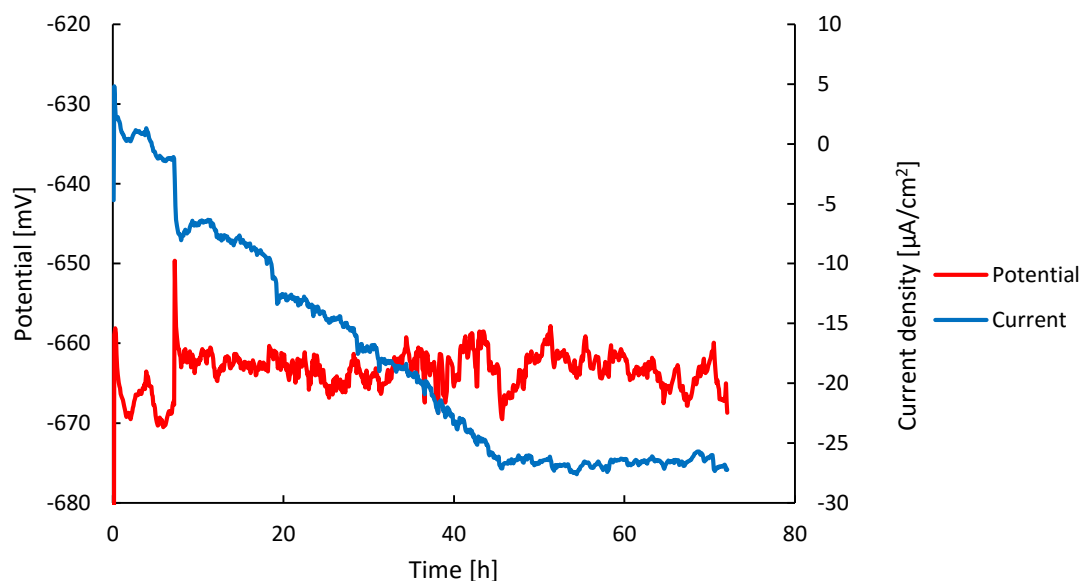
Figure 4.14. Galvanic crevice corrosion test between X65 carbon steel and 6005 aluminium in seawater. Recorded coupling potential and galvanic current as a function of time. The samples were coupled in a simulated crevice of 100 μm.

The measurements were relatively stable in NaCl where little change in current and potential was seen during testing. The current density was somewhat smaller than for the corresponding test without the factor of crevice corrosion. The measurements differed greatly in seawater as can be seen in figure 4.14. The current steadily increased in cathodic direction up until 45 hours into the test, where it stabilized at the same value as in NaCl. An important observation is that the galvanic current between the samples was positive, i.e. the current measured on steel was anodic during the first 10 hours of the experiment. The potential was relatively stable, with a jump of 20 mV as the current shifts from anodic to cathodic.

The crevice device was carefully lifted up from the test cell and dismantled post testing. By placing a pH strip onto the metal surfaces, an indication of the crevice inside the crevice was acquired. For NaCl and seawater, the pH was measured to 3 and 4 respectively.

4.3.2 Three-metal coupling

The results from galvanic crevice corrosion testing between X65 carbon steel, 6005 aluminium and AlZnIn can be seen in figure 4.15 and 4.16. Recall that the circuitry is the same as for the corresponding galvanic corrosion test (figure 3.7). The steel and aluminium was coupled in the crevice device, whereas the anode was placed adjacent to coupling in the solution.
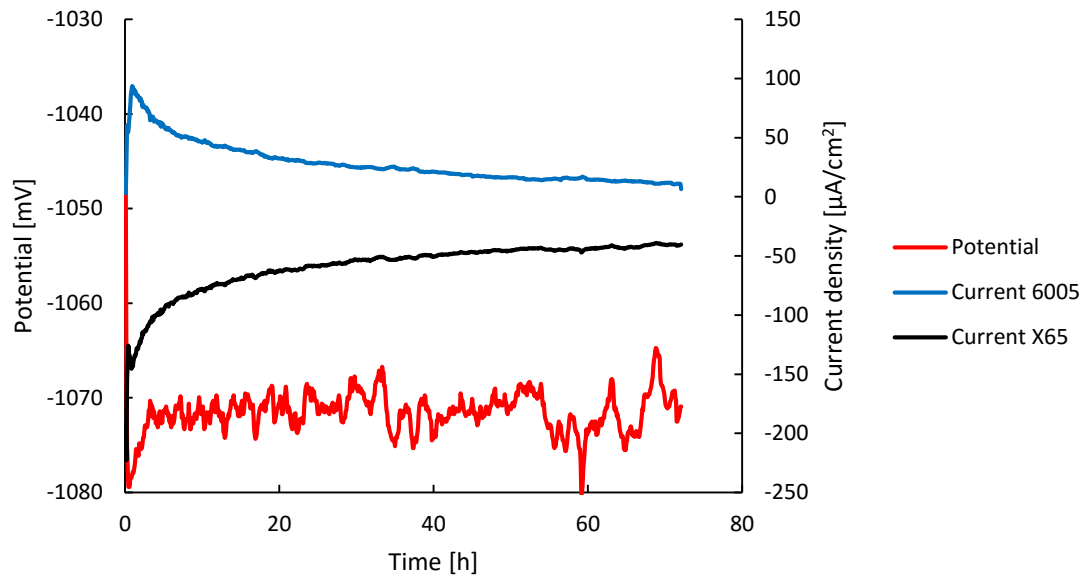
Figure 4.15. Galvanic crevice corrosion test between X65 carbon steel and 6005 aluminium with cathodic protection in NaCl. Recorded coupling potential and galvanic current as a function of time. X65 CS and 6005 Al were coupled in a simulated crevice of 100 μm.
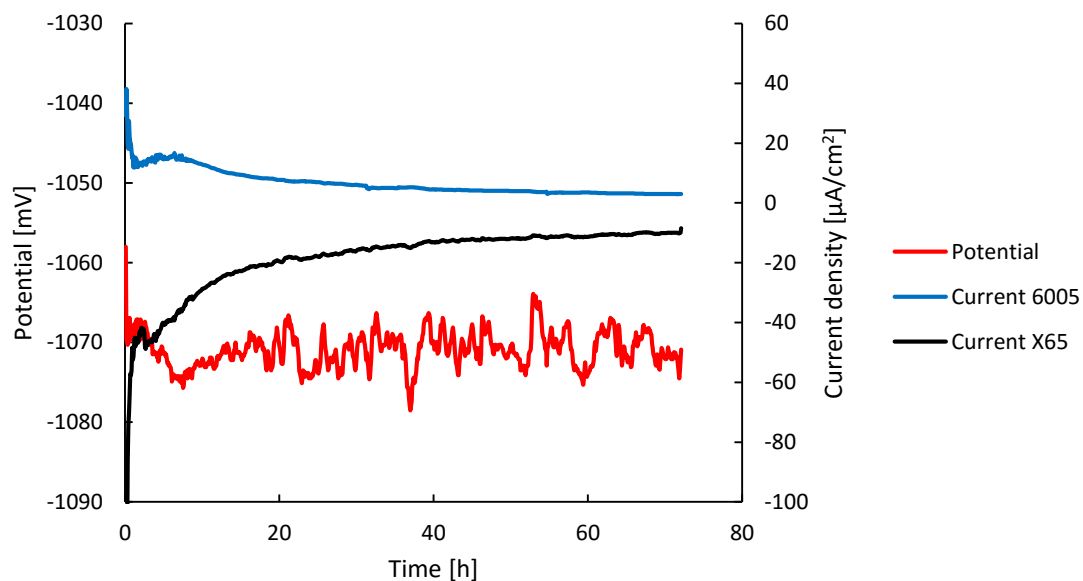

Figure 4.16. Galvanic crevice corrosion test between X65 carbon steel and 6005 aluminium with cathodic protection in seawater. Recorded coupling potential and galvanic current as a function of time. X65 CS and 6005 Al were coupled in a simulated crevice of 100 μm.

The measured current on steel and aluminium had opposite signs; cathodic current was measured on steel whereas anodic current was measured on aluminium. In NaCl a maximum value was observed for both current curves approximately 1 hour into the test. For the remaining time, a steady decay towards zero was seen for both metals. From figure 4.15, it can be seen that the curves make a symmetric shape around a value of about -15 μA/cm². The potential was controlled by the anode, and varied no more than 15 mV. Similar observations was made in

seawater, with the most distinct difference being lower current densities on both metals. The pH inside the cavity was measured to approximately 10 in both solutions.

4.4 Potential sweep

The polarization curves for all three alloys in NaCl was recorded in the author's specialization project [30], and is presented in figure 4.17. Corresponding measurements for curves in seawater was attempted but the results were not satisfactory and will not be presented. Figure 4.18 shows the results from polarization of a steel sample covered with calcareous deposits from a three-metal galvanic corrosion test. The curve is plotted along with the linear part of the cathodic polarization curve of steel in NaCl from figure 4.17.
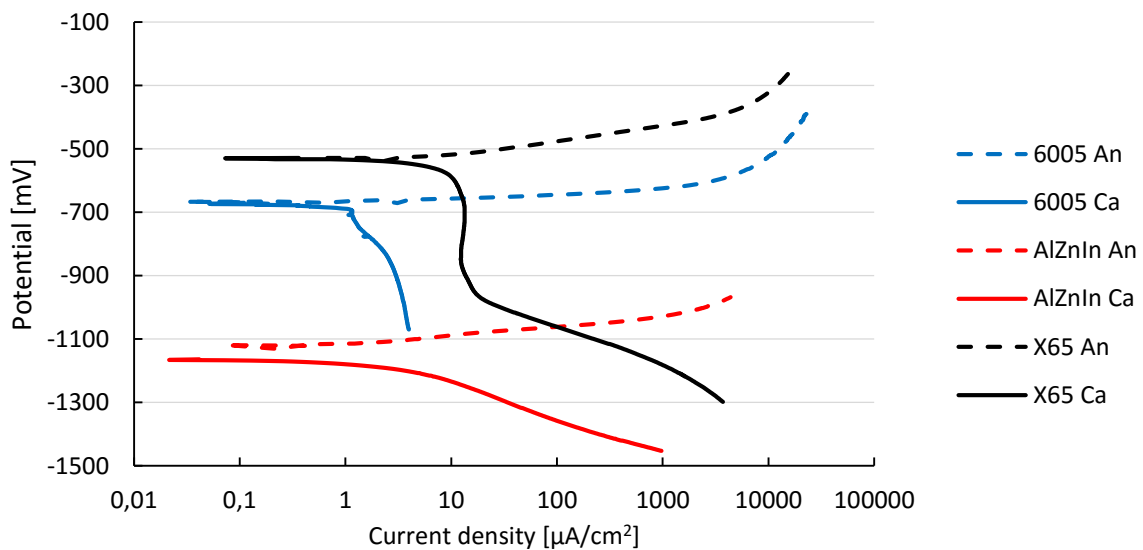

Figure 4.17. Polarization curves for X65 carbon steel, 6005 aluminium and AlZnIn in 3.5% NaCl solution. Recorded in the author's specialization project [30].
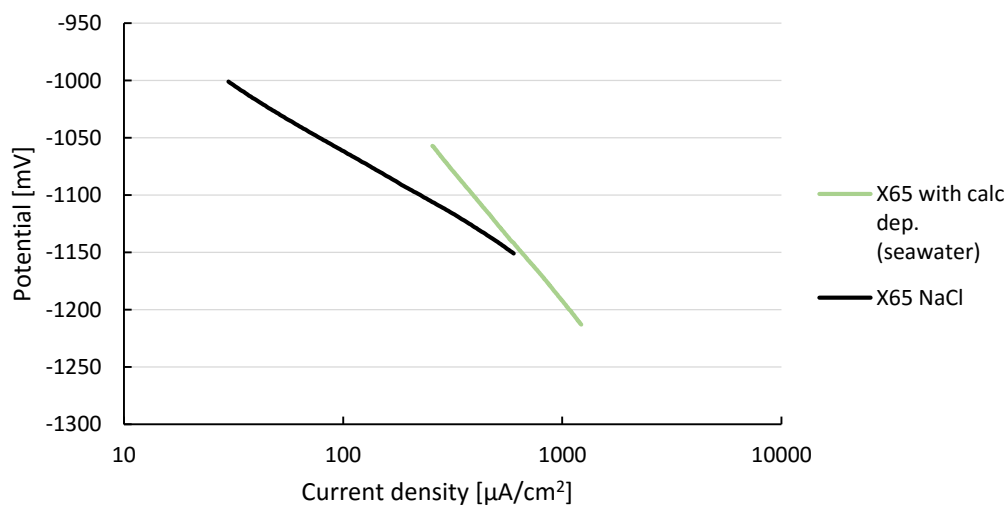

Figure 4.18. Polarization curves for a sample of X65 carbon steel covered with calcareous deposits in artificial seawater, and bare X65 carbon steel sample in NaCl.

43

Results

The anodic and cathodic curve for AlZnIn in figure 4.17 does not intersect at the open circuit potential. 6005 Al was not polarized sufficiently in cathodic direction to intersect the anodic curve for AlZnIn. From the cathodic curve of X65 CS, the Tafel slope of hydrogen evolution was found to be approximately -115 mV/dec. From figure 4.18 the Tafel slope of hydrogen evolution on steel covered with calcareous deposits in seawater was approximated to -230 mV/dec.

Using the curves in figure 4.17, the current density and coupling potential can be found for a galvanic connection between the various alloys. Graphical analysis gave the results shown in table 4.1. The cathodic curve for 6005 Al was extrapolated until it intersected with the anodic curve for AlZnIn.

Table 4.1: Theoretical coupling potential and current density for various galvanic couples.

Coupling	$|i_c| = i_a$ [μA/cm²]	E_c [mV]
X65 CS / 6005 Al	12.9	-650
X65 CS / AlZnIn	112.2	-1065
6005 Al / AlZnIn	4.5	-1100
X65 CS / 6005 Al / AlZnIn	116.2	-1045

In three-metal coupling the value for current is the total cathodic current, i.e. the sum of currents on X65 CS and 6005 Al.

4.5 Weight loss measurements

Weight loss measurements were performed for all samples and will be presented in this section with the unit $\frac{mg}{cm^2 \cdot 24h}$. As mentioned earlier, the method of determining weight loss of carbon steel can be found in appendix A.

4.5.1 X65 carbon steel

Table 4.2 shows the measured weight loss of X65 CS samples from the various electrochemical tests performed.

Table 4.2. Weight loss of X65 carbon steel samples from electrochemical testing. Unit is $\frac{mg}{cm^2 \cdot 24h}$

Type	Coupling	NaCl	Seawater
Open circuit	X65	0.92	0.79
Galvanic	X65 CS / 6005 Al	0.18	0.25
	X65 CS / AlZnIn	0.28	0.27
	X65 CS / 6005 Al / AlZnIn	0	0
	X65 CS / 6005 Al / AlZnIn (96 h)	-	0.03
Galvanic crevice	X65 CS / 6005 Al	0.02	0.05
	X65 CS / 6005 Al and AlZnIn	0	0

From table 4.2 it is evident that X65 CS coupled with 6005 Al or AlZnIn reduces the corrosion rate of steel significantly; the measured weight loss of steel was decidedly largest for the open circuit tests. When coupled to AlZnIn, the steel suffered a slightly higher corrosion rate than when coupled to 6005 Al. Three-metal coupling gave no measurable weight loss in either test solution, and the 96-hour test gave only a very slight metal loss. Similarly, in two-metal crevice coupling, the steel hardly suffered corrosion at all, with the measured weight loss being below that of two-metal coupling without crevice. Moreover, when cathodic protection was applied to the crevice, the steel suffered no measurable corrosion. When comparing the two test solutions, there is no unambiguously result whether NaCl is more corrosive than seawater.

4.5.2 6005 aluminium

Table 4.3 shows the measured weight loss of 6005 Al samples from the various electrochemical tests performed.

Table 4.3. Weight loss of 6005 aluminium samples from electrochemical testing. Unit is $\frac{mg}{cm^2 \cdot 24h}$

Type	Coupling	NaCl	Seawater
Open Circuit	6005 Al	0.13	0.16
Galvanic	X65 CS / 6005 Al	0.50	0.18
	6005 Al / AlZnIn	0.11	0.08
	X65 CS / 6005 Al / AlZnIn	0.24	0.11
	X65 CS / 6005 Al / AlZnIn (96 h)	-	0.07
Galvanic crevice	X65 CS / 6005 Al	0.38	0.25
	X65 CS / 6005 Al and AlZnIn	0.39	0.15

From table 4.3 it can be seen that the self corrosion rate of 6005 Al is relatively low in both test solutions. When coupled to steel, the corrosion rate increased significantly in NaCl, but a difference barely measurable was seen in seawater. The weight loss decreased slightly when coupled to the anode, with the greatest difference being in seawater. Three-metal coupling gave an increase in corrosion rate compared to the OCP test, whereas the opposite was seen in seawater, both for the 24- and 96-hour test. Introduction of the crevice increased the corrosion rate further. An important observation is that the highest corrosion rate was seen for coupling with steel in NaCl without crevice. Furthermore, seawater seems to be less corrosive to 6005 Al than NaCl. The only test that contradicts this is the OCP test.

4.5.3 AlZnIn

Table 4.3 shows the measured weight loss of 6005 Al samples from the various electrochemical tests performed.

Table 4.4. Weight loss of AlZnIn samples from electrochemical testing. Unit is $\frac{mg}{cm^2 \cdot 24h}$

Type	Coupling	NaCl	Seawater
Open circuit	AlZnIn	0.16	0.13
Galvanic	X65 CS / AlZnIn	1.45	1.84
	6005 Al / AlZnIn	0.26	0.18
	X65 CS / 6005 Al / AlZnIn	1.74	3.11
	X65 CS / 6005 Al / AlZnIn (96 h)	-	1.47
Galvanic crevice	X65 CS / 6005 Al and AlZnIn	0.54	0.37

From table 4.4 one can see that the self corrosion rate of the anode is relatively low. When coupled to steel, the consumption of the anode was very high compared to coupling with 6005 Al. Further, when X65 CS and 6005 Al were coupled in crevice connection, the corrosion rate of the anode decreased significantly.

4.6 Macroscopic surface characterization

The samples were inspected visually after electrochemical testing. Photographs were taken after rinsing in distilled water and ethanol. The photographs will be presented in the same order as the electrochemical tests. The only tests lacking are 6005 Al vs AlZnIn in NaCl and three-metal 96-hour.

4.6.1 Open circuit

Photographs taken of samples after open circuit testing in NaCl and seawater can be seen in figure 4.19 and 4.20 respectively.
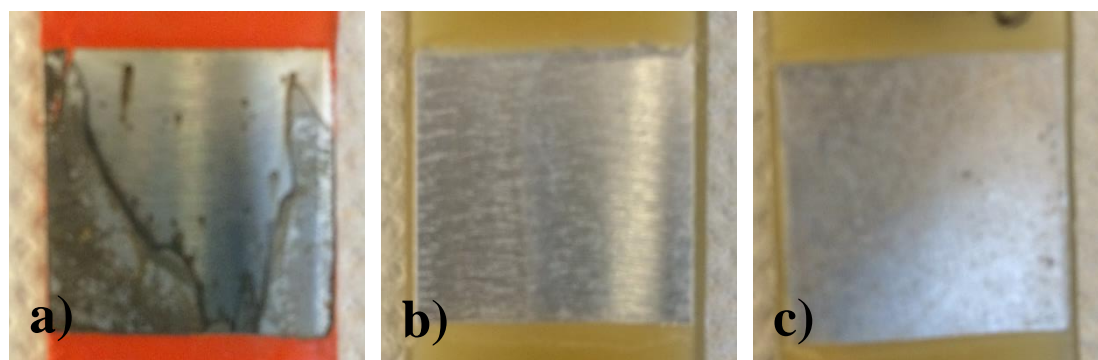

Figure 4.19. Pictures of samples after open circuit testing in NaCl. a) X65 CS, b) 6005 Al, c) AlZnIn
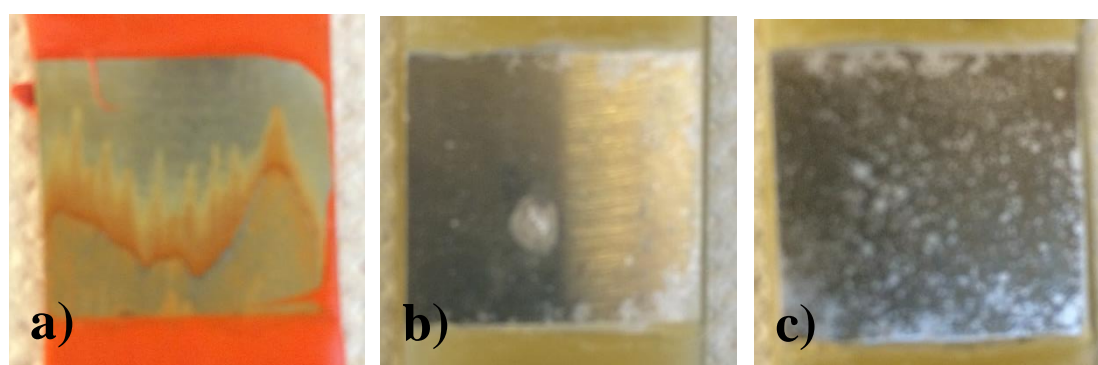

Figure 4.20. Pictures of samples after open circuit testing in seawater. a) X65 CS, b) 6005 Al, c) AlZnIn.

Black and brown rust could be seen on parts of the steel surface tested in NaCl, whereas hardly any corrosion was visible on the aluminum and anode surface. Orange rust was seen on the steel surface tested in seawater, and minor deposits and/or corrosion products were visible on 6005 Al and AlZnIn.

4.6.2 Galvanic corrosion

Figure 4.21 and 4.22 show pictures of samples from galvanic corrosion testing between X65 CS and 6005 Al.
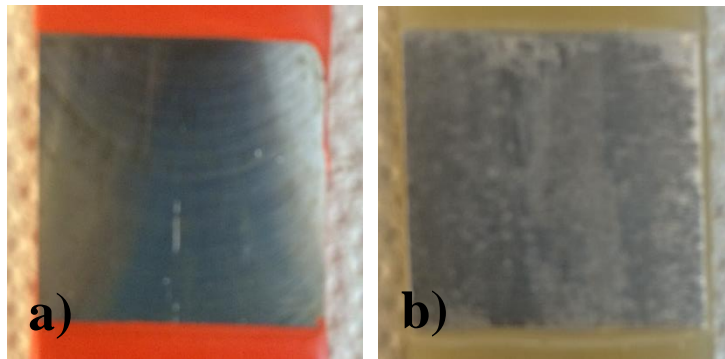
Figure 4.21. Pictures of samples from galvanic corrosion testing between a) X65 CS and b) 6005 Al in NaCl.
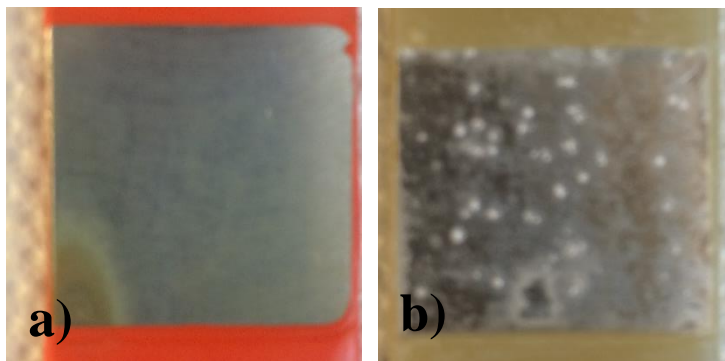

Figure 4.22. Pictures of samples from galvanic corrosion testing between a) X65 CS and b) 6005 Al in seawater.

In NaCl, the steel sample showed little sign of corrosion, with only minor local corrosion could be observed. The aluminium sample had clearly corroded. In seawater, orange rust was seen on the steel sample, localized in a small area in one of the corners only. Corrosion products and deposits was seen on the 6005 Al sample.

Photographs taken of samples after galvanic corrosion testing between X65 CS and AlZnIn can be seen in figure 4.23 and 4.24.
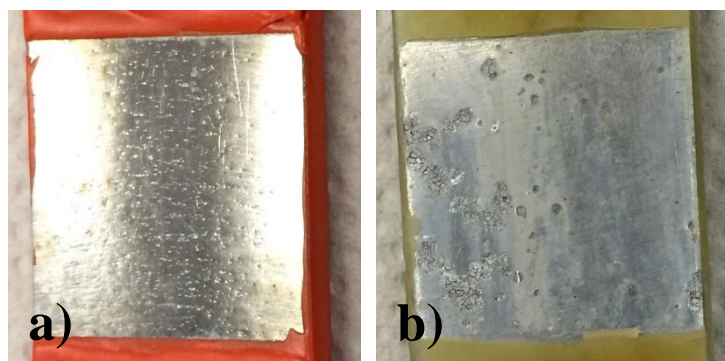

Figure 4.23. Pictures of samples after galvanic corrosion testing between a) X65 CS and b) AlZnIn in NaCl.
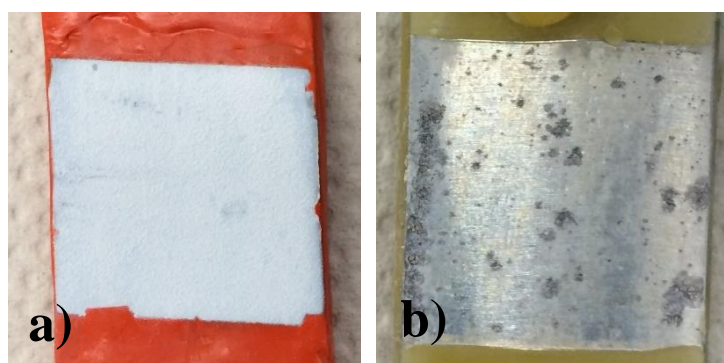
Figure 4.24. Pictures of samples after galvanic corrosion testing between a) X65 CS and b) AlZnIn in seawater.

The steel sample tested in NaCl showed little sign of corrosion, and only slight localized corrosion was observed. Calcareous deposits was seen on the steel sample tested in seawater. Pitting corrosion was seen on the anode for both test solutions.

Figure 4.25 shows the sample surfaces of 6005 Al and AlZnIn after galvanic corrosion testing in seawater. Photographs were not taken of the samples tested in NaCl.
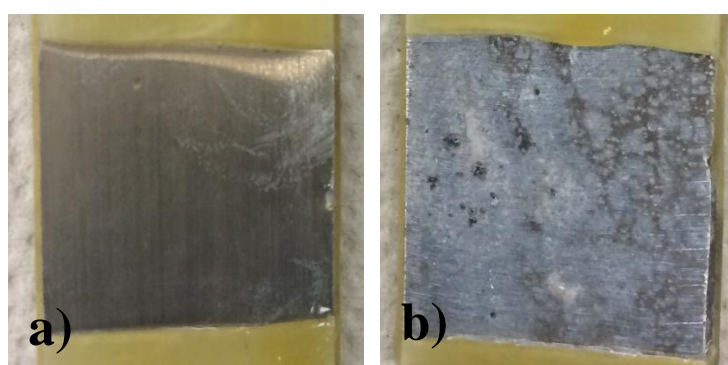

Figure 4.25. Pictures of samples from galvanic corrosion testing between a) 6005 Al and b) AlZnIn in seawater.

From figure 4.25 one can see that the 6005 Al sample seemed almost unaffected, whilst corrosion and deposits was seen on the anode.

Pictures taken of samples after three-metal galvanic corrosion testing between X65 CS, 6005 Al and AlZnIn can be seen in figure 4.26 and 4.27.
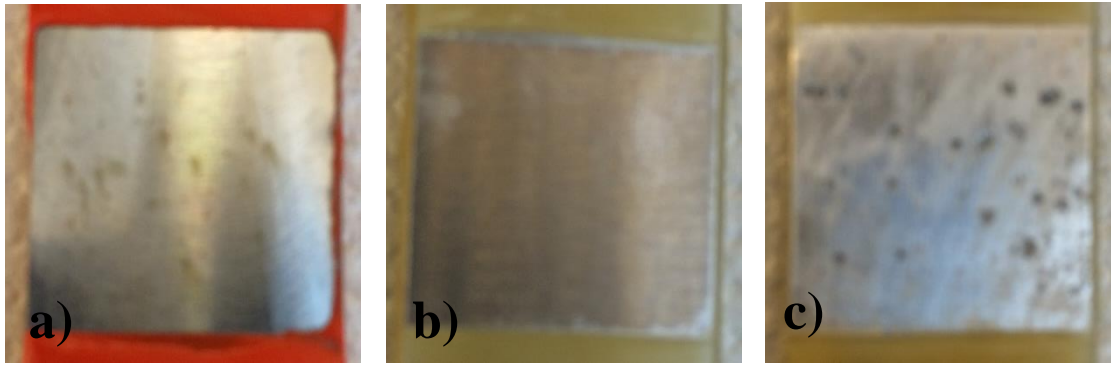
Figure 4.26. Pictures of samples after three-metal galvanic corrosion testing in NaCl. a) X65 CS, b) 6005 Al, c) AlZnIn.
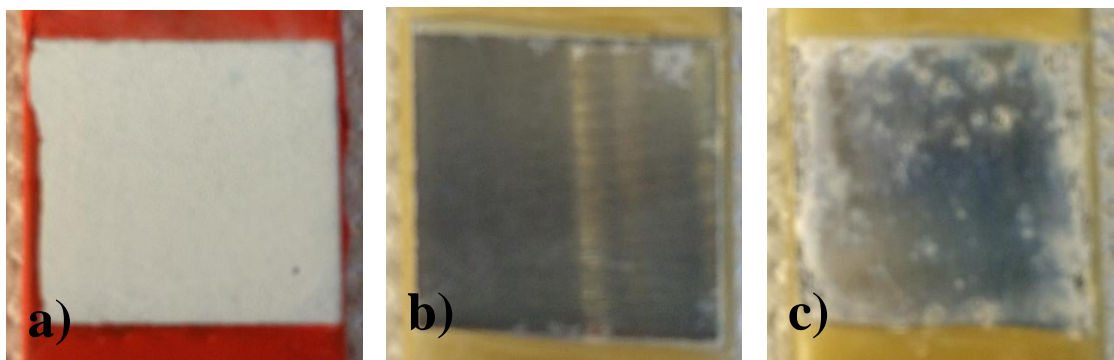

Figure 4.27. Pictures of samples after three-metal galvanic corrosion testing in seawater. a) X65 CS, b) 6005 Al, c) AlZnIn.

Minor localized corrosion was observed on the steel sample tested in NaCl, whilst for seawater, the steel was covered with calcareous deposits. Only slight corrosion was observed on the 6005 Al surfaces. Consumption of the anode was clearly visible in form of pitting corrosion.

4.6.3 Galvanic crevice corrosion

Figure 4.28 and 4.29 shows pictures of samples after galvanic crevice corrosion testing of X65 CS and 6005 Al in NaCl and seawater respectively. The photographs were taken just after the crevice coupling was opened.
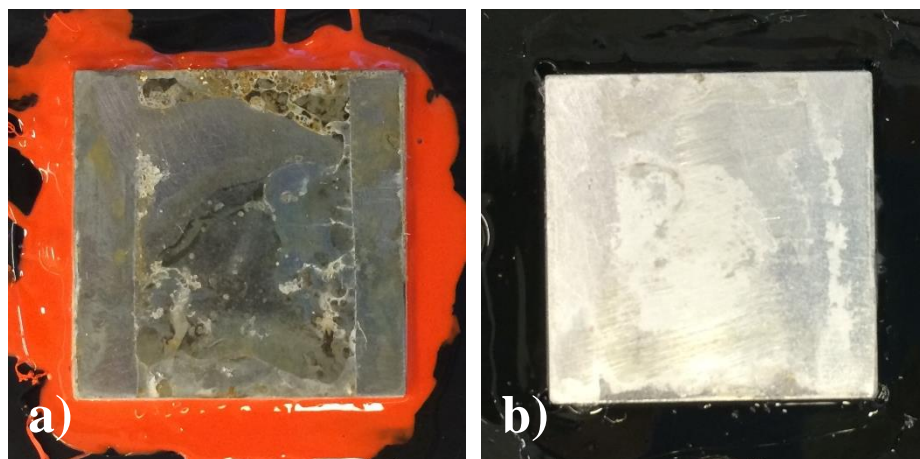
Figure 4.28. Pictures of samples after galvanic crevice corrosion testing in NaCl. a) X65 CS, b) 6005 Al.
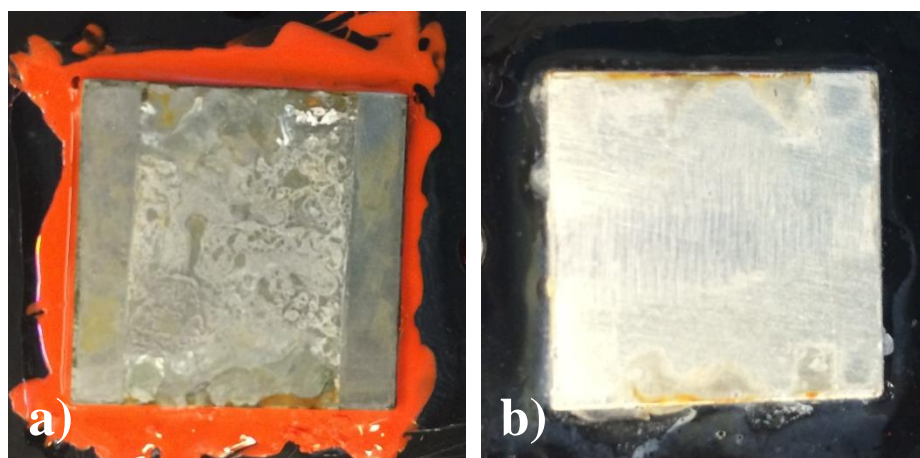

Figure 4.29. Pictures of samples after galvanic crevice corrosion testing in seawater. a) X65 CS, b) 6005 Al.

From figure 4.28 one can see that the steel surface tested in NaCl was covered with black and brown corrosion products. The distribution of these deposits was not even; the top area near the crevice mouth seemed the area with highest degree of corrosion, while other areas seemed rather unaffected. Minor corrosion was also visible where the two Teflon strips had been placed. Further, the aluminium sample seemed to be somewhat corroded, but similarly to the steel sample not evenly; certain parts of the sample appeared to be unaffected.

From figure 4.29 it can be seen that the steel sample was covered with white or grey corrosion products or deposits. Orange rust was also visible. Slight corrosion was observed under the Teflon strips. The aluminium sample appeared to be rather unaffected with exception of orange rust at the mouth of the crevice.

Photographs of samples taken after galvanic crevice corrosion testing with cathodic protection can be seen in figure 4.30 and 4.31. Pictures of the anode is not included.
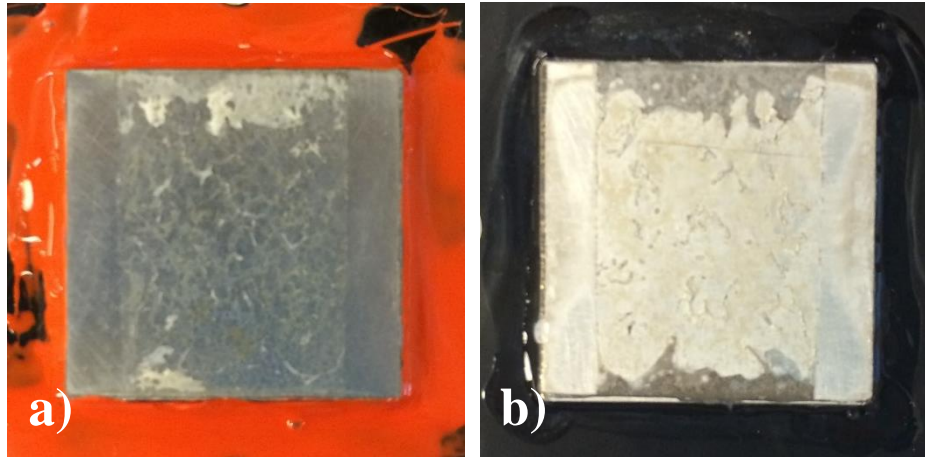

Figure 4.30. Pictures of samples after galvanic crevice corrosion testing with cathodic protection in NaCl. a) X65 CS, b) 6005 Al.
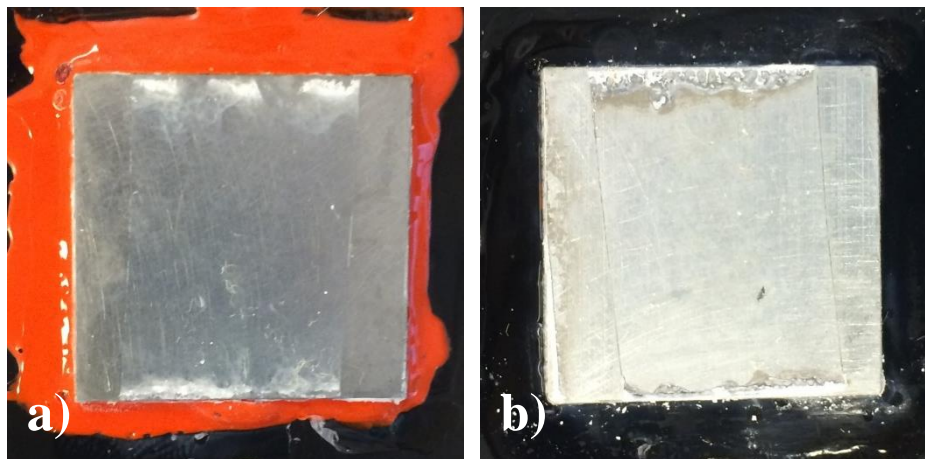

Figure 4.31. Pictures of samples after galvanic crevice corrosion testing with cathodic protection in seawater. a) X65 CS, b) 6005 Al.

White or grey deposits was seen on the steel surface tested in NaCl. The deposits were concentrated near the crevice opening while only a minor degree of deposits was seen in the middle of the sample. No corrosion was visible under the Teflon strips. Heavy corrosion damage was observed on the aluminium sample near the crevice mouth; a distinct loss of metal was visible 2-3 mm from the edge of the sample.

In seawater, no change in steel surface was visible with exception of white deposits at the edge of the crevice opening. Significant corrosion was observed on the corresponding area of the aluminium sample, whilst the remaining part of the surface seemed unaffected.

4.7 Microscopic surface characterization

SEM and EDS were used to characterize specimens microscopically both before and after chemical cleaning, for all experiments with exception of the open circuit tests. Only selected micrographs and analyses from EDS will be presented; additional data can be found in appendix B. In general, micrographs of the anode will not be presented.

4.7.1 Galvanic corrosion

Figure 4.32 shows SEM images of the surfaces of X65 CS and 6005 Al as received that were used in galvanic corrosion testing.
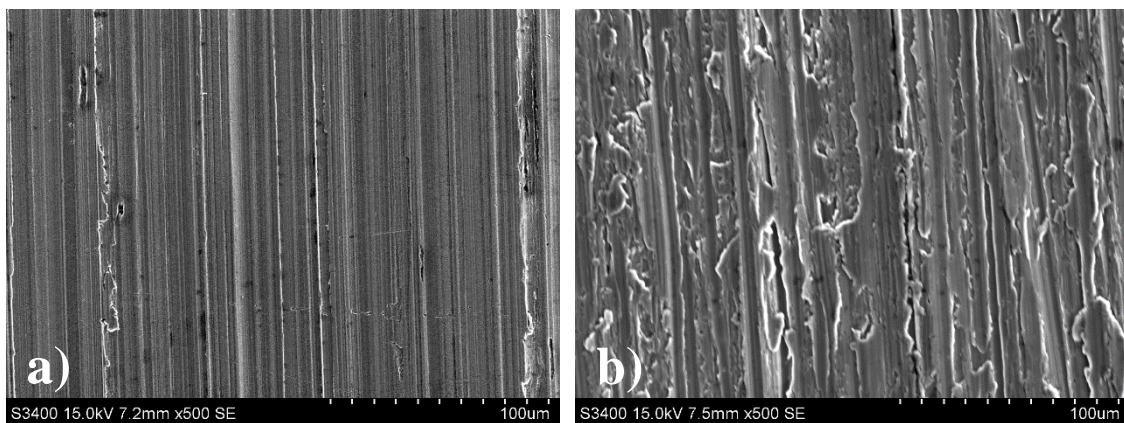
Figure 4.32. SEM images of the surfaces of alloys used in galvanic corrosion testing, as received. a) X65 CS, b) 6005 Al.

Figure 4.33 shows a SEM image of a 6005 Al sample after galvanic corrosion testing against X65 CS in NaCl, corresponding to the sample in figure 4.21b). The image was taken post chemical cleaning.
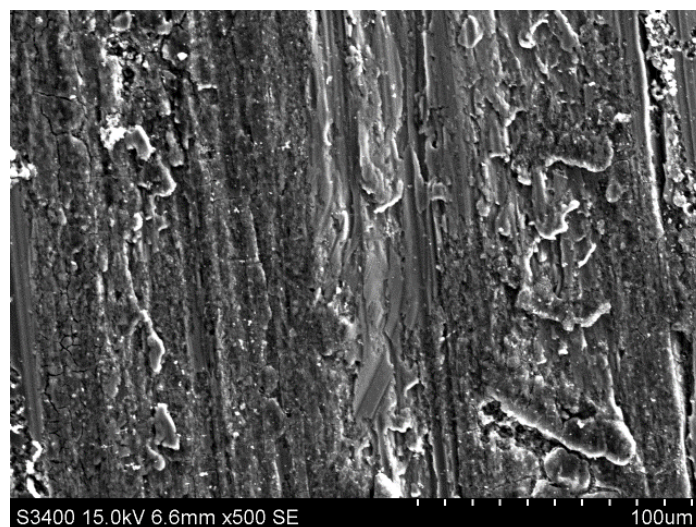

Figure 4.33. SEM image of a 6005 Al sample after galvanic corrosion testing with X65 CS in NaCl. The image was taken post chemical cleaning.

It is evident from figure 4.33 that aluminium suffers from corrosion when coupled to steel in a NaCl solution. By comparing with figure 4.32b one can see that the surface morphology has clearly changed.

Figure 4.34 shows a SEM image of a 6005 Al sample after galvanic corrosion testing against X65 CS in seawater (figure 4.22a). The image was taken prior to chemical cleaning.
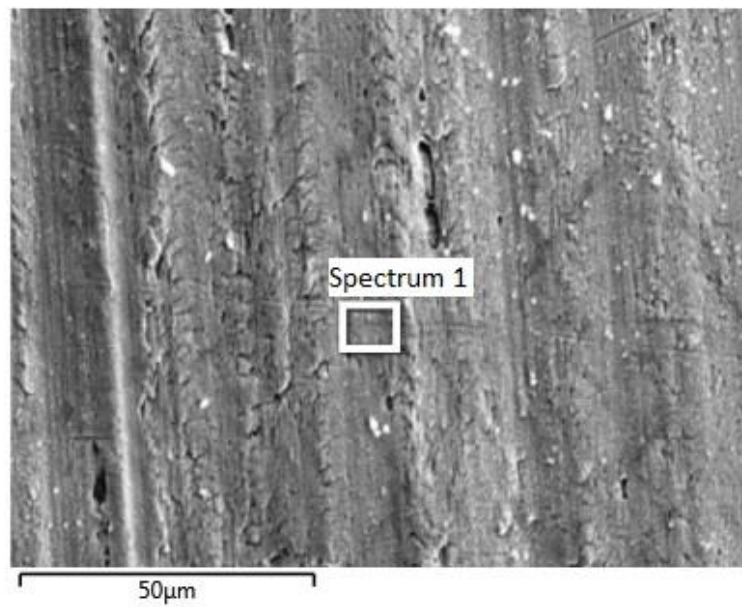

Figure 4.34. SEM image of an X65 CS sample after galvanic corrosion testing with 6005 Al in seawater, including area for EDS analysis. The image was taken prior to chemical cleaning.

The SEM image shown in figure 4.34 was taken at a representative area of the steel sample. Before being analyzed in SEM, the sample was rinsed in distilled water and ethanol. Deposits or corrosion products seems to be present on the metal surface. EDS analysis was performed for spectrum 1 in the figure, and the results can be seen in table 4.5.

Table 4.5. EDS analysis for spectrum 1 in figure 4.34.

Element	wt%
Fe	87.31
O	4.98
C	4.37
Mg	2.02
Mn	1.32

From the results in table 4.5, the layer on the steel surface is presumably a combination of corrosion products and small deposits containing Mg. However, no Ca was detected.

Figure 4.35 shows SEM images of 6005 Al samples from galvanic corrosion testing against AlZnIn in NaCl and seawater. The images were taken post chemical cleaning.
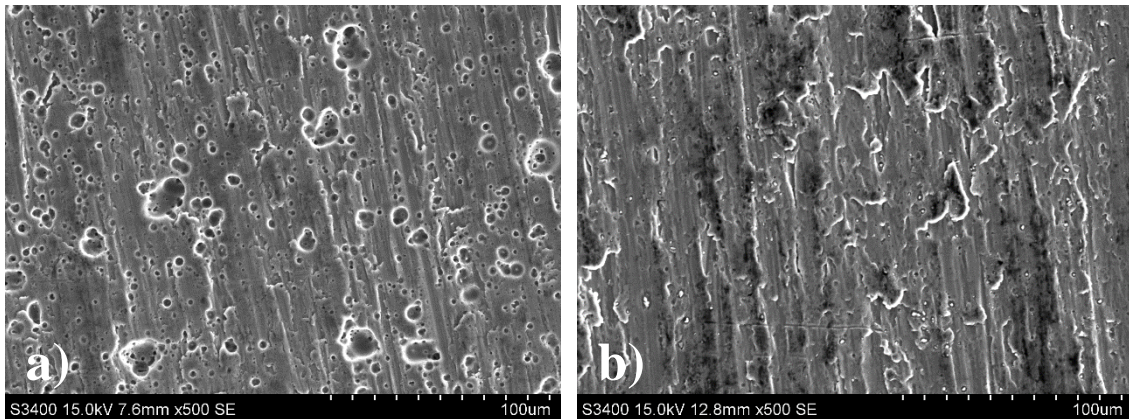

Figure 4.35. SEM images of 6005 Al samples from galvanic corrosion testing against AlZnIn in a) NaCl, b) seawater. The images were taken post chemical cleaning.

From figure 4.35 one can see that the surface of the aluminium sample tested in NaCl was covered with small pits no larger than 20 μm, whereas no such phenomena was seen for seawater; the surface morphology seems unaltered from the unexposed surface.

SEM images of X65 CS and 6005 Al from three-metal coupling in NaCl can be seen in figure 4.36. The images were taken post chemical cleaning.
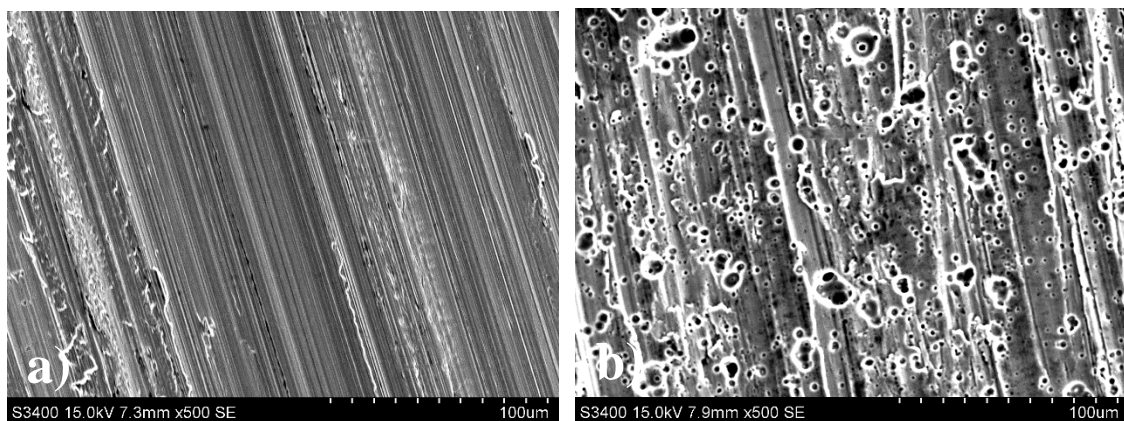
Figure 4.36. SEM images of a) X65 CS and b) 6005 Al samples from three-metal galvanic corrosion testing in NaCl. The images were taken post chemical cleaning.

The steel sample appeared to be unaltered after electrochemical testing. The aluminium sample however, suffered from pitting attacks on the surface, similar to what was found for two-metal testing with AlZnIn.

Figure 4.37 and 4.38 shows SEM images of calcareous deposits formed on the steel sample during three-metal galvanic corrosion testing seawater.
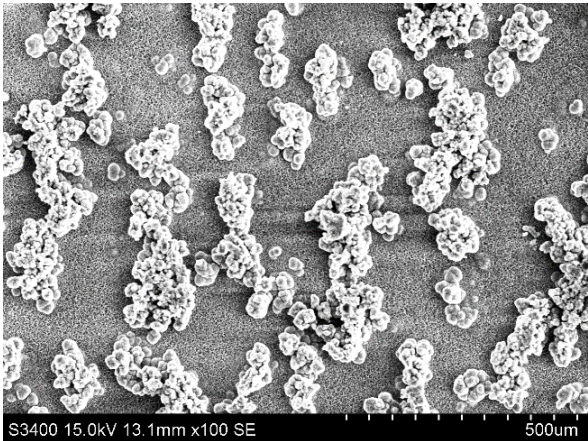
Figure 4.37. SEM image of calcareous deposits formed on steel during three-metal galvanic corrosion testing in seawater.
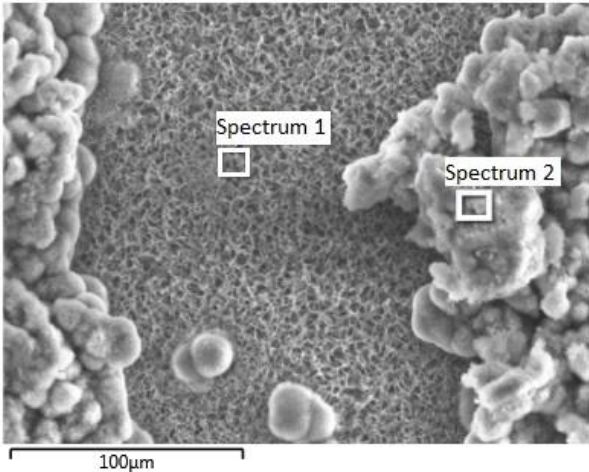
Figure 4.38. SEM image of calcareous deposits formed on steel during three-metal galvanic corrosion testing in seawater, including areas for EDS analysis.

From figure 4.37 and 4.38 one can see that clusters of deposits formed on a uniform deposit layer on steel. EDS analysis was performed on both, and the results can be seen in table 4.6.

Table 4.6. EDS analysis for spectrum 1 and 2 in figure 4.38.

Element	wt%	
	Spectrum 1	Spectrum 2
O	53.28	51.9
Mg	41.42	41.75
C	2.86	4.84
Cl	1.11	1.33
Na	0.43	0.44
Fe	0.87	0.57
K	0.03	-

Before being analyzed, the sample was rinsed in distilled water and ethanol. As one can see from table 4.6, there was hardly any difference between the two spectra. The composition of the calcareous deposits is presumably $Mg(OH)_2$; no Ca was detected whatsoever.

The calcareous deposits were mechanically scraped off the sample all the way down to the metal surface, exposing the deposits that formed adjacent to the steel. Figure 4.39 shows a SEM image of these deposits along with areas for EDS analysis, which can be seen in table 4.7.
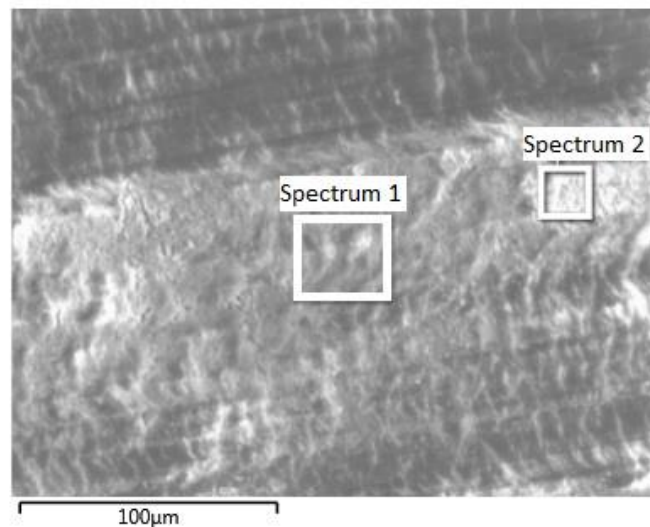
Figure 4.39. SEM image of a steel sample with calcareous deposits, where the deposits have been mechanically scraped off, down to the metal surface.

Table 4.7. EDS analysis for spectrum 1 and 2 in figure 4.39.

Element	wt%	
	Spectrum 1	Spectrum 2
O	51.36	50.75
Mg	32.98	19.98
Ca	5.02	16.97
C	5.91	8.79
Cl	2.49	1.52
Fe	1.03	0.98
Na	0.87	0.74
S	0.34	0.27

Analysis of the calcareous deposits located near the metal surface revealed a significant amount of Ca. The composition of the deposits near the metal surface was thus found to be a combination of $CaCO_3$ and $Mg(OH)_2$. The amount of Ca found in the two spectra differs by a factor of 3, suggesting a non uniform composition. Additional areas were also analyzed and showed varying amount of Ca.

Figure 4.40 shows SEM images of X65 CS and 6005 Al samples from three-metal galvanic corrosion testing in seawater. The images were taken post chemical cleaning.
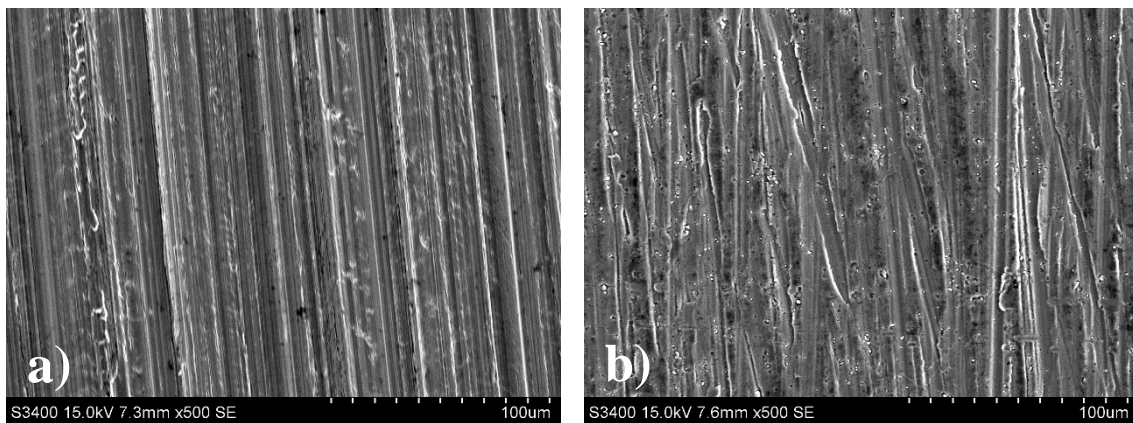
Figure 4.40. SEM images of a) X65 CS and b) 6005 Al samples from three-metal galvanic corrosion testing in NaCl. The images were taken post chemical cleaning.

The steel sample showed little or no sign of corrosion, and only slight change in surface morphology was seen for the aluminium sample.

Figure 4.41 shows a backscatter image of the 6005 Al sample from 96 hour three-metal galvanic corrosion test. The image was taken post chemical cleaning. EDS analysis for one of bright spots in the Al matrix can be found in table 4.8.
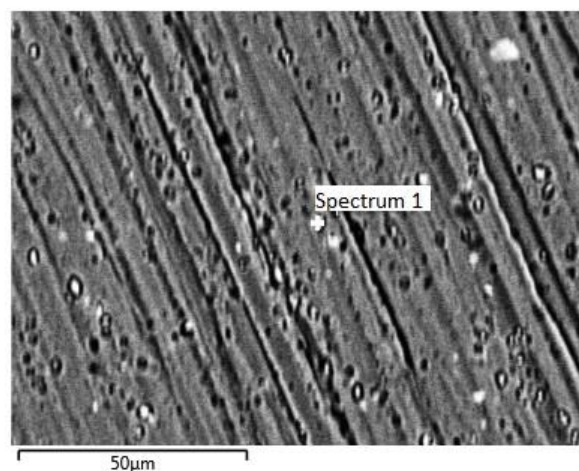
Figure 4.41. SEM (backscatter) image of the 6005 Al sample from 96h three-metal galvanic corrosion testing in seawater. The image was taken post chemical cleaning.

**Table 4.8.** EDS analysis for spectrum 1 in figure 4.41.

Element	wt%
Al	69.2
Fe	14.16
C	8.32
Si	4.06
Mn	2.04
O	1.11
Mg	0.27

EDS analysis of the bright spot in the Al matrix confirms that Fe-rich intermetallic inclusions was present after the electrochemical test. Thus, no alkaline etching process as seen in NaCl was seen in seawater after an extended period of time.

4.7.3 Galvanic crevice corrosion

Figure 4.42 shows SEM images of the surfaces of X65 CS and 6005 Al as received that was used in galvanic crevice corrosion testing.
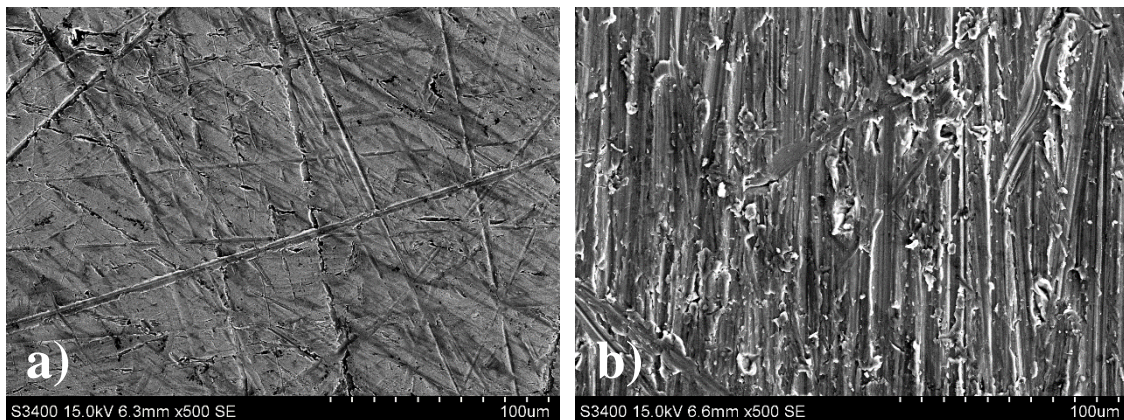
Figure 4.42. SEM images of the surfaces of alloys used in galvanic crevice corrosion testing, as received. a) X65 CS, b) 6005 Al.

Figure 4.43 shows a SEM image of the steel sample from two-metal galvanic crevice corrosion testing in NaCl. The image is taken prior to chemical cleaning, in the top area of the sample near the crevice mouth (see figure 4.28a).
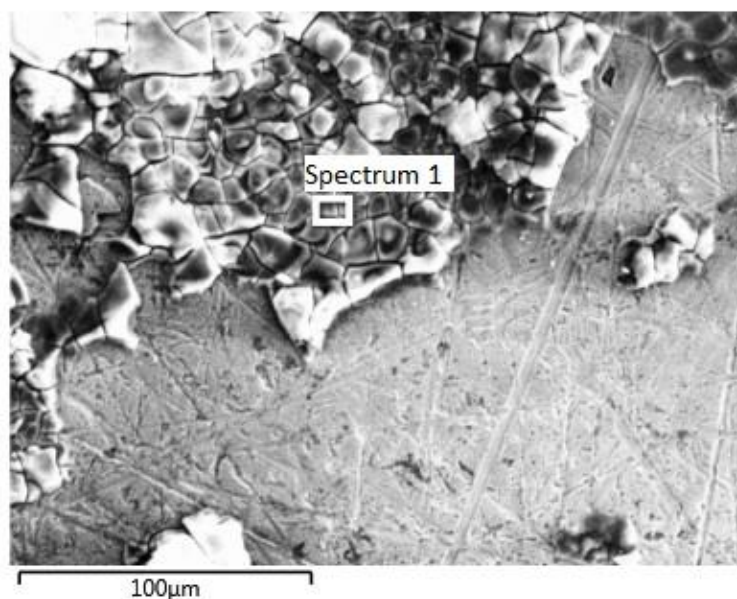
Figure 4.43. SEM image of the steel sample from two-metal galvanic crevice corrosion testing in NaCl. The image was taken prior to chemical cleaning.

A layer of deposits can be seen in figure 4.43, whilst the bare steel surface is seen in the other half of the image. EDS analysis was performed for the deposits, which can be found in table 4.9.

Table 4.9. EDS analysis for spectrum 1 in figure 4.43.

Element	wt%
Al	27.42
Fe	15.09
O	43.33
Cl	8.92
C	5.24

From table 4.9 it is evident that the deposits seen on the steel sample is a combination of corrosion products from both steel and aluminium.

Figure 4.44 shows SEM images of X65 CS and 6005 Al samples from two-metal galvanic crevice corrosion testing in NaCl, taken after chemical cleaning.
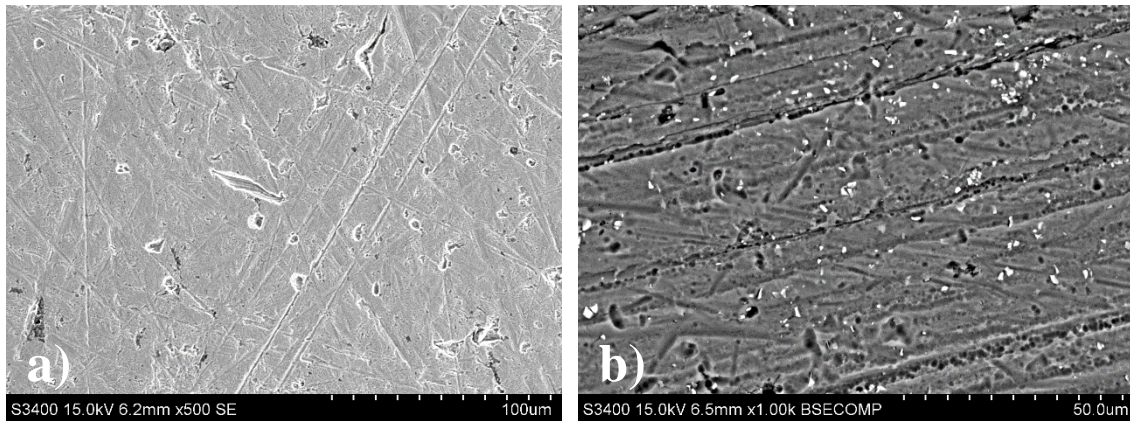
Figure 4.44. SEM images of a) X65 CS and b) 6005 Al samples after two-metal galvanic crevice corrosion testing in NaCl. The images were taken post chemical cleaning.

Some minor pitting corrosion was observed on the steel sample, with no severe corrosion attack. No significant corrosion damage was seen on the Al sample, and the backscatter image in figure 4.44b) shows the presence of the intermetallic particles in the Al matrix.

SEM images of X65 CS and 6005 Al samples from two-metal galvanic crevice corrosion testing in seawater can be seen in figure 4.45. The images were taken post chemical cleaning.
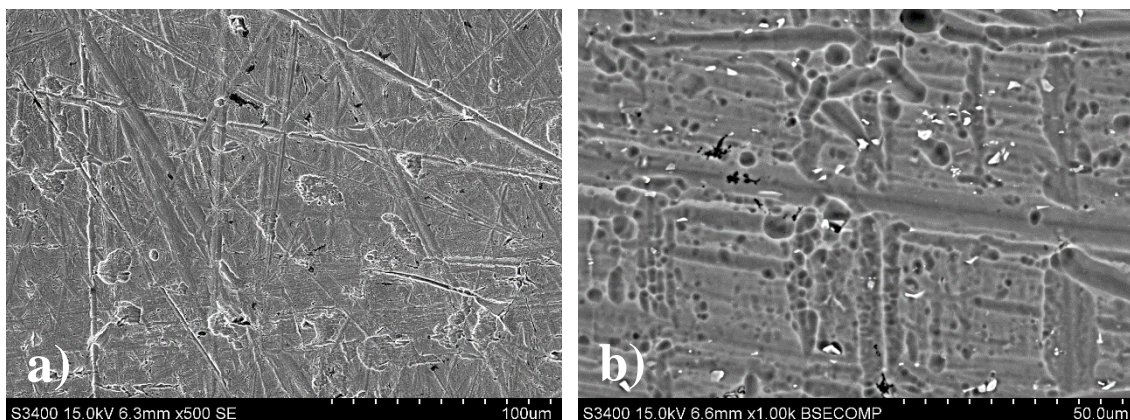
Figure 4.45. SEM images of a) X65 CS and b) 6005 Al samples after two-metal galvanic crevice corrosion testing in seawater. The images were taken post chemical cleaning.

Similar to what was seen for the corresponding test in NaCl, minor pitting corrosion was observed on the steel sample with no severe corrosion attack on the metal. However, the Al sample showed partial etching of intermetallic particles where some still were present in the Al matrix.

Figure 4.46 shows a SEM image of the white deposits found on the steel sample from galvanic crevice corrosion testing with cathodic protection in NaCl. The results from EDS analysis of the deposits can be found in table 4.10.

61
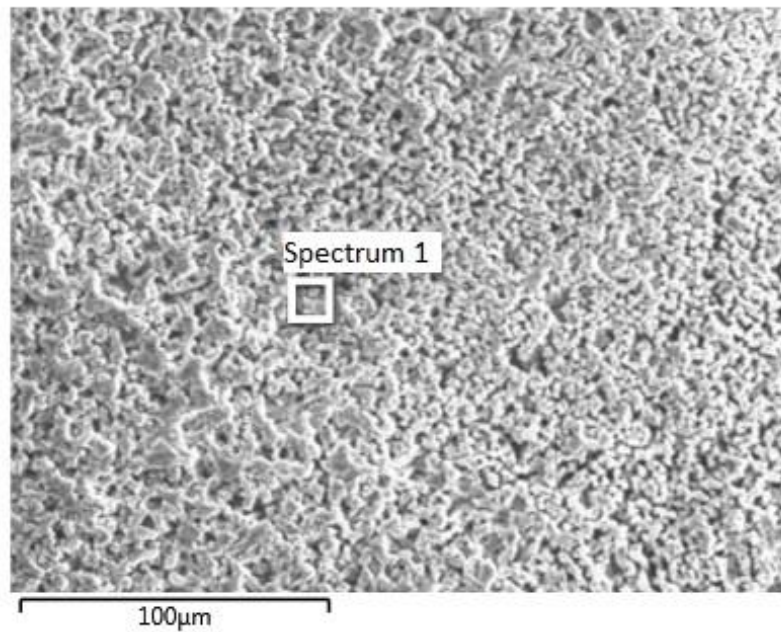
Figure 4.46. SEM image of the white deposits seen on the steel sample from galvanic crevice corrosion testing with cathodic protection in NaCl.

Table 4.10. EDS analysis for spectrum 1 in figure 4.46.

Element	wt%
O	58.38
Al	35.7
Fe	1.53
C	4.39

EDS analysis showed that the deposits found on the steel sample was corrosion products from the aluminium sample. Hardly any iron was detected. Additional areas of the sample was analyzed, and only trace elements were detected besides iron.

SEM images of X65 CS and 6005 Al from galvanic crevice corrosion testing with cathodic protection in NaCl can be seen in figure 4.47. The images were taken in the middle of the samples, post chemical cleaning.

Figure 4.47. SEM images of a) X65 CS and b) 6005 Al samples after galvanic crevice corrosion testing with cathodic protection in NaCl. The images were taken in the middle of the samples, post chemical cleaning.

The steel sample seemed unaffected by the test. Images were taken at additional locations, with the same results. Etching around the cathodic inclusions was seen on the aluminium sample. The backscatter image in figure 4.47b indicated that new particles are exposed at the bottom of some pits. Additional images were taken from the edge of the sample, near the crevice mouth and can be seen in figure 4.48.

Figure 4.48. SEM images of the 6005 Al sample from galvanic crevice corrosion testing with cathodic protection in NaCl. Both images were taken near the crevice mouth, post chemical cleaning. a) Area near crevice mouth, b) adjacent area.

Hemispherical pits were observed near the crevice mouth, appearing in dense clusters. Varying size of the pits were observed, with the largest being approximately 100 μm across. In contrast to the etching process observed in middle of the sample (figure 4.47b), these pits were not limited around intermetallic particles.

Figure 4.49 shows SEM images of X65 CS and 6005 Al samples from galvanic crevice corrosion testing with cathodic protection in seawater. The images were taken in the middle of the samples post chemical cleaning.
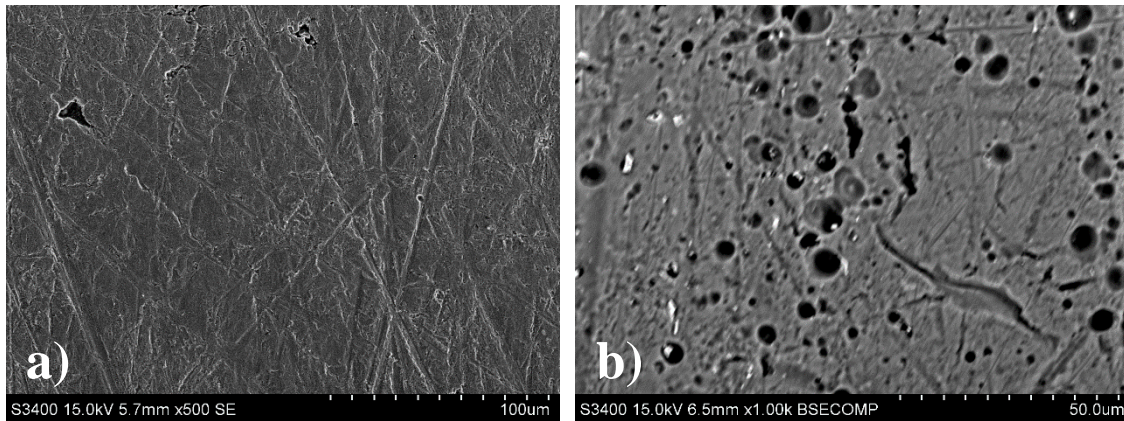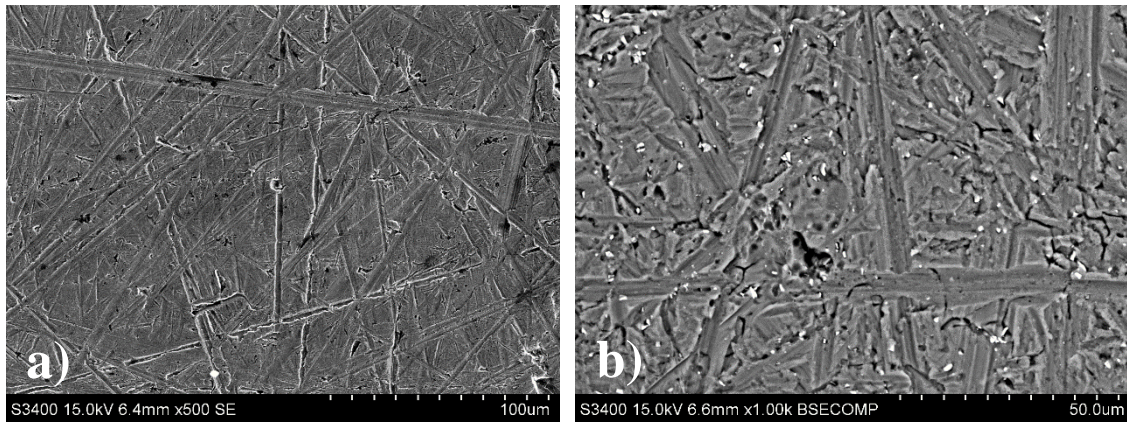
Figure 4.49. SEM images of a) X65 CS and b) 6005 Al samples after galvanic crevice corrosion testing with cathodic protection in seawater. The images were taken in the middle of the samples, post chemical cleaning.

Similar to the corresponding test in NaCl, the steel appeared unaffected. No etching process was observed on the aluminium surface in this part of the sample. Additional images were taken from the edge of the sample, near the crevice mouth and can be seen in figure 4.50.
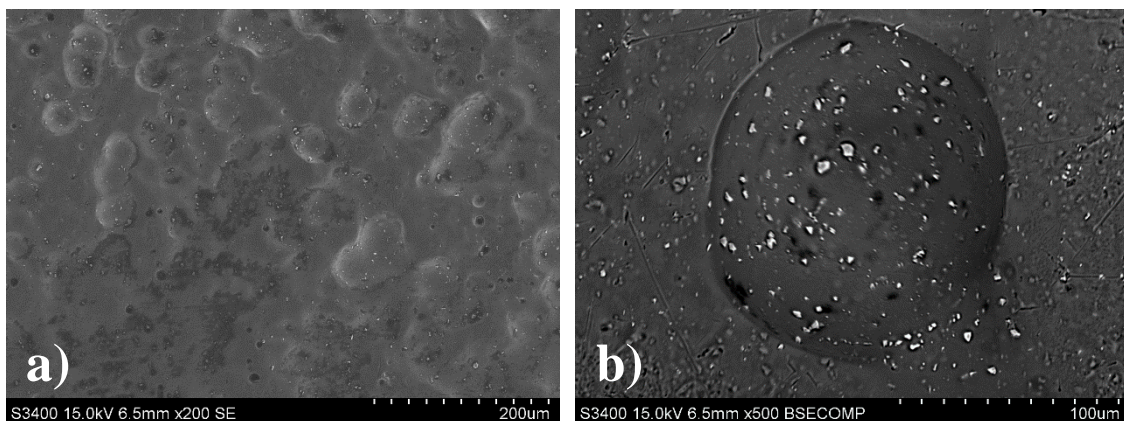

Figure 4.50. SEM image of the 6005 Al sample from galvanic crevice corrosion testing with cathodic protection in seawater. The image was taken near the crevice mouth, post chemical cleaning.
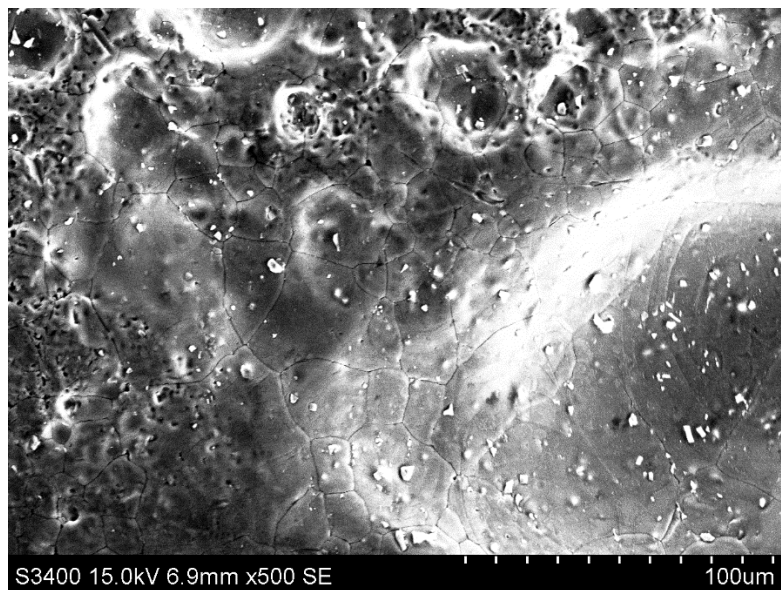
Near the crevice opening, dense clusters of hemispherical pits of varying size were seen. The pits were not limited around intermetallic inclusions, similar to what was seen in NaCl.

Chapter 5

Discussion

This chapter contains the discussion of the results and experimental work. The discussion will consist of the following parts: Electrochemical behavior, corrosion rates, surface characterization and experimental work. Finally, suggestions for further work will be presented. Similar to the previous chapter, all potentials are given versus the saturated Ag/AgCl electrode.

5.1 Electrochemical behavior

The electrochemical behavior of a coupling between X65 CS, 6005 Al and AlZnIn was thoroughly studied through galvanic corrosion tests of different couplings between the alloys. The two-metal tests were conducted to have a basis for comparison before all three alloys were coupled.

X65 CS coupled to 6005 Al in NaCl gave a net galvanic current density of approximately -35 μA/cm^2 on steel. This value is in the same order of magnitude as previous studies [5], [6] for slightly different materials. Literature for the same alloys has not been found. The current flow was relatively stable, slightly decreasing as a function of time. A certain change of the metal surfaces will occur from corrosion and corrosion products. Thus, a slight decay in current density is expected. A distinct difference was seen for the same test performed in seawater, where the potential was approximately the same, -680 mV, but the galvanic current decayed exponentially towards zero. As the only difference between the experiments is the test solution, there are two causes to be considered: deposits on the metal surfaces from the seawater and electrochemical behavior of the two metals in the different solutions. The former will be discussed later in the surface characterization section. The latter relates to the open circuit measurements performed. From figure 4.1 one can see that the potential of X65 CS is more active in seawater than in NaCl. In fact, from comparing with figure 4.2, it can be seen that the potential of X65 CS and 6005 Al becomes almost identical in seawater which can explain the very low net current between them in galvanic corrosion testing. Nevertheless, aluminium

Discussion

supplies protective current to steel in the coupling discussed above, and the steel is partially protected. The theoretical values for net current and coupling potential found from the polarization curves in figure 4.17 deviate somewhat from the measured values. A possible explanation for this is that the samples were not stabilized for a sufficient period in the solution before recording of polarization curves began. The open circuit potential of steel can be found to be -530 mV from figure 4.17 whereas in figure 4.1, the potential drops below -600 mV as time proceeds. Thus, the polarization curve for X65 CS would probably be shifted in the active direction if the sample were immersed for a longer time.

Galvanic corrosion testing between X65 CS and AlZnIn gave a coupling potential of approximately -1070 mV, well below the protection potential of steel [11], and a reduction current in the range of 100 μA/cm^2 was measured in NaCl. These values correspond well with the theoretical values presented in table 4.1. From figure 4.6 and 4.7 it can be seen that after a short initial period where the anode is activated, a decay in the current can be seen for both test solutions. As discussed before, a slight decay is expected as time progresses due to the change in the metal surface. Although, not much corrosion is expected at these potentials. Further, calcareous deposits were formed on the steel surface in seawater, which are known to reduce the reduction rate on steel. However, the dominating reduction reaction at a potential of -1070 mV is expected to be hydrogen evolution, which the calcareous deposits have little or no effect on [16]. Thus, the decay rate of the reduction current in NaCl and seawater is expected to be similar at a potential controlled by AlZnIn. Further examination of the results reveal that the current density was significantly larger in seawater than in NaCl, roughly by a factor of 1.5. Studies have shown that $Mg(OH)_2$ may catalyze the hydrogen evolution reaction [17]. These findings are supported by the polarization curves presented in figure 4.18. The sample covered with calcareous deposits gave a Tafel slope twice that of bare steel in NaCl. However, at -1070 mV, the current density is substantially larger in seawater. The slope found in NaCl was close to the theoretical value of -118 mV/dec, and consequently smaller (less negative) than what was found in previous studies [8], [16].

The net current measured from galvanic corrosion testing between 6005 Al and AlZnIn was below 10 μA/cm^2 for both test solutions. Thus, the current requirement of aluminium under cathodic protection is significantly lower than that of steel, as expected. The reduction reactions on aluminium occur on the Fe-rich intermetallic particles in the Al matrix, which only make up for a fraction of the surface area [18]. The current density measured in seawater quickly stabilized, whereas an exponential decay towards zero was seen in NaCl. The shape of the

current curve resembles the current-time behavior shown in figure 2.9. The mechanism of the current behavior is presumably that proposed by Gundersen and Nisancioglu [21]. As aluminium is polarized by the anode, an alkaline diffusion layer will form near the cathodic sites. The amphoteric oxide layer will corrode, and the intermetallic particles will eventually become detached. A final current density of 1 $\mu A/cm^2$ was measured in NaCl, where the curve showed a tendency of further decrease. The very low current suggests that the pH at the surface gives rise to detachment of near all particles in the matrix without exposing new ones. In seawater however, the larger buffer capacity presumably prevents the pH on the metal surface from reaching sufficiently high values for alkaline etching.

In galvanic three-metal coupling, the measurements on steel and aluminium showed the same behavior as in two-metal coupling with AlZnIn. Thus, cathodic protection of steel-aluminium galvanic couples in the absence of a crevice seems possible in terms of electrochemical behavior; the anode supplies cathodic current to both metals similar as in a two-metal system. The results from three-metal testing further supports that the reduction current on steel is larger in seawater compared to NaCl. The final current observed on steel in seawater was twice that of NaCl. For the 96-hour test, the current density was somewhat lower, but still larger than in NaCl after 24 hours. Furthermore, no significant decay in the reduction reaction rate on aluminum was seen after 96 hours. Thus, the pH at the surface was presumably too low to cause alkaline etching, and the cathodic sites are expected to be intact.

The introduction of a crevice between X65 CS and 6005 Al gave somewhat unexpected results. Galvanic crevice corrosion testing in NaCl without cathodic protection gave a slightly smaller net current than for the corresponding test without crevice. A possible cause could be presence of air inside the cavity, reducing the exposed metal area. However, electrolyte was forced inside the crevice before testing by use of a pipette. For testing in seawater, the current stabilized at the same value as in NaCl after 45 hours. During the first 10 hours, a positive current was measured on steel, indicating an initial high corrosion rate on steel. The chemistry inside the cavity becomes very different from that of the bulk solution due to the limited diffusion, and it is difficult to predict the environment. A cavity pH of 3 and 4 was measured for NaCl and seawater respectively. The change in pH is not easily explained as the samples are galvanically coupled. All parts of the samples were coated except the crevice area. Thus, current from Al dissolution should give reduction current on steel, neutralizing the lower pH from hydrolysis of Al ions.

Discussion

The results from galvanic crevice corrosion with cathodic protection shown in figure 4.15 and 4.16, indicate that aluminium suffers from corrosion, initially at a high rate. Anodic current was measured on aluminium through the entire test period in both NaCl and seawater, even though the metal was connected to a sacrificial anode. The results are in contrast to what was found for three-metal galvanic corrosion testing without the factor of crevice corrosion, where cathodic current was measured on both steel and aluminium. The poor resistance to changes in pH that aluminium has can explain this. The high reduction rate on steel combined with limited diffusion inside the crevice give rise to a high pH, which is detrimental to aluminium. A cavity pH of approximately 10 was measured for both test solutions. This value corresponds well with measurements from previous studies [24] where the crevice distance was ten times of what was used in this work. The actual pH of the cavity is expected to be higher than what was measured because of the way the measurement was carried out. At the end of the test, the crevice device was lifted out of the test cell before it was opened. Although this was performed with great caution, the movement caused convection, and the chemistry inside the cavity was presumably diluted. However, the anodic current decayed towards zero at the end of the test, indicating that corrosion of aluminium was only an initial stage. The mechanism will be discussed more in detail in the surface characterization section.

5.2 Corrosion rates

5.2.1 Steel

The corrosion rate of steel was significantly reduced when coupled to 6005 Al or AlZnIn. When coupled to 6005 Al, a slightly higher corrosion rate was measured in seawater than NaCl. This can be explained by the very low net current measured between the samples in seawater. However, at a potential of -680 mV, the steel is not expected to be fully protected. On the contrary, when coupled to AlZnIn, the steel is expected to be protected as the potential was approximately -1070 mV. From table 4.2 one can see that the corrosion rate of steel was larger in coupling with AlZnIn than with 6005 Al. This is unexpected and not easily explained. Further, when coupled to both AlZnIn and 6005 Al, no metal loss whatsoever was found. Similarly, the 96-hour test gave a weight loss barely measurable. The protective current provided by 6005 Al is presumably close to negligible compared to what is provided by the anode. Thus, the corrosion rate in the coupling X65 CS / AlZnIn was expected to be considerably lower. Another surprising observation is that the weight loss found for galvanic crevice corrosion testing without cathodic protection is close to zero. The corresponding test without the factor of crevice corrosion gave a higher corrosion rate. A cavity pH of 3 and 4 was

measured in NaCl and seawater respectively, which should not be beneficial to steel. From the Pourbaix diagram in figure 2.4 an increased corrosion rate is expected as the pH decreases. Nevertheless, steel seems to be well protected by 6005 Al. Galvanic crevice corrosion testing with cathodic protection gave no measurable corrosion on steel in either test solution. A cavity pH of 10 was measured in both NaCl and seawater. From the Pourbaix diagram of steel, immunity of steel is expected at this pH and a potential of approximately -1070 mV. Based on the corrosion rate of steel, cathodic protection of steel-aluminium galvanic couples is possible, with or without the factor of crevice corrosion.

5.2.2 Aluminium

There was relatively little variation in weight loss of 6005 Al between the different experiments, where the highest weight loss was measured for two-metal testing with steel in NaCl. A high corrosion rate was expected for this test, as the galvanic current was stable between -30 and -40 $\mu A/cm^2$ on steel through the entire test period. The corrosion rate was lower in seawater, where the net current approached zero, and little protective current was provided to the steel sample. Coupling to AlZnIn gave a slight reduction in weight loss compared to what was found for open circuit testing. In three-metal coupling, the corrosion rates were in the same range, close to the values of self-corrosion. This indicates that the protective current provided from the anode to 6005 Al had little effect. Complete corrosion protection of aluminium is not expected as the metal is passive, and a certain part of the corrosion of the metal cannot be stopped electrochemically. It was also suggested that the immune area of the Pourbaix diagram for aluminium does not exist at all [19]. Thus, the term anodic protection is more applicable, rather than cathodic protection. However, the corrosion rates measured were very low, and application of aluminium in a three-metal system seems thus far possible. Further, a slight increase in corrosion rate was observed when the effect of crevice corrosion was introduced, especially in NaCl. This was expected, as the change in pH associated with crevice corrosion can be detrimental to aluminium. For galvanic crevice corrosion without cathodic protection, a pH of 3 and 4 was measured in NaCl and seawater respectively, which can explain the difference in measured weight loss between the two test solutions. Also, anodic current was measured on steel in the beginning of the test, suggesting that 6005 Al received reduction current in this period. With the application of cathodic protection, a cavity pH of 10 was measured for both solutions; however, the weight loss found in seawater is in the range of the open circuit measurements. This is not explained easily, but could be related to the accuracy of the pH measurements, which will be discussed in detail later.

5.2.3 AlZnIn

From table 4.4 it becomes evident that the higher reduction rate measured on steel gives rise to a high anode consumption. Comparison of the anode consumption between coupling with steel and with Al is in correspondence with the current density measured for the couplings. Thus, the consumption of the anode is to a high degree determined by the reduction current density on steel. This is evidenced by the lower weight loss measurements found for experiments involving crevice corrosion. A higher corrosion rate of aluminium was observed in these tests, however the reduction current on steel quickly decayed, reducing the anode consumption.

5.3 Surface characterization

The photographs of the steel samples from galvanic corrosion testing between X65 CS and 6005 Al showed little corrosion, indicating that the samples were well protected, though not completely. This is in correspondence with the electrochemical readings and weight loss measurements. From the micrograph in figure 4.33 it can be seen that aluminium clearly suffered from corrosion when coupled to steel in NaCl. This was also the sample that gave the highest corrosion rate of 6005 Al. EDS analysis of the steel sample tested in seawater against 6005 Al gave no indication of a protective surface layer containing Ca. Such a layer could contribute to the very low current densities measured in seawater (figure 4.5). Thus, the exponential decay in current is thus presumed to be caused by the almost identical open circuit potential of X65 CS and 6005 Al in seawater at the given time span.

The unexpected high weight loss of steel samples from galvanic corrosion testing with AlZnIn was not clarified from surface characterization. Only minor signs of localized corrosion was observed from macroscopic analysis, and the microscopic analysis, though not presented, showed very local pits with maximum size of 100 μm. The same morphology was seen on steel samples from three-metal galvanic corrosion testing, which gave no measurable corrosion. There is a certain error in the weight loss measurements of steel, related to the solution used for chemical cleaning; however, not enough to account for a weight loss this significant. Another explanation is the possibility of crevice corrosion between the metal sample and the lacquer coating. This was generally not a problem, but it is possible that it could have occurred on these samples and remained undetected, especially on the edges of the samples.

Microscopic analysis of 6005 Al samples that had been tested under cathodic protection in NaCl showed clear evidence of the alkaline etching process described by Gundersen and Nisancioglu [21]. From figure 4.35 one can see that the surface of the sample tested in NaCl was covered

with small pits no larger than 20 μm, whereas the sample tested in seawater showed no sign of such a process. The same morphology was seen for both two-metal testing with AlZnIn and three-metal testing. During the 96-hour test, the reduction current on 6005 Al showed only a very slight decay, and the cathodic sites were expected to be intact. From figure 4.41 one can see that most of the particles were intact, where only small dark spots indicate detachment. Although the test was run for a timespan of four times the primary duration, 96 hours is a very short period in terms of corrosion. Thus, it is expected that further detachment of cathodic sites would occur if the experiment were prolonged for a sufficient amount of time.

EDS analysis of the calcareous deposits formed on steel under cathodic protection revealed that no Ca was present on the surface of the deposits. However, when the deposits were scraped off the surface, and the layer of deposits close to the metal surface was analyzed, a significant amount of Ca was detected. The distribution of Ca was not found to be uniform. These results suggests that a thin layer of calcareous deposits with protective properties forms initially, close to the test initiation. As described by Okstad [15], there is a very fine balance between applied potential and convection, which determines the composition and thereby the protectiveness of calcareous deposits. From figure 2.5, it can be seen that the Ca/Mg ratio is expected to be close to zero under the conditions used in this work. The pH at which $CaCO_3$ and $Mg(OH)_2$ precipitate was calculated in previous studies [14], [15], and the conclusion was that $CaCO_3$ forms before $Mg(OH)_2$. This is supported by the results from this work. The thin layer containing Ca presumably forms as the steel surface becomes alkaline from reduction of water and hydrogen evolution. As the pH increases, the driving force for precipitation of $Mg(OH)_2$ is enhanced, and no further Ca precipitates due to inhibiton by Mg, as described by Okstad [15].

Analysis of the metal surfaces from galvanic crevice corrosion testing without cathodic protection revealed that the deposits found on the steel surface was a combination of corrosion products from both steel and aluminium. The measured weight loss of steel was close to zero for both test solutions, though. Microscopic analysis post chemical cleaning revealed that the only corrosion damage visible on steel was micropits. The aluminium surface also showed little sign on corrosion in NaCl, although the measured weight loss for this sample was considerable higher. However, the surface morphology was not completely uniform, and the SEM image in figure 4.44 was taken from a representative area of the sample. In seawater, 6005 Al showed some sign of an etching process on the surface, though the corrosion rate of this sample was smaller than for the sample tested in NaCl. Nevertheless, the acidic pH measured in these tests did thus not cause devastating corrosion damage to either metals.

71

Discussion

Examination of the sample surfaces from galvanic crevice corrosion testing with cathodic protection revealed that steel was protected, whereas aluminium suffered from localized corrosion. EDS analysis of steel samples prior to chemical cleaning showed that the white deposit layer shown in figure 4.30 and 4.31, consisted mainly of corrosion products from the aluminium sample. The deposits were concentrated near the crevice mouth, and correspondingly, corrosion damage was visible on the aluminium samples, primarily at the edge of the crevice. SEM images taken post chemical cleaning showed that the steel was completely protected, as suggested by the weight loss measurements. The aluminium however, suffered from significant corrosion damage near the crevice opening. Some minor corrosion was also visible in the middle of the samples, with some alkaline etching around cathodic inclusions, particularly in NaCl. However, the corrosion morphology at the edge of the samples consisted of hemispherical pits of varying size, some above 100 μm. The pits were not limited to cathodic sites, indicating a high pH, as described by Nisancioglu et al. [22]. The cavity pH was measured to 10 for both test solutions, but is assumed to be higher, as discussed earlier. Thus, the slightly higher corrosion rate of aluminium in galvanic crevice corrosion testing with cathodic protection is due to highly localized corrosion near the crevice mouth, and the phenomena could be detrimental for the lifetime of a structure where such a metal system was applied. However, from the electrochemical measurements, it was seen that the anodic current on aluminium decayed towards zero, indicating that the high corrosion rate is only an initial stage.

From the electrochemical measurements and results from surface characterization, the mechanism of galvanic crevice corrosion of steel and aluminium with cathodic protection can be explained. As suggested in previous studies and crevice corrosion theory [4], [23], [24], there is initially of potential and current distribution along the crevice due to ohmic potential drop, and the current is concentrated at the crevice mouth. As oxygen is depleted inside the crevice the current density decreases. The distribution of potential and current also becomes more even as a function of time. Based on this, the current behavior in three-metal galvanic corrosion testing can be explained by the following mechanism: The reduction current density on steel is initially high, and concentrated at the crevice mouth. The very high local reduction rate causes a high pH, which causes the aluminium to corrode at a rate sufficiently high to give positive net current. As the current density on steel decreases due to depletion of oxygen, and the distribution becomes more even, the reduction rate at the crevice mouth decreases, and the pH is lowered by diffusion. The corrosion rate of aluminium is consequently reduced. Thus, the symmetric shape of the current curves of steel and aluminium in figure 4.15 and 4.16 is

explained. The reduction rate on steel is the controlling factor; the anodic current on aluminium is controlled by the local pH, which is kept in balance by diffusion and the reduction rate on steel.

5.4 Experimental work

5.4.1 Experimental procedures

Before electrochemical testing began, all electrical circuits were checked for ohmic resistance. As described in the experimental section, connection of samples involved direct contact with a copper wire, excluding the use of extra clamps, which can contribute to electric resistance. All contacts were checked, and all readings were below 0.1 Ω. During galvanic corrosion testing, the connection point on the sample was placed above the solution; however, the contact was covered completely with a coating, as a precaution. For galvanic crevice corrosion testing, the crevice device, and thereby the connection points, were submerged in the electrolyte. Thus, once the test was completed, the coating was removed and all electric contacts were checked for corrosion and/or exposure to the solution. The samples were inspected visually for corrosion beneath the coating, and the conductivity in the wires were measured. There was no sign of exposure in any cases, and the experimental coupling method was regarded satisfactory.

Two experimental setups were used simultaneously: two potentiostats, two cells and two reference electrodes. The potential difference between the reference electrodes was measured to a few mV, and the difference was regarded negligible. Also, several test runs were performed for the two potentiostats to check if the results were reproducible between them. No significant difference was observed. However, it was not possible to conclude that the readings were completely consistent between the two setups, thus a certain degree of deviation between parallel testing could be related to the use of different setups.

Three different coatings were used; the Miccro lacquer and the nail polish was easily removed from the samples post testing. However, the bee wax required boiling of the samples for complete removal. Several test specimens coated with the wax was boiled and weighed to check if the removal process caused metal loss, or if the wax was in fact completely removed. The only measurable change in mass was 0.1 mg, which is the error of the weight used. Thus, removal of the coating is not a source of error in the weight loss measurements. However, the use of bee wax caused some practical difficulties, especially during microscopic surface characterization prior to chemical cleaning. As the samples needed to be analyzed in SEM before being immersed in boiling water, the specimens were coated with wax during analysis.

Discussion

Proper electric contact during SEM analysis was challenging, and was achieved by applying a silver tape from the specimen holder onto the exposed surface of the sample. Although the method proved to be satisfactory, an alternative to the wax would have been preferred. Another aspect regarding the coatings is the possibility of crevice corrosion. This was only seen as minor problem for the lacquer coating applied on steel; no sign of such a problem was observed on samples coated with bee wax or nail polish.

The weight loss measurements of X65 CS carry a fair amount of error related to the solution used for chemical cleaning. The solution does not only remove corrosion products, but causes some metal loss as well. The weight loss caused by corrosion has to be estimated by plotting accumulated weight loss and number of cleaning cycles (see appendix A), as well as using an uncorroded reference sample. The use of a reference sample became an issue as the measured weight loss of corroded samples sometimes was very low, on the limit of what was measurable. This was a problem particularly for steel samples that had been tested under cathodic protection. The weight loss of the reference sample could exceed that of the tested sample. Very low corrosion rates was a general problem. Distinguishing corrosion rates of different samples was sometimes very difficult, as the measured weight loss was close to the limit of the scale used, 0.1 mg. Thus, very small differences in reported corrosion rates could be associated with the error of the analytical weight. Another issue regarding weight loss measurements is that the experiments were not run for the same period of time, ranging from 24 to 96 hours. The corrosion rate is not expected to be constant during testing. Thus, comparison of results from experiments of different durations might not give a realistic picture.

After galvanic crevice corrosion testing, a pH strip was placed on the metal surfaces in attempt to measure the pH of the cavity. The reported pH measurements are regarded rather inaccurate. At the end of the test, the crevice device was carefully lifted up from the test cell. Even though this was done with great caution, the effect of convection certainly caused dilution of the crevice chemistry to some degree. Also, when the device was opened, exposing the samples, there was barely enough electrolyte on the metal surfaces to get a reading off the pH strip. It was necessary to pass the strip over the whole surface of both samples, and even then, the wetting of the strip seemed inadequate. Thus, a larger volume of the crevice chemistry might have given a slightly different reading.

Further, a weakness in the work performed in this project is the lack of parallel testing. For the galvanic corrosion tests, a considerable amount of parallel testing was performed in the author's specialization project [30]; however, little or no parallel testing was performed for the

remaining experiments due to time constraints and unforeseen events. Thus, the results carry little statistical reliability.

5.4.2 Limitations: laboratory conditions versus real conditions

Small scale laboratory testing may provide an answer to whether application of steel-aluminium galvanic couples is possible; however, the experimental conditions used in this work does not reflect the conditions that a real structure would be subjected to. All experiments were conducted at a temperature of 25 ºC. A temperature closer to subsea temperatures would presumably have a significant effect on corrosion rates, electrochemical behavior and the kinetics of precipitation of calcareous deposits. Another important factor is convection. The present work was performed in stagnant solutions, whereas a certain flow rate would be present in real conditions. This factor would greatly affect the results, as many of the processes discussed are controlled by a change of pH in the diffusion layer, particularly corrosion of aluminium and composition of the calcareous deposits on steel.

Although artificial seawater is better than NaCl as a substitute for ocean water, it lacks the biological factors, which has to be considered for real application of the three-metal system. Marine growth and biological factors along with the deposits from the chemistry of seawater would give a different surface layer than what is found in a laboratory test using artificial seawater. Furthermore, the duration of the tests is a very short time in terms of corrosion. Some of the electrochemical phenomena found in this project might be a short initial stage, and to extrapolate the measured corrosion rates from a 24 hour test to several years is unrealistic. Thus, the weight loss measurements might not reflect the corrosion rate of a real structure, but can still be compared to each other.

5.5 Further work

Based on the experimental work performed in this thesis and discussions of the results, suggestions for further work have been made. The following bullet points present work which purpose is to further investigate whether cathodic protection of steel-aluminium galvanic couples is possible.

- Perform parallel testing of present results to confirm the findings and give the results statistical reliability.
- Perform experiments over an extended period of time (weeks) in order to investigate a) whether or not 6005 Al undergoes an etching process in seawater similar to what is seen

in NaCl, b) if the anodic current measured on 6005 Al in galvanic crevice corrosion testing with cathodic protection drops below zero.

- Change test parameters so that the experimental conditions to a higher degree reflect that of a real structure: Natural seawater, convection and lower temperatures.

- Develop a more sophisticated setup for conducting galvanic crevice corrosion testing. It would be interesting to measure the distribution of potential and current along the crevice. Also, a more accurate method of measuring pH inside the cavity is desirable.

- Perform crevice corrosion tests of each metal against an inert plane (no galvanic coupling), to get a better understanding of the behavior of each metal under crevice corrosion.

- Record polarization curves for all three alloys in seawater.

- The duration of the galvanic corrosion tests should be extended from 24 hours. All tests should be run with the same primary duration, making measurements more easy to compare, particularly the corrosion rates.

- Increase the exposed area of the samples. This too is related to the corrosion rates. Higher weight losses would make a more clear pattern regarding different couplings and test solutions; the difference between samples would be more evident, and the error related to very low corrosion rates would no longer be an issue.

- Further investigate the protective properties of the calcareous deposits formed on steel, possibly introducing new methods of analysis, such as XRD.

Chapter 6

Conclusions

X65 carbon steel, 6005 aluminium and AlZnIn has been studied in laboratory testing in order to answer whether cathodic protection of steel-aluminium galvanic couples is possible. The testing has involved electrochemical experiments, weight loss measurements and surface characterization. The following has been found:

- Cathodic protection of steel-aluminium galvanic couples is possible in the absence of crevice corrosion.

- The sacrificial anode supplied cathodic current to both steel and aluminium, in a similar way as for cathodic protection of each metal by itself.

- Steel required near all current from the anode. The reduction rate on steel was between 1 and 2 orders of magnitude larger than that on aluminiumum. For aluminium, the reduction reactions occur only on the Fe-rich intermetallic particles in the Al matrix, i.e. a small fraction of the surface area. Reduction may occur on the entire steel surface.

- During cathodic protection of steel in seawater, calcareous deposits formed on the metal surface. The composition of the deposits were not uniform; close to the metal surface, the deposits contained $CaCO_3$, whilst the remaining deposits consisted of mainly $Mg(OH)_2$. The deposits gave little or no reduction of the current density on steel, as the dominating reduction reaction is hydrogen evolution at a potential controlled by AlZnIn. Further, compared to testing in NaCl, the calcareous deposits seemed to enhance hydrogen evolution. The Tafel slope of the hydrogen evolution reaction was found to be -230 mV/dec on steel covered with calcareous deposits and -115 mV/dec on bare steel in NaCl. At a potential of -1070 mV (Ag/AgCl), the reduction current density was significant larger in seawater.

- During cathodic protection of aluminium in NaCl, the current density decayed towards zero. This was due to alkaline etching of the cathodic sites, made possible by the alkaline

diffusion layer formed under cathodic protection. No such phenomena was seen in seawater due to a higher buffer capacity.

- Galvanic crevice corrosion between steel and aluminium without cathodic protection gave an increased corrosion rate of aluminium due to a low cavity pH. The steel appeared to be near fully protected.

- When cathodic protection was applied to the galvanic crevice coupling between steel and aluminium, a positive net current was measured on aluminium, i.e. anodic. The measured weight loss of aluminium was relatively low, but surface characterization showed that the corrosion damage was highly localized near the crevice mouth. The steel was completely protected. A cavity pH of 10 was measured in both test solution.

- The morphology of the corrosion and electrochemical measurements were explained by the presence of a potential and current distribution along the crevice. The current was initially concentrated near the crevice mouth. The very high local reduction rate on steel gave a high local pH, which caused aluminium to corrode at a rate sufficiently high to give positive net current. As oxygen was depleted inside the crevice, the reduction rate decreased. The lower reaction rate on steel, combined with diffusion reduced the pH, and thereby the corrosion rate of aluminium. The anodic current decayed towards zero.

- Although being seen as an initial stage, the local corrosion on aluminium could be detrimental to a structure, and the phenomena needs further investigation.

References

1. C. Knutsen, I. Kvale, J. H. Nordlien, *Aluminium Applied for Subsea Structures: Possibilities and Challenges,* Stavanger, 2001.
2. *Kompetanseprosjekt for næringslivet, mal for prosjektbeskrivelse,* 2010.
3. DNV, *Cathodic Protection Design,* in *Recommended Practice DNV-RP-B401,* 2011.
4. K. Nisancioglu, *Corrosion Basics and Engineering,* Norwegian University of Science and Technology, 2014.
5. M. J. Pryor and D. S. Keir, *Galvanic corrosion. Current Flow and Polarization Characteristics of the Aluminium-Steel and Zinc-Steel Couples in Sodium Chloride Solution,* Journal of the Electrochemical Society, 1957.
6. F. Mansfeld and E. P. Parry, *Galvanic corrosion of bare and coated Al alloys coupled to stainless steel 304 or Ti-6Al-4V,* Corrosion Science, 1973.
7. J. Fournier et al., *Hydrogen Evolution Reaction in Alkaline Solution,* Journal of the Electrochemical Society, 1996.
8. M. Stern, *The Electrochemical Behavior, Including Hydrogen Overvoltage, of Iron in Acid Environments,* Journal of the Electrochemical Society, 1955.
9. Gamry Instruments, *Reference Electrodes,* 2016. [cited 27.05.16]; available from: http://www.gamry.com/products/accessories/reference-electrodes/
10. F. Gaalsgard, L. V. Nielsen, *AC/DC interference corrosion in pipelines,* Metricorr, 2006.
11. NORSOK, *Cathodic Protection M-503,* in *Common Requirements,* 1997.
12. Ph. Refait et al., *Corrosion and cathodic protection of carbon steel in the tidal zone: products, mechanisms and kinetics,* Corrosion science, 2015.
13. S. Elbeik, A. C. C. Tseung and A. L. Mackay, *The formation of calcareous deposits during the corrosion of mild steel in sea water,* Corrosion science, 1986.
14. Y. Yang, J. D. Scantlebury and E. V. Koroleva, *a Study of Calcareous Deposits on Cathodically Protected Mild Steel in Artificial Seawater,* metals, 2015.
15. T. Okstad, *Hydrogenutvikling ved katodisk beskyttelse av karbonstål i naturlig sjøvann,* Master's thesis, NTNU, 2005.
16. T. Okstad et al., *Significance of Hydrogen Evolution During Cathodic Protection of Carbon Steel in Seawater,* Corrosion, 2007.
17. S. H. Salleh et al., *Enhanced hydrogen evolution on $Mg(OH)_2$ covered Mg surfaces,* Electrochimica Acta, 2015.
18. K. Nisancioglu, *Corrosion and protection of aluminum alloys in seawater.* Corrosion behavior of copper and aluminium alloys in seawater, 2007.
19. G. G. Perrault, *The Role of Hydrides in the Equilibrium of Aluminum in Aqueous Solutions,* Journal of the Electrochemical Society, 1979.
20. N. L. Sukiman et al., *Durability and Corrosion of Aluminium and its Alloys: Overview, Property Space, Techniques and Developements,* Aluminium Alloys – New trends in Fabrication and Applications, chapter 2, 2012.

21. R. Gundersen, K. Nisancioglu, *Cathodic protection of Aluminum in Seawater,* Corrosion, 1990.
22. K. Nisancioglu, K. Y. Davanger and Ø. Strandmyr, *Cathodic Behavior of Impure Aluminum in Aqueous Media,* Journal of the Electrochemical Society, 1981.
23. S. Joma et al., *Incongruent dissolution of copper in an Al-Cu assembling. Influence of local pH changes,* Surface and Interface Analysis, 2013.
24. Z. Li, F. Gan and X. Mao, *A study on cathodic protection against crevice corrosion in dilute NaCl solutions,* Corrosion Science, 2002.
25. H. Möller, E. T. Boshoff and H. Froneman, *The corrosion behavior of a low carbon steel in natural and synthetic seawater,* Journal of the South African institute of mining and metallurgy, 2006.
26. K. Nisancioglu, *Personal communication,* NTNU, 2016.
27. A. Bergin, *Alternating Current Corrosion of Steel in Seawater,* Master's thesis, NTNU, 2015.
28. ASTM, *Standard Practice for the Preparation of Substitute Ocean Water,* in *D1141*, 2013.
29. ASTM, *Standard Practice for Preparing, Cleaning and Evaluating Corrosion Test Specimens,* in *G1,* 2011.
30. S. Røstbø, *Cathodic protection of steel-aluminium galvanic couples for a new generation of light-weight subsea structures,* Specialization project, NTNU, 2015.
31. K. Nisancioglu, *Personal communication,* NTNU, 2015.
32. K. Forthun, *Alternating Current Corrosion of Aluminium Sacrificial Anodes,* Master's thesis, NTNU, 2013.
33. K. Nisancioglu, *Personal communication,* NTNU, 2015

List of symbols

Symbol	Explanation	Unit
C_b	Bulk concentration	$mol \cdot m^{-3}$
C_s	Surface concentration	$mol \cdot m^{-3}$
D	Diffusion coefficient	$m^2 \cdot s^{-1}$
dc/dx	Concentration gradient	$mol \cdot m^{-4}$
E_C	Coupling potential	V
E_{corr}	Corrosion potential	V
E_h	Potential at crevice opening	V
E_{in}	Potential inside crevice	V
E_M	Potential of metal M	V
E_N	Potential of metal N	V
E_{out}	Potential outside crevice	V
E_p	Protection potential	V
F	Faradys constant	$C \cdot mol^{-1}$
i	Current density	$A \cdot m^{-2}$
i_0	Exchange current density	$A \cdot m^{-2}$
I_{corr}	Corrosion current	A
$I_{corr(M-\underline{N})}$	Corrosion current of metal N due to galvanic coupling of metal M	A
$I_{corr(\underline{M}-N)}$	Corrosion current of metal M due to galvanic coupling of metal N	A
I_g	Galvanic current	A
i_{lim}	Limiting current density	$A \cdot m^{-2}$
i_{max}	Maximum current density	$A \cdot m^{-2}$
I_{net}	Net current	A
$I_{ox,M}$	Oxidation current of metal M	A
$I_{ox,N}$	Oxidation current of metal N	A
i_{ss}	Steady state current density	$A \cdot m^{-2}$
$I_{red,M}$	Reduction current of metal M	A
$I_{red,N}$	Reduction current of metal N	A

J_{O_2}	Flux of O_2	$mol \cdot m^{-2} \cdot s^{-1}$
n	Number of electrons	-
R	Gas constant	$J \cdot K^{-1} \cdot mol^{-1}$
R_{el}	Resistance in electrolyte	Ω
R_{ext}	Resistance in external circuit	Ω
T	Temperature	K
t_{max}	Time corresponding to maximum current density	S
t_{ss}	Time corresponding to steady state current density	S
α	Charge transfer coefficient	-
δ	Crevice thickness	m
δ_N	Thickness of Nernst diffusion layer	m
η	Overpotential	V
η_c	Concentration overpotential	V
σ	Conductivity	$S \cdot m^{-1}$
φ_g	Galvanic potential	V

APPENDICES

Appendix A: Weight loss of X65 carbon steel

Removal of corrosion products from X65 carbon steel was done by chemical cleaning according to ASTM G-1 [29]. The cleaning solution caused metal loss of the sample, and a weight loss graph as shown in figure A.1 was used to determine weight loss due to corrosion testing. The sample was chemically cleaned in several cycles, and weight loss was determined between each cycle. Accumulated weight loss was plotted against number of cleaning cycles, and the resulting curve can be divided into two trend lines, where the mass loss due to corrosion is given by the intersection of the lines. An untested reference sample was used to correct for metal loss.
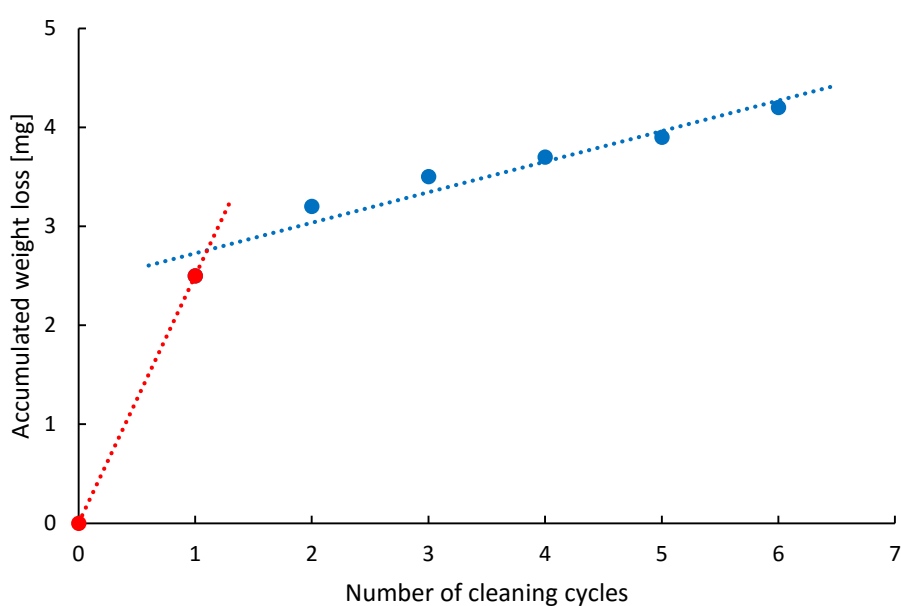
Figure A.1. Weight loss graph for X65 carbon steel.

Appendix B: Additional SEM and EDS data

Galvanic corrosion: X65 CS and 6005 Al
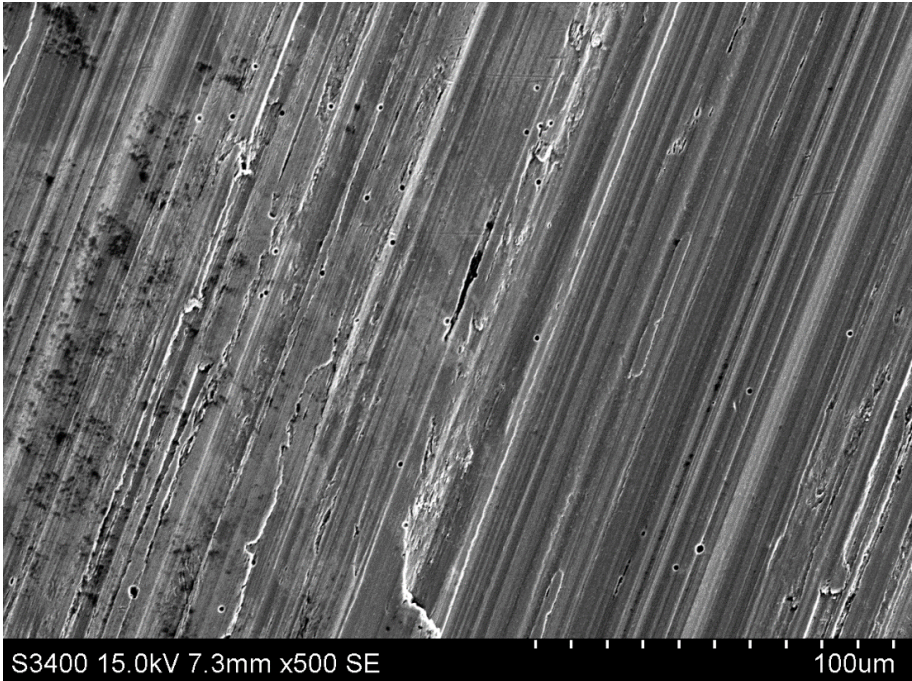
Figure B.1. SEM image of an X65 CS sample from galvanic corrosion testing between X65 CS and 6005 Al in NaCl. The image was taken post chemical cleaning.
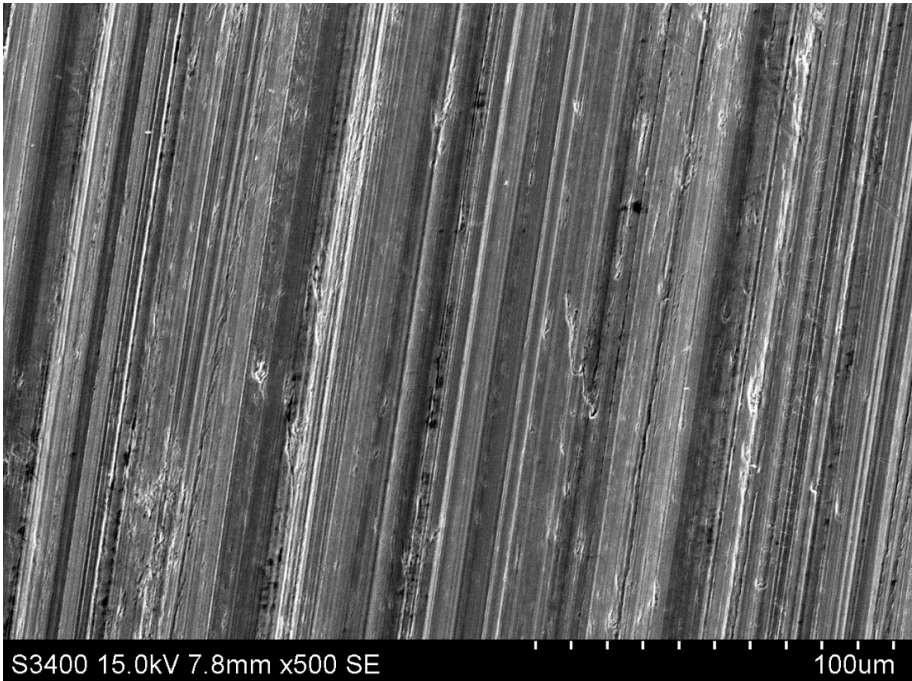
Figure B.2. SEM image of an X65 CS sample from galvanic corrosion testing between X65 CS and 6005 Al in seawater. The image was taken post chemical cleaning.
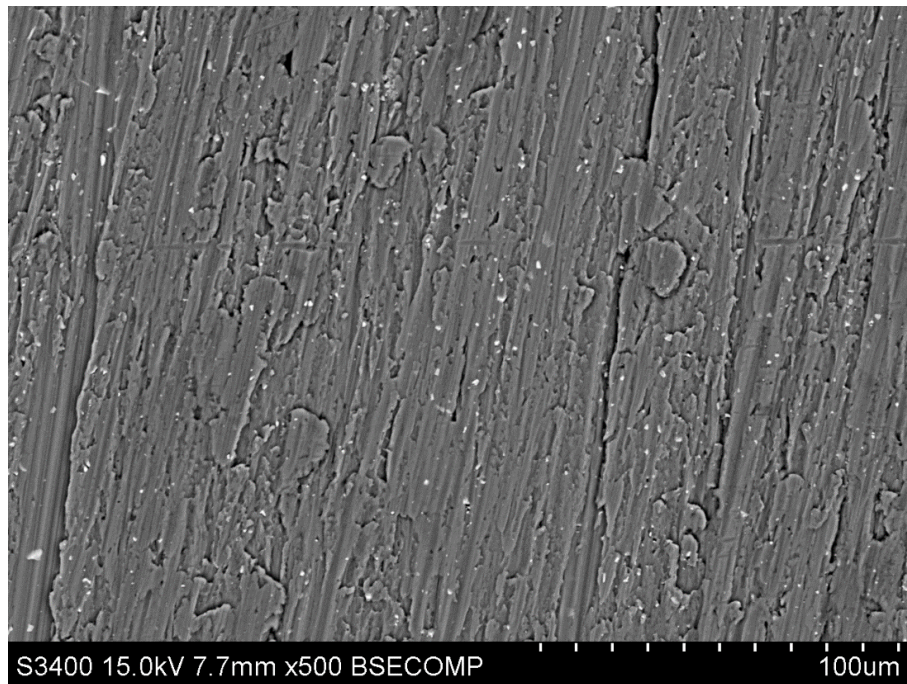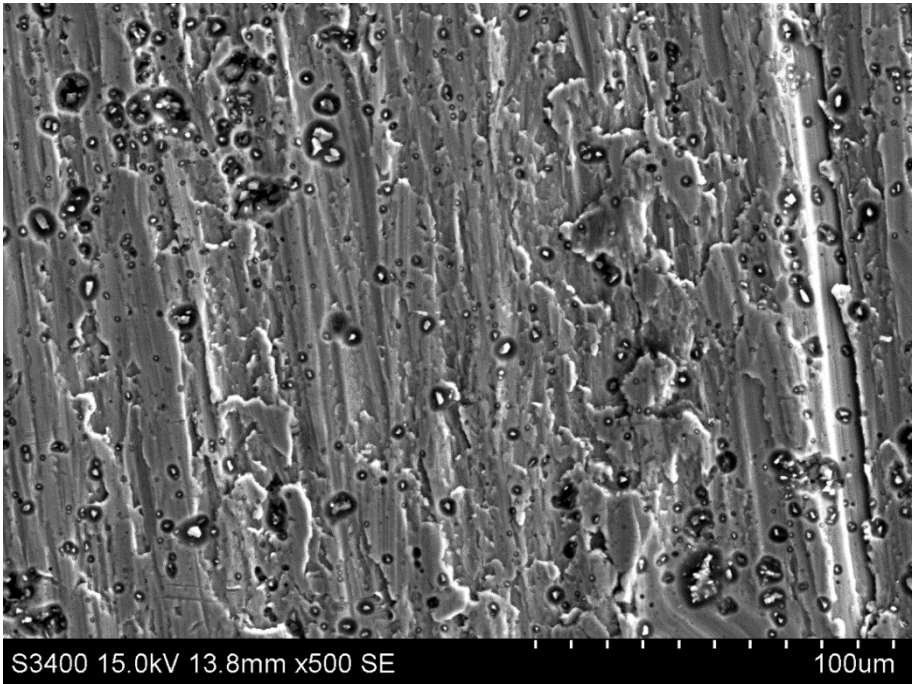
Figure B.3. SEM (backscatter) image of a 6005 Al sample from galvanic corrosion testing between X65 CS and 6005 Al in seawater. The image was taken post chemical cleaning.

Figure B.4. SEM image of an X65 CS sample from galvanic corrosion testing between X65 CS and AlZnIn in NaCl. The image was taken prior to chemical cleaning.
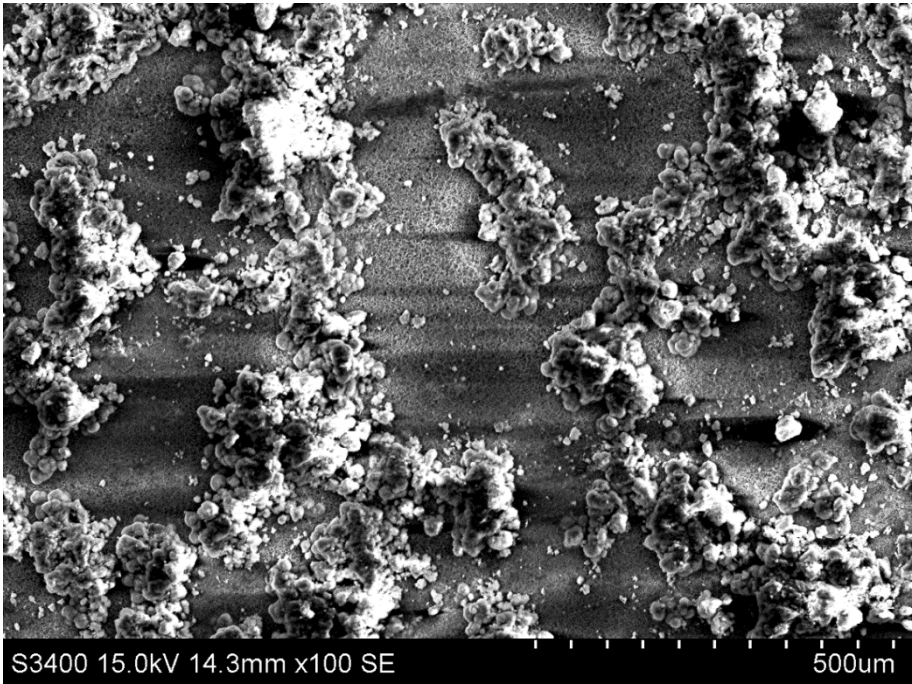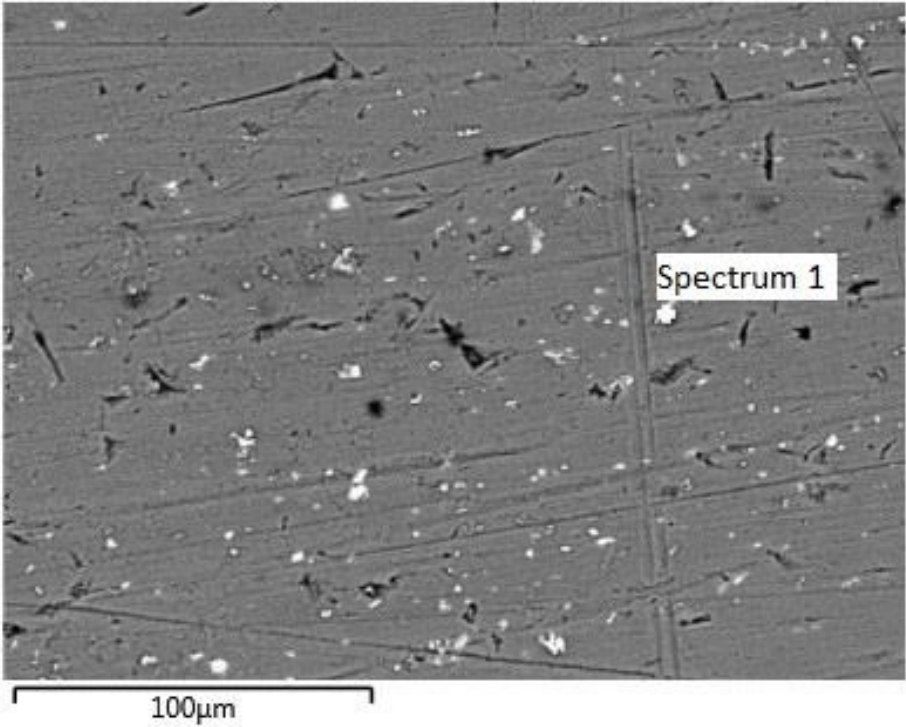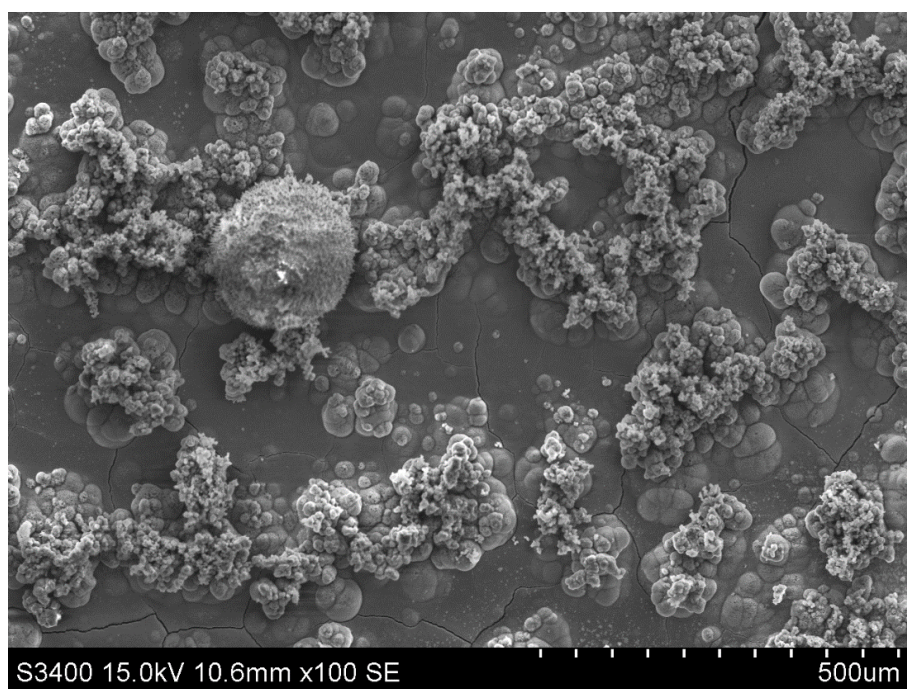
Figure B.5. SEM image of an X65 CS sample covered with calcareous deposits from galvanic corrosion testing between X65 CS and AlZnIn in seawater.
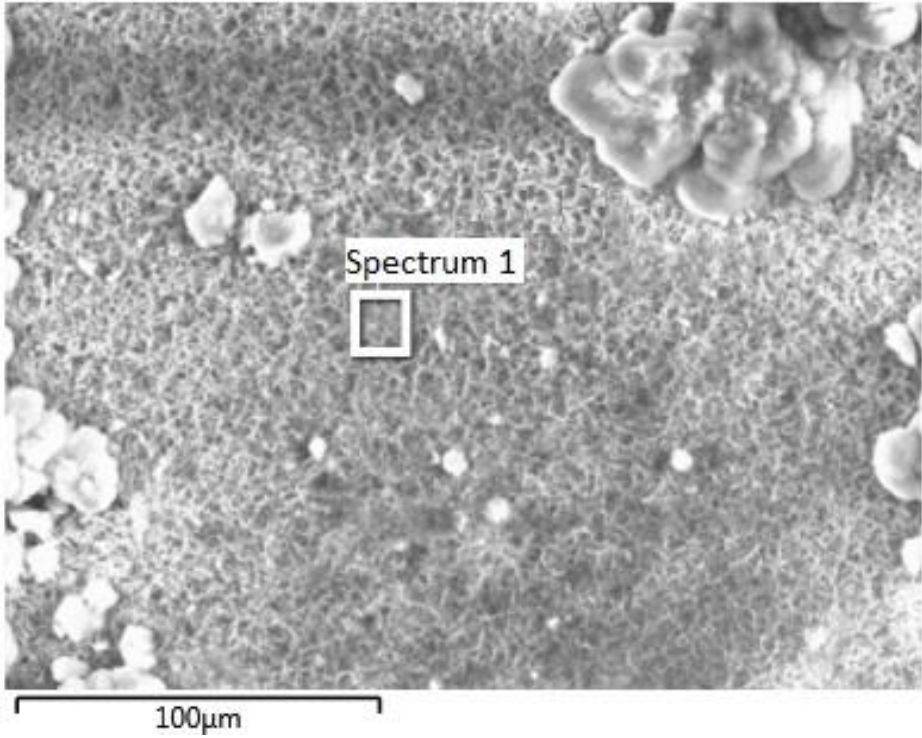
Figure B.6. SEM image of an X65 CS sample covered with calcareous deposits from galvanic corrosion testing between X65 CS and AlZnIn in seawater, including area of EDS analysis.

Table B.1. EDS analysis for spectrum 1 in figure B.6.

Element	wt%
O	52.48
Mg	39.86
C	4.11
Cl	1.87
Na	0.87
Fe	0.56
Ca	0.25

S3400 15.0kV 7.4mm x500 SE   100um
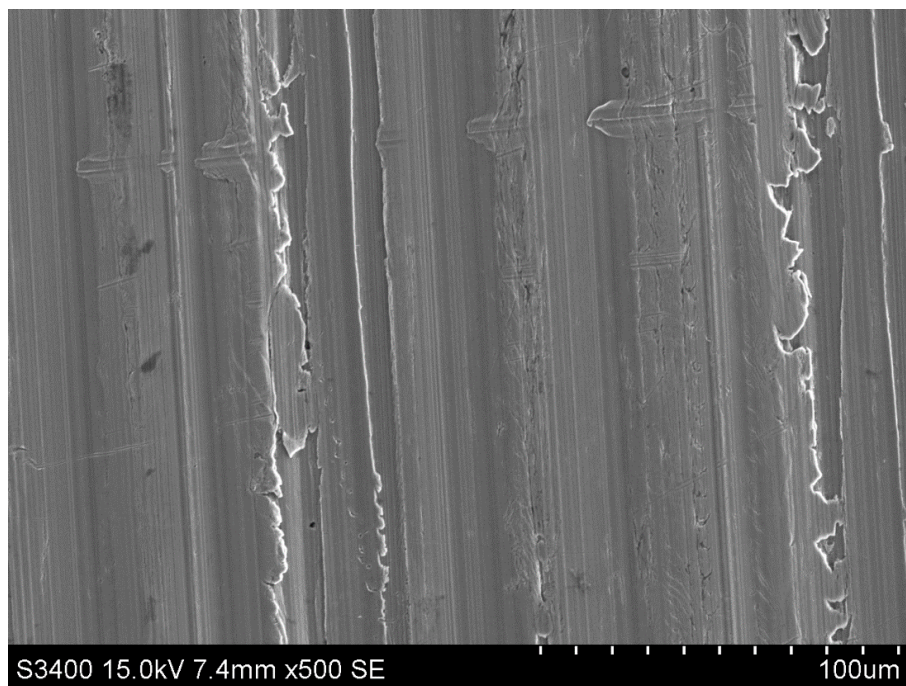
Figure B.7. SEM image of an X65 CS sample from galvanic corrosion testing between X65 CS and AlZnIn in seawater. The image was taken post chemical cleaning.

Figure B.8. SEM image of a 6005 Al sample from galvanic corrosion testing between 6005 Al and AlZnIn in NaCl. The image was taken prior to chemical cleaning.

Figure B.9. SEM (backscatter) image of a 6005 Al sample from galvanic corrosion testing between 6005 Al and AlZnIn in seawater, including area of EDS analysis. The image was taken post chemical cleaning.

Table B.2. EDS analysis for spectrum 1 in figure B.9.

Element	wt%
Al	74.64
Fe	10.45
C	8.25
Si	3.33
Mn	1.95
O	0.97
Mg	0.41

S3400 15.0kV 10.6mm x100 SE 500um

Figure B.10. SEM image of an X65 CS sample covered with calcareous deposits from 96-hour three-metal galvanic corrosion testing in seawater.
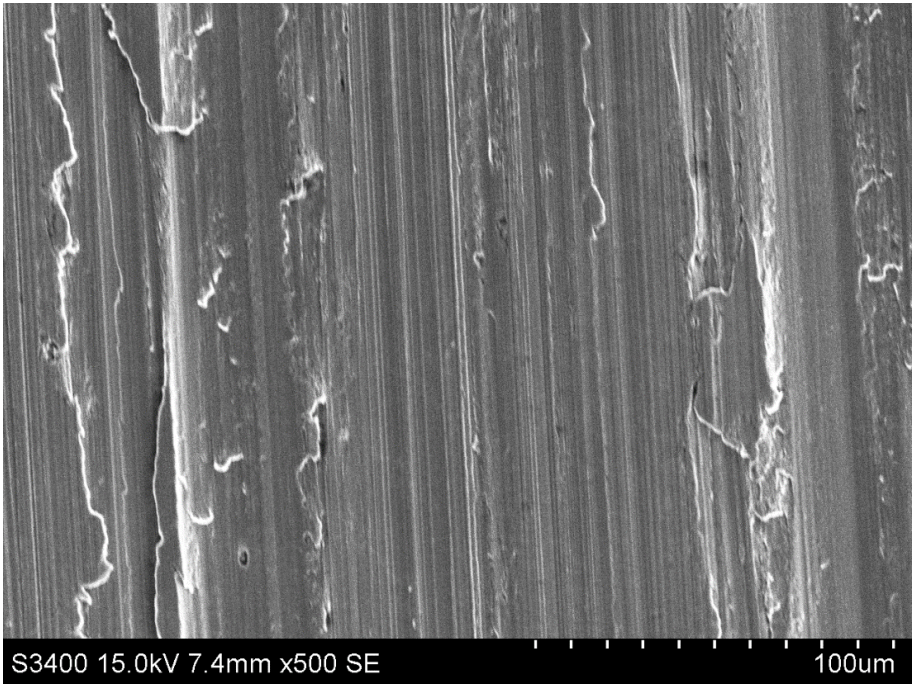
Figure B.11. SEM image of an X65 CS sample from 96-hour three-metal galvanic corrosion testing seawater. The image was taken post chemical cleaning.
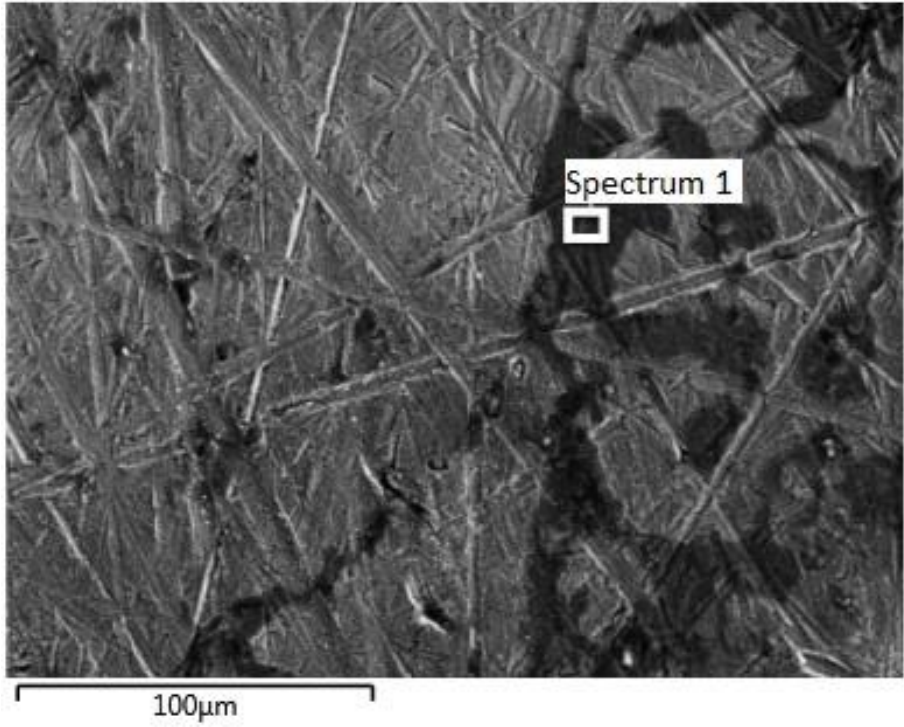
Figure B.12. SEM image of an X65 CS samples after two-metal galvanic crevice corrosion testing in seawater, including area of EDS analysis. The image was taken prior to chemical cleaning.

Table B.3. EDS analysis for spectrum 1 in figure B.12.

Element	wt%
Fe	70.45
Al	5.78
O	15.32
C	6.48
Mn	0.91
Cl	0.38
Na	0.68
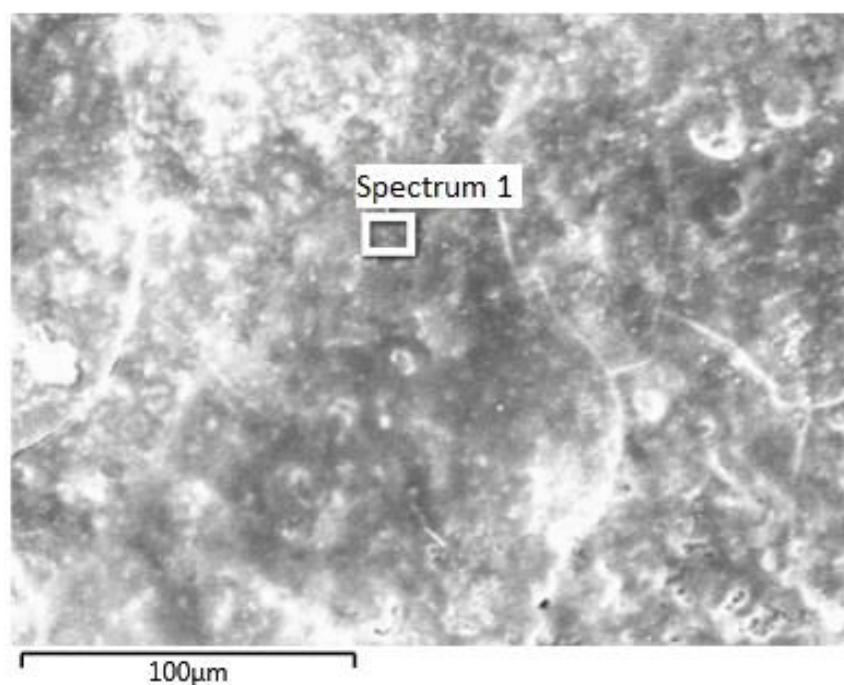
Figure B.13. SEM image of the white deposits seen on the 6005 Al sample from galvanic crevice corrosion testing with cathodic protection in seawater, including area of EDS analysis. The image was taken near the crevice mouth, prior to chemical cleaning.

Table B.4. EDS analysis for spectrum 1 in figure B.13.

Element	wt%
O	59.07
Al	33.51
C	5.72
Ca	0.91
Mg	0.79

Appendix C: Data from previous work

The following data was recorded in the author's specialization project [30]. Figure C.1 and C.2 shows the results from galvanic corrosion testing of X65 CS and 6005 Al in NaCl and seawater respectively. Potential measurements for parallel 1 in NaCl and parallel 2 in seawater is lacking due to a defect reference electrode used in these experiments.
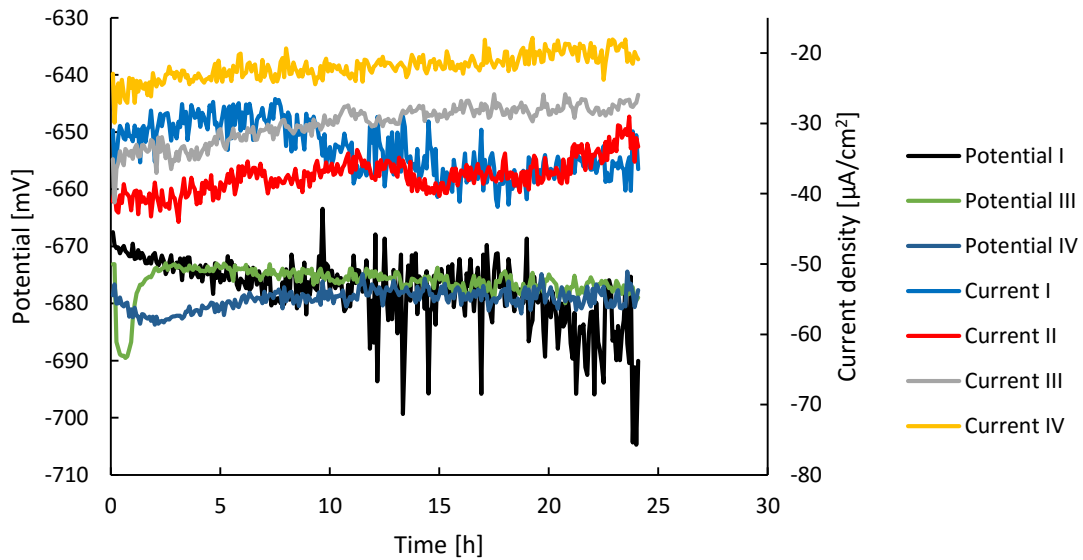
Figure C.1. Galvanic corrosion test between X65 carbon steel and 6005 aluminium in 3.5% NaCl solution. Recorded coupling potential and galvanic current as a function of time.
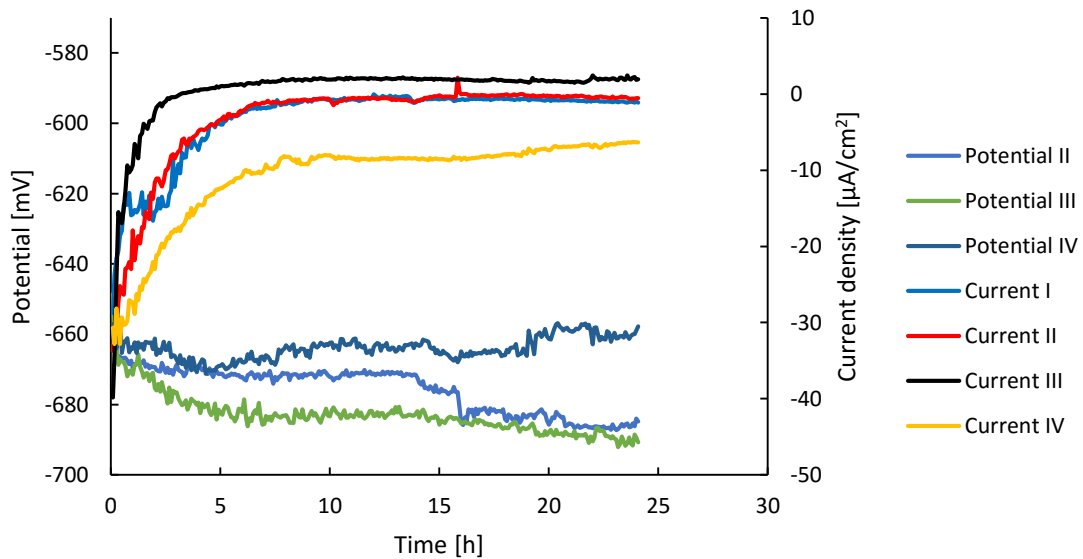
Figure C.2. Galvanic corrosion test between X65 carbon steel and 6005 aluminium in artificial seawater. Recorded coupling potential and galvanic current as a function of time.

Figure C.3 and C.4 shows the results from galvanic corrosion testing of X65 CS and AlZnIn in NaCl and seawater respectively.
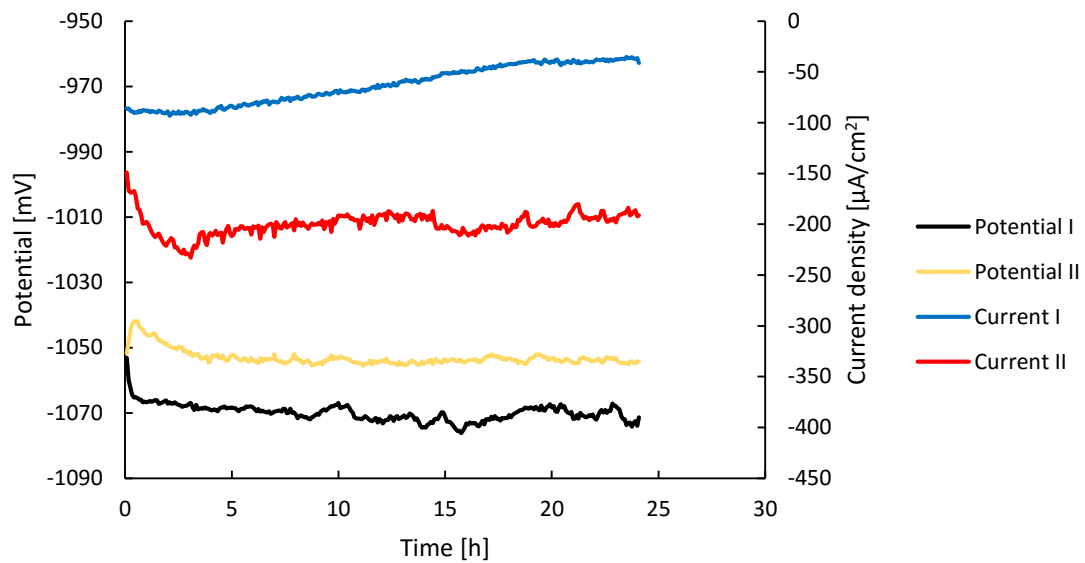
Figure C.3. Galvanic corrosion test between X65 carbon steel and AlZnIn in 3.5% NaCl solution. Recorded coupling potential and galvanic current as a function of time.
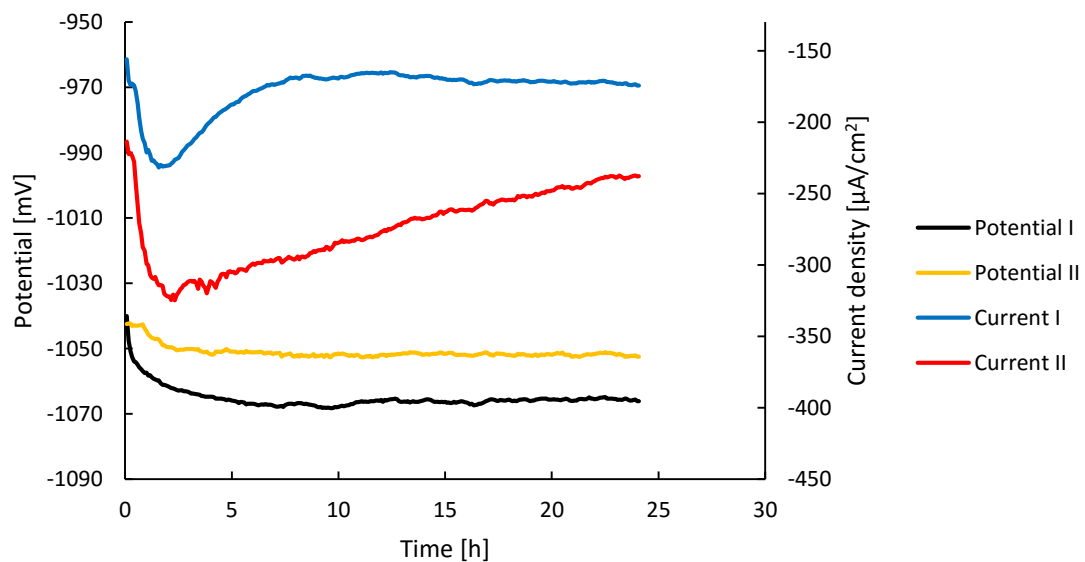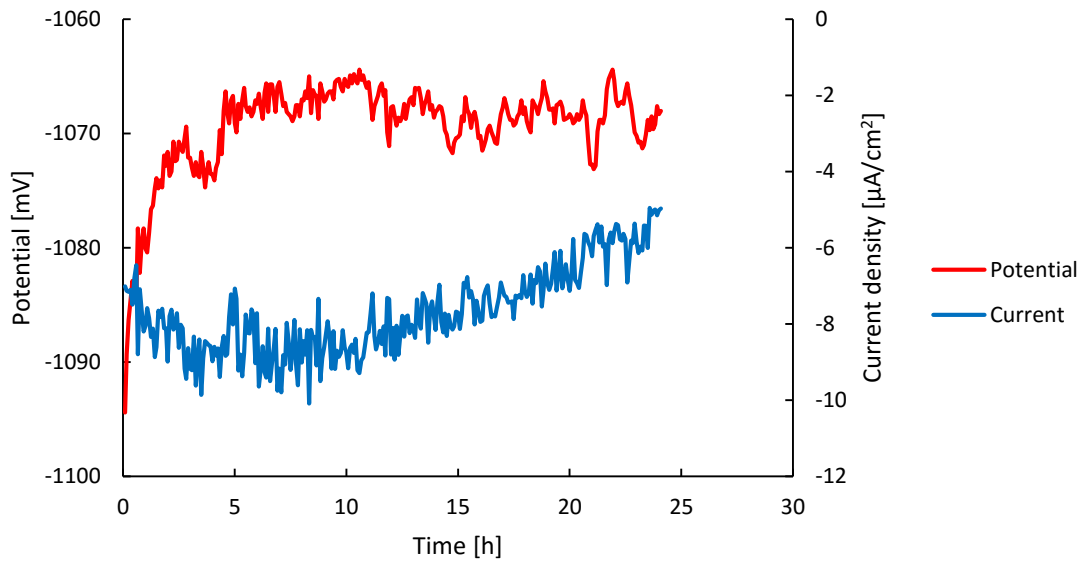

Figure C.4. Galvanic corrosion test between X65 carbon steel and AlZnIn in artificial seawater. Recorded coupling potential and galvanic current as a function of time.

Appendix C

Figure C.5 and C.6 shows the results from galvanic corrosion testing of 6005 Al and AlZnIn in NaCl and seawater respectively.

Figure C.5. Galvanic corrosion test between 6005 aluminium and AlZnIn in 3.5% NaCl solution. Recorded coupling potential and galvanic current as a function of time.
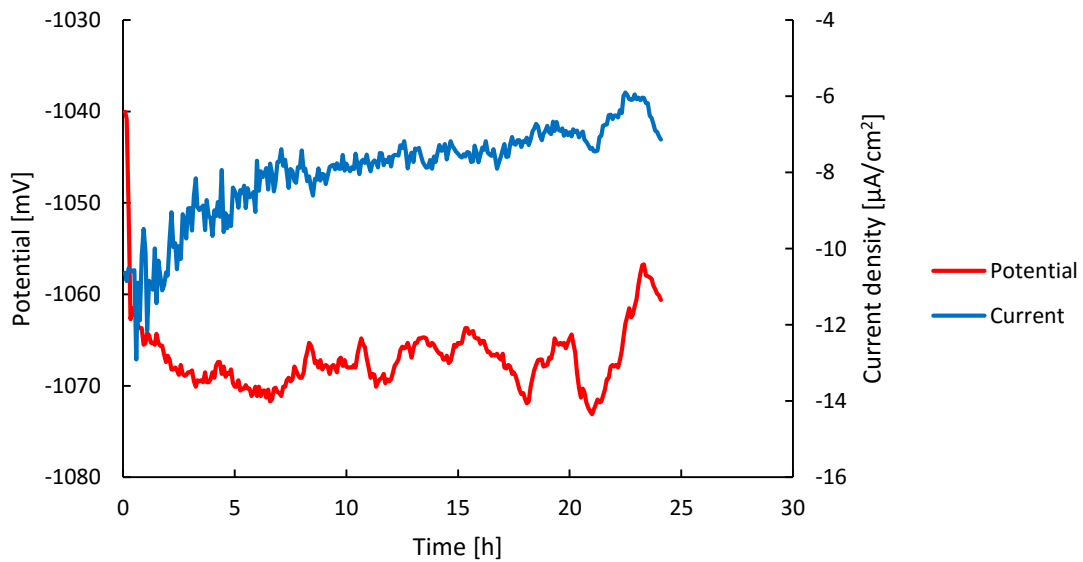

Figure C.6. Galvanic corrosion test between 6005 aluminium and AlZnIn in artificial seawater. Recorded coupling potential and galvanic current as a function of time.

Figure C.7 through C.10 shows the results from galvanic corrosion testing of 6005 Al and AlZnIn in NaCl and seawater. Two parallels for each solution was performed, and is presented separately.
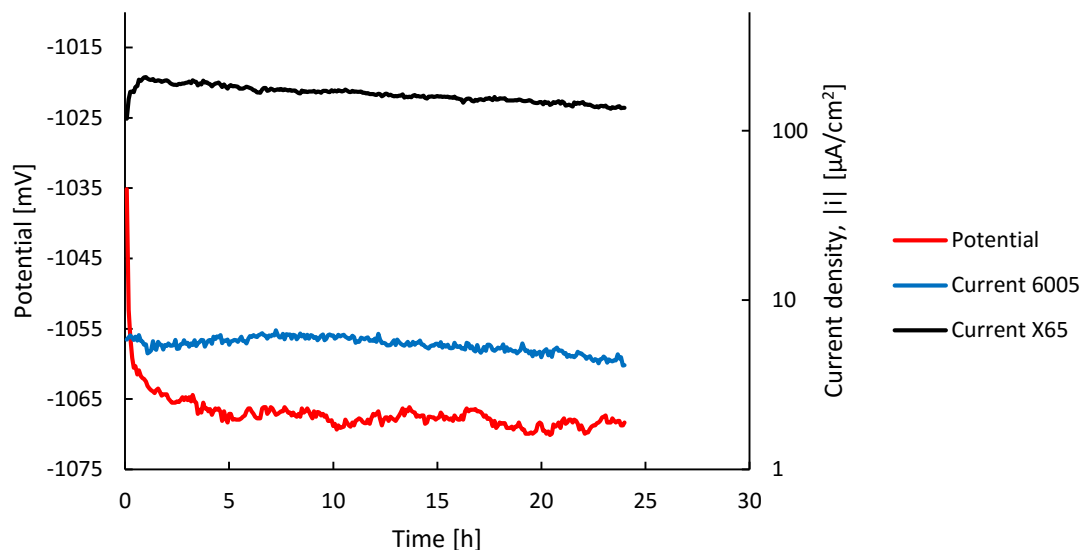

Figure C.7. Parallel 1 of galvanic corrosion test between X65 carbon steel, 6005 aluminium and AlZnIn in 3.5% NaCl solution. Recorded coupling potential and galvanic current as a function of time.
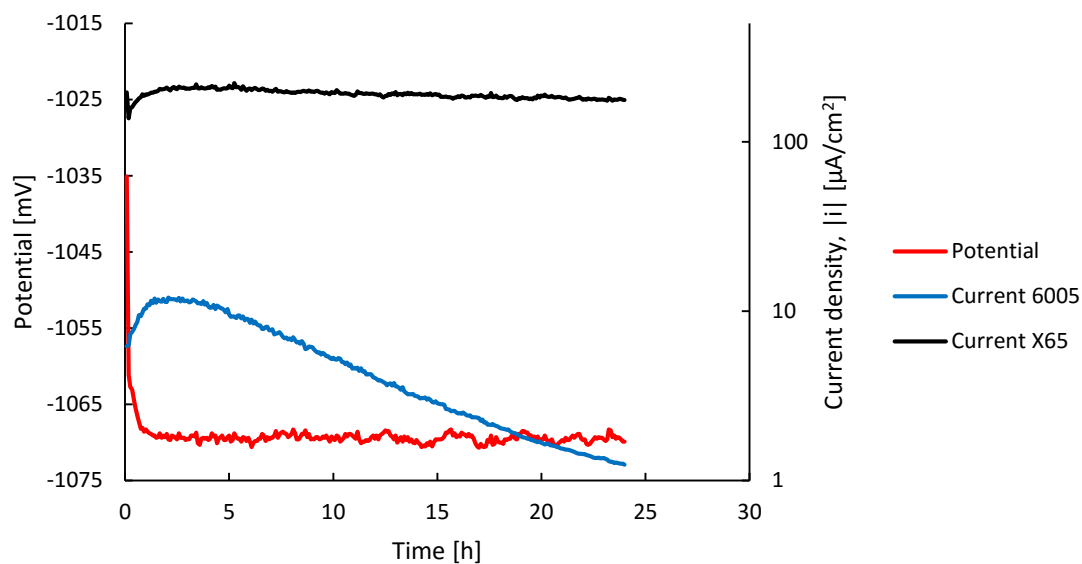

Figure C.8. Parallel 2 of galvanic corrosion test between X65 carbon steel, 6005 aluminium and AlZnIn in 3.5% NaCl solution. Recorded coupling potential and galvanic current as a function of time.
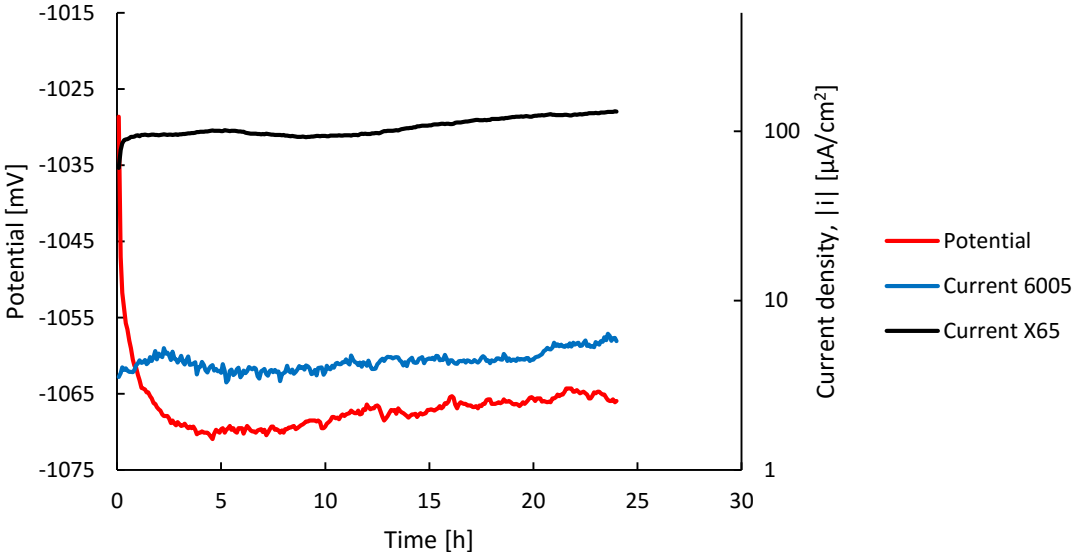
Figure C.9. Parallel 1 of galvanic corrosion test between X65 carbon steel, 6005 aluminium and AlZnIn in artificial seawater. Recorded coupling potential and galvanic current as a function of time.
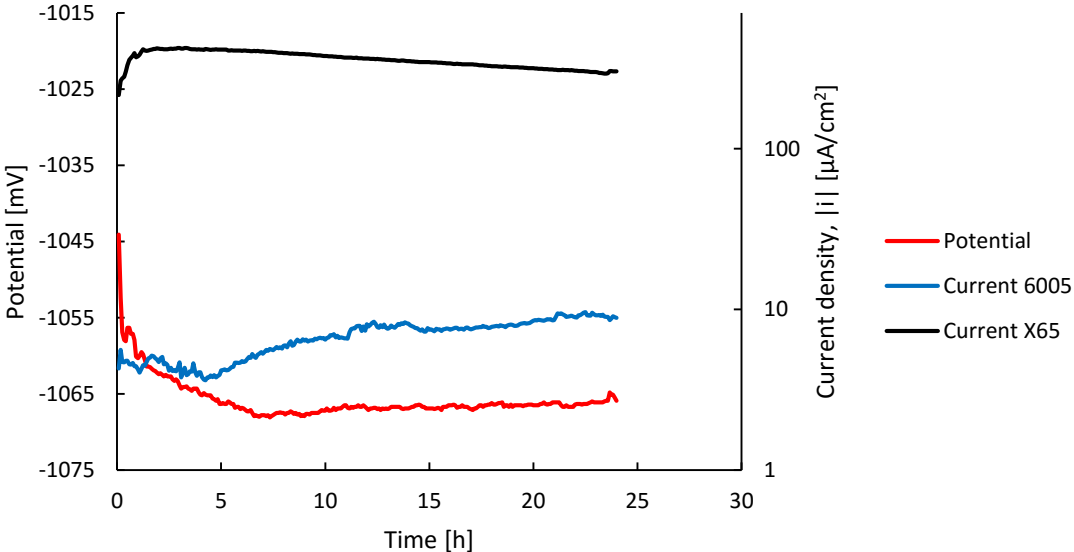

Figure C.10. Parallel 2 of galvanic corrosion test between X65 carbon steel, 6005 aluminium and AlZnIn in artificial seawater. Recorded coupling potential and galvanic current as a function of time.